UNIVERSIDADE
FEDERAL DO CEARÁ

Universiteit
Antwerpen

Diego de Lucena Camarão

Diffusive properties of soft condensed matter systems under external confinement

---

Diffuse eigenschappen van zachte gecondenseerde materie systemen met uitwendige opsluiting

Fortaleza / CE / Brazil

2014

Diego de Lucena Camarão

Diffusive properties of soft condensed matter systems under external confinement

Doctoral thesis presented to the Department of Physics of Federal University of Ceará as part of the prerequisites to obtain the title of Doctor of Science (D.Sc.)

Federal University of Ceará

Department of Physics

Graduation Program in Physics

Supervisor: Prof. Dr. Wandemberg Paiva Ferreira

Co-supervisor: Prof. Dr. François M. Peeters

Fortaleza / CE / Brazil

2014

Diego de Lucena Camarão
Diffusive properties of soft condensed matter systems under external confinement/ Diego de Lucena Camarão. – Fortaleza / CE / Brazil, 2014-
141 p. : il. (color.) ; 30 cm.

Supervisor: Prof. Dr. Wandemberg Paiva Ferreira

Doctoral Thesis – Federal University of Ceará
Department of Physics
Graduation Program in Physics, 2014.

1. Soft condensed matter. 2. Colloids. 3. Computer simulation. I. Prof. Dr. Wandemberg Paiva Ferreira. II. Federal University of Ceará. III. Department of Physics. IV. Title

CDU xx:xxx:xxx.x

Diego de Lucena Camarão

Diffusive properties of soft condensed matter systems under external confinement

Doctoral thesis presented to the Department of Physics of Federal University of Ceará as part of the prerequisites to obtain the title of Doctor of Science (D.Sc.)

Approved doctoral thesis. Fortaleza / CE / Brazil, 27/08/2014:

Prof. Dr. Wandemberg Paiva Ferreira
Supervisor (UFC, Brazil)

Prof. Dr. François M. Peeters
Co-supervisor (UAntwerpen, Belgium)

Prof. Dr. Ramón Castañeda-Priego
University of Guanajuato, Mexico

Prof. Dr. Fabrício Q. Potiguar
UFPA, Brazil

Prof. Dr. Gil de Aquino Farias
UFC, Brazil

Prof. Dr. Raimundo N. da Costa Filho
UFC, Brazil

Fortaleza / CE / Brazil
2014

To my mother, Socorro, whose endless support and love are indispensable.

Acknowledgements

I would like to kindly express my full gratitude to my supervisor Prof. Wandemberg Paiva Ferreira, for all the support during the development of this thesis. Not less important is my gratitude towards my co-supervisor Prof. François Peeters for all his insightful comments to improve this thesis, and specially his endless patience. I would also like to thank Prof. Felipe Munarin, Dr. Kwinten Nelissen and Dr. Vyacheslav Misko for all the support during the preparation of some of the works presented in this thesis.

Scientific developments are certainly not a result of individual achievement, therefore I would like to thank all people involved in my life during all these (almost) four years of my PhD studies, specially my family and my friends. It would be unfair if I forgot any names, so I'll just keep it simple and plain: Thank you very much for all the support throughout these years.

I would also like to thank all the employees from the Department of Physics of Federal University of Ceará (UFC) and from the Department of Physics of University of Antwerp (UA). Last but not least, I would like to thank the Brazilian agencies CAPES and CNPq, and the Flemish agency FWO, for financial support.

Diego
August, 2014

“The first principle is that you must not fool yourself.
And you are the easiest person to fool.”
– Richard P. Feynman

Abstract

In this thesis we study the influence of external confinement potentials on the dynamical properties of soft condensed matter systems. We analyze the diffusive properties of two specific systems by means of Langevin and Brownian Dynamics simulations. In Chapter 1, we introduce the subject of soft condensed matter. We show several theoretical and experimental aspects of these type of systems. We make a brief introduction to the topic of diffusion (Sec. 1.5), where we discuss main aspects of Brownian motion. We introduce the single-file diffusion (SFD) problem (Sec. 1.5.3) and discuss it in the context of soft condensed matter systems, both theoretically and experimentally. In Chapter 2, we introduce the computational method used in this thesis. We discuss Molecular Dynamics (MD) and its variants, Langevin and Brownian Dynamics simulations. We also introduce numerical algorithms used in the following chapters. In Chapters 3, 4 and 5, we analyze two different systems, namely (i) a system of interacting Yukawa particles confined in a parabolic *quasi*-one-dimensional (q1D) channel and (ii) a system of magnetic colloidal particles under the influence of both a parabolic confinement potential and a periodic external modulation along the unconfined direction. In the former, we study the transition from the single-file diffusion (SFD) regime to the two-dimensional (2D) diffusion regime. In the latter, we study the influence of several parameters that characterizes the system, *e.g.*, the strength of an external magnetic field and the periodic modulation along the unconfined direction, on its dynamical properties. Finally, we present the summary of the main findings reported in this thesis and we show some open questions as perspectives for future research in the field of diffusion in soft condensed matter systems.

Key-words: soft condensed matter. colloids. computer simulation.

Resumo

Nesta tese estudamos a influência de potenciais de confinamento externos nas propriedades dinâmicas de sistemas de matéria condensada mole. Analisamos as propriedades difusivas de dois sistemas específicos utilizando simulações computacionais (Dinâmica Molecular de Langevin e Dinâmica Browniana). No Capítulo 1, introduzimos o tópico sobre matéria condensada mole. Mostramos vários aspectos teóricos e experimentais neste tipo de sistema. Fazemos uma breve introdução ao tópico de difusão (Sec. 1.5), onde discutimos os principais aspectos do movimento Browniano. Introduzimos o problema de difusão em linha (SFD, do inglês *single-file diffusion*) (Sec. 1.5.3) e o discutimos, teorica e experimentalmente, no contexto de sistemas de matéria condensada mole. No Capítulo 2, introduzimos os métodos computacionais utilizados nesta tese. Discutimos os métodos de Dinâmica Molecular e suas variantes, o método de Dinâmica de Langevin e Dinâmica Browniana. Também introduzimos algoritmos de integração utilizados nos capítulos posteriores. Nos Caps. 3, 4 e 5, analisamos dois sistemas distintos, (i) um sistema de partículas de Yukawa confinadas em um canal parabólico *quasi*-unidimensional (q1D) e (ii) um sistema de colóides magnéticos sob a influência de um potencial parabólico e uma modulação periódica externa ao longo da direção não confinada. No primeiro sistema, estudamos a transição do regime de difusão em linha (SFD) para o regime de difusão normal (2D). No segundo sistema, estudamos os efeitos de vários parâmetros que caracterizam o sistema (*e.g.*, a magnitude do campo magnético externo e a presença da modulação periódica externa) em suas propriedades dinâmicas. Finalmente, apresentamos um sumário dos principais resultados obtidos nesta tese e mostramos algumas questões em aberto como perspectivas para pesquisas futuras na área de difusão em sistemas de matéria condensada mole.

Palavras-chave: matéria condensada mole. colóides. simulação computacional.

Samenvatting

In deze thesis werd de invloed van uitwendig aangelegde inperkingspotentialen onderzocht op de dynamische eigenschappen van zacht gecondenseerde materie systemen. De diffusie eigenschappen van twee specifieke systemen werden onderzocht doormiddel van Langevin en Brownse dynamische simulaties. In Hfst. 1 wordt het onderwerp van zacht gecondenseerde materie geintroduceerd. Verschillende theoretische en experimentele aspecten van dit type van systemen worden vermeld. Ook wordt er een korte inleiding gegeven van het onderwerp diffusie (Sec. 1.5), waar de verschillende hoofd aspecten van Brownse beweging worden vermeld. Het probleem van 'single file' diffusie (SFD) (Sec. 1.5.3) wordt geintroduceerd en besproken in de context van zacht gecondenseerde materie systemen, zowel theoretisch als experimenteel. In Hfst. 2, wordt de computationele methode besproken die in deze thesis werd aangewend. We bespreken de Moleculaire Dynamica (DM) simulatie methode en de varianten zoals Langevin and Brownse dynamische simulaties. De numerieke algoritmen die in de volgende hoofstukken worden aangewend worden geintroduceerd. In de Hfst. 3, 4 en 5 analyzeren we twee verschillende systemen, namelijk: (i) een systeem van interagerende Yukawa deeltjes die opgesloten zijn in een parabolische kwasi-één-dimensionaal (q1D) kanaal, en (ii) een systeem van magnetisch colloidale deeltjes onder de invloed van een parabolische inperkingspotentiaal en een periodisch externe modulatie langs de vrije richting. In het eerste systeem bestuderen we de overgang van het 'single-file' diffusie regime naar het twee-dimensionaal diffusie regime. We bestuderen de invloed van de verschillende parameters die het systeem karakteriseren, bijv. de sterkte van het uitwendig magneetveld en de aanwezigheid van een periodische modulatie langs de vrije richting op de dynamische eigenschappen. Eindelijk, presenteren we de overzicht van de thesis en we vermelden een aantal open vragen die interessant zijn voor toekomst onderzoek in het gebied van diffusie van zacht gecondenseerde materie systemen.

Sleutelwoorden: zachte gecondenseerde materie. colloïden. computersimulatie.

List of Figures

Contents

Part I

Literature review

1 Soft condensed matter

In this chapter we introduce the topic of Soft Condensed Matter. We define colloidal dispersions and we give motivation for using these particles as model systems for testing theoretical predictions of statistical physics. Many of the ideas presented here can be found in the following much more specialized textbooks: “Soft condensed matter” by R. A. L. Jones and “Soft matter physics” by Masao Doi.

1.1 General considerations

Condensed matter physics is a discipline in the field of Physical Sciences which studies the physical properties of condensed phases of matter (1). It is mainly concerned in addressing problems related to liquid and solid systems, but it also deals with different condensed phases as, for instance, the Bose-Einstein condensate (BEC) in cold atomic systems (2) and the superconducting phase (3) found in low temperature materials.

However, there is a variety of materials found in nature which do not fall into the category of either simple liquids or crystalline solids. For instance, glues, paints, soaps, and colloidal gels (Fig. 1) are examples of these type of materials. They are usually referred to as *soft condensed matter* systems (4) or *soft matter*, for short. These systems are formed of colloidal particles (solute) which are dispersed in another liquid (solvent). For example, fat and proteins in milk are types of colloidal dispersions ($\sim 0.1\ \mu$m of diameter) embedded in water.

All of these soft matter systems share some common characteristics. For example, the characteristic length scale of colloidal dispersions is in an intermediate regime between the atomic scale and the macroscopic scale. It is therefore usual to refer to colloidal dispersions as a class of *mesoscopic* systems. The diameter of the colloidal particles ranges between 10 nm and 10 μm. Another feature is that the common physical properties of these materials (*e.g.*, self-assembly and non-linear response to external perturbations) are related to the fact that the energy scales involved are of the order of the thermal energy, k_BT. This means that quantum effects do not play an important role in the properties of soft matter systems, which make them strong candidates for testing theoretical models in statistical physics using relatively simple experimental setups.

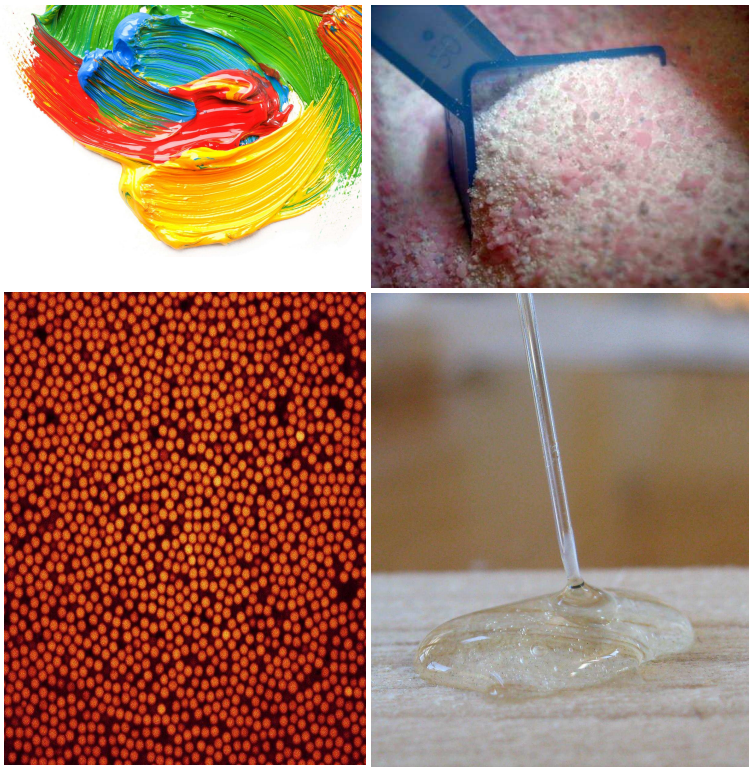

Figure 1 – Examples of soft condensed matter systems. Top panel: (left) Paints, and (right) powder soap. Bottom panel: (left) A colloidal gel dispersion, and (right) glue.

1.2 Colloidal dispersions

A colloidal particle of diameter $\sim 1\ \mu$m at room temperature $T = 300$ K in water has a characteristic relaxation time[1] $\tau_s \sim 1$ s. Therefore, the dynamics of this particle can be time resolved using an experimental technique called *video microscopy*, which consists in recording the particle's trajectory to extract useful information not only about the dynamics of the particle itself, but also about the fluid properties in which it is embedded in.

On the other hand, in atomic systems, where particles have a diameter of a few angstroms, the characteristic relaxation time is of the order of $\tau_s \sim 10^{-9}$ s, which is too short for time-resolved experiments with atomic resolution. In principle it is also possible to study atomic systems by means of atomic force microscopy (AFM), but colloidal dispersions are usually more simple and flexible. The main experimental tools to study the static and dynamical properties of colloidal suspensions are static and dynamic light scattering (SLS and DLS, respectively) (5, 6).

Furthermore, mesoscopic systems can be much more easily tuned in experiments. The interaction of colloids with external fields and the inter-particle interaction potential between

[1] This is called the structural relaxation time, which is the time needed for a particle to diffuse a distance comparable with its diameter.

pairs of colloids are customizable in order to allow the study of different basic physical problems in statistical physics. For instance, colloidal crystals show similar diffraction patterns (7) as X-ray diffraction in atomic systems. One could also, for example, use colloidal crystals as model systems to study kinetics of crystallization (8, 9), a much more difficult task to achieve using atomic systems.

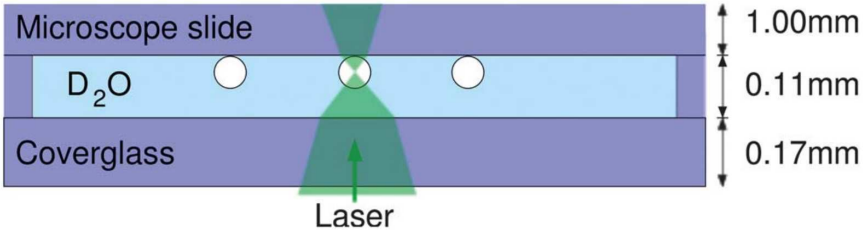

Figure 2 – Schematic representation of polystyrene colloidal particles of radius $R = 1.4\ \mu$m dispersed in heavy water (D_2O) and confined by external laser beams. Taken from Ref. (10).

As stated above, one major advantage of using colloidal particles as model systems to study theoretical predictions of statistical physics is the possibility to tune inter-particle interaction potentials. For instance, colloids can interact through a screened Coulomb potential (commonly known as the Yukawa potential) or through a dipole-dipole potential, just to cite a few. In the first case, the strength of interaction between colloids can be tuned by changing the salt concentration of the solution in which the particles are moving in. In the second case, the magnetic interaction (dipole-dipole) can be adjusted by introducing an external magnetic field which induces a magnetic dipole moment inside the colloidal particles. The strength of this interaction is then proportional to the magnitude of the external magnetic field. The Yukawa potential has an exponential decay form, $V(r) \propto \exp(-r/\lambda_D)/r$ and the dipole-dipole interaction has a $1/r^3$ dependence, where r is the center-to-center distance between a pair of colloids and λ_D is the so-called Debye screening length (11).

Besides the tuning of the inter-particle interaction potential by adjusting external parameters, it is also possible to experimentally control the interaction of colloidal particles with external fields (cf. Fig. 2). For instance, colloidal dispersions can be placed on the top of modulated (either periodic or random) substrates which are created by using, *e.g.*, light fields (10, 12, 13). Furthermore, several types of external potential shapes can be also realized experimentally by using topographic patterns (14, 15).

One of the devices used to experimentally trap colloidal charged particles is called a Penning trap, where both an electric and a magnetic field are used to confined the particles. This device usually has a cylindrical symmetry (Fig. 3) and batteries are placed on the tips of the cylinder to produce the external fields (16). An additional laser beam is used to decrease the

temperature of the system to very low values, where liquid and crystal phases are found.

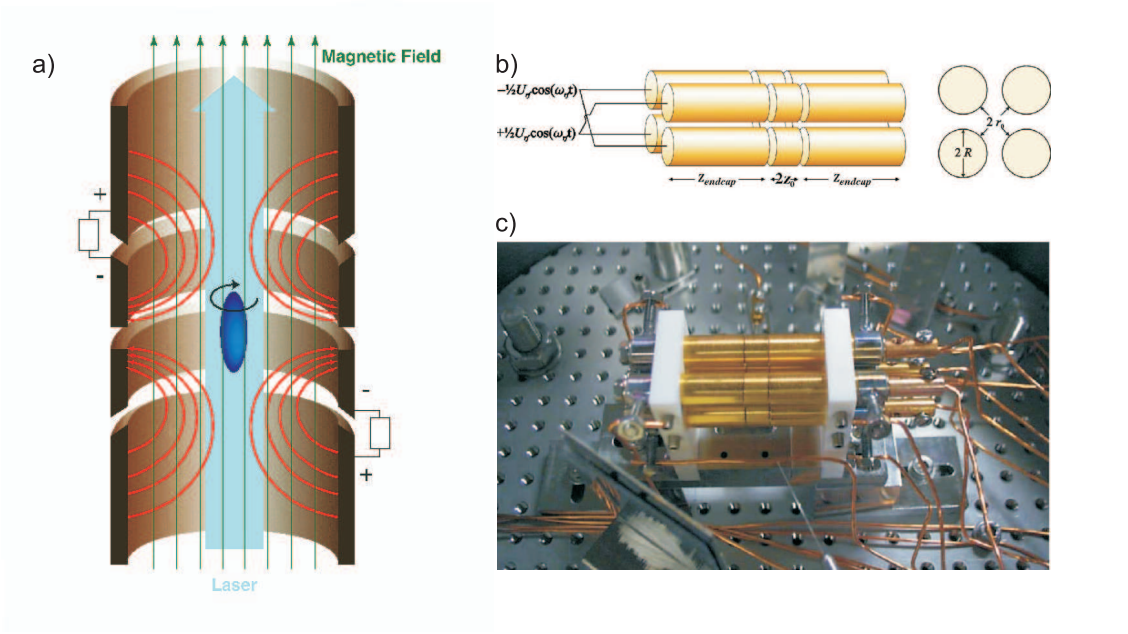

Figure 3 – (a) Schematic representation of a Penning trap, where charged particles are confined by using electric and magnetic fields. (b) Sketch of the experiment used to confine the particles and (c) image of the actual device used in the experiments of Ref. (16).

1.3 Pair interaction between colloidal particles

1.3.1 van der Waals forces

In general, colloidal particles interact with each other through van der Waals forces. In the case of the spherical particles, the van der Waals potential is given by the analytical expression (17, 18)

$$V(r_{ij}) = -C\left[\frac{2R^2}{r_{ij}^2 - 4R^2} + \frac{2R^2}{r_{ij}^2} + \ln\left(1 + \frac{4R^2}{r_{ij}^2}\right)\right], \tag{1.1}$$

where r_{ij} is the center-to-center distance between a pair of particles i and j, $R = \sigma/2$ is the radius of each particle, and C is a constant that depends on the type of colloidal particle and the medium where it is embedded[2]. Note that the negative sign in Eq. (1.1) indicates that this interaction is strongly attractive and therefore colloidal particles tend to stick together, which is known as the coagulation effect. In order to study different kind of effects other than the coagulation, it is of course desirable to have stabilized colloidal suspensions. This is mainly achieved by introducing repulsive interaction between the particles, which can be done, *e.g.*, by electrostatic stabilization techniques (19).

[2] For instance, for polystyrene particles dispersed in water, $C \approx 0.23 \times 10^{-20}$ J.

1.3.2 Debye-Hückel inter-particle interaction potential

The surface of a colloidal particle is covered by molecules which are electrically neutral. However, when a colloidal particle is dispersed in water (for instance) the positive charged counter ions of the molecules are dissolved due to water molecule polarization (20). Therefore, the surface of the particle is negatively charged and the entropy tends to spread the ions over the whole volume. When equilibrium is reached, the balance between energy and entropy creates an electric double layer (21). This layer consists of the positively charged cloud of counter ions around the colloidal particle and the negatively charged surface of the colloidal particle itself. Therefore, the cloud of counter ions around the particle is responsible for screening the interaction between colloidal particles.

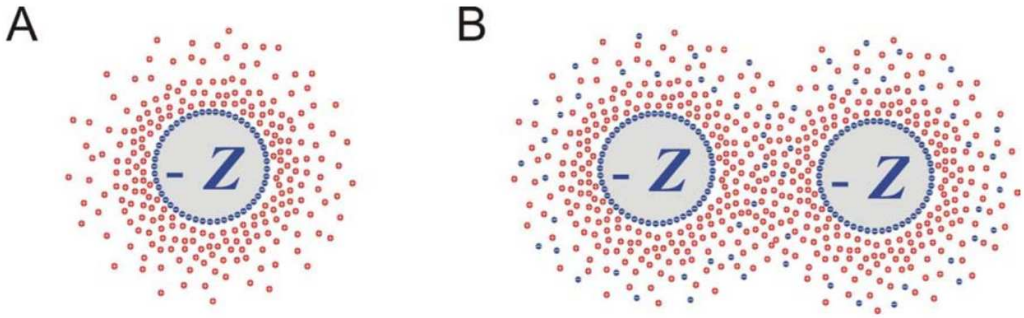

Figure 4 – (a) Schematic representation of the electric double layer, which consists of the positively charged cloud of counter ions around the colloidal particle and the negatively charged surface (total charge Z) of the colloidal particle. (b) Two colloidal particles interact with each other through a repulsive inter-particle interaction potential which is screened by the cloud of counter ions. Taken from Ref. (20).

In order to calculate the inter-particle interaction potential for this case, the Poisson-Boltzmann (PB) equation

$$\varepsilon_0 \varepsilon_W \nabla^2 \phi(r) \propto \exp\left(-\frac{z_i e \phi(r)}{k_B T}\right), \tag{1.2}$$

can be solved analytically (11) in the first-order approximation case (*i.e.*, by linearization of the PB equation). By doing so, one gets the potential $\phi(r)$ created by a colloidal particle at a point r in space as

$$\phi(r) = \frac{Ze}{4\pi\varepsilon_0\varepsilon_W} \frac{\exp(\sigma/2\lambda_D)}{(1+\sigma/2\lambda_D)} \frac{\exp(-r/\lambda_D)}{r}, \tag{1.3}$$

where Z is the total charge (in units of the elementary charge e) on the surface of the colloidal particle, ε_0 and ε_W are the permittivity of vacuum and water, respectively. The Debye screening length is given by $\lambda_D^{-1} = \sqrt{\varepsilon_0 \varepsilon_W k_B T / s}$ with $s = \sum_i (e z_i^2) c_i$ (z_i and c_i are the valence and the bulk concentration of the counter ions of type i, respectively). Linear superposition of Eq. (1.3) leads to the well-known Debye-Hückel (22) inter-particle interaction potential

$$V(r_{ij}) = \frac{(Ze)^2}{4\pi\varepsilon_0\varepsilon_W} \left(\frac{\exp(\sigma/2\lambda_D)}{(1+\sigma/2\lambda_D)}\right)^2 \frac{\exp(-r_{ij}/\lambda_D)}{r_{ij}}, \tag{1.4}$$

for a pair of colloidal particles i and j separated by a distance r_{ij}. Note that the screening effect is directly related to the concentration of ions present in the sample, *i.e.*, $\lambda_D^{-1} \propto 1/\sqrt{s}$. Therefore, it is possible to experimentally tune the inter-particle interaction potential by adjusting the salt (ions) concentration of the sample, as previously stated.

Note that, as opposed to the potential of Eq. (1.1), the Debye-Hückel potential is positive, which means the interaction between particles is repulsive. Consequently, experimental techniques such as the electrostatic stabilization are mainly based on the adjustment of the salt concentration of the samples. These adjustments prevent particles agglomeration and allows the creation of well-defined 2D and 3D lattices of colloidal suspensions, *e.g.*, nanocrystals (23, 24).

1.4 Structural and dynamical properties of colloidal dispersions

1.4.1 Wigner crystals

In 1934, physicist Eugene Wigner predicted that a gas of electrons could present a phase transition from a liquid phase to a solid (crystalline) structure (25). This solid phase is now usually called a *Wigner crystal*. The main physical mechanism behind this effect is that for a certain value below a critical density ($n < n_c$), the potential energy of the electrons dominates over the kinetic energy. Therefore, the spatial arrangement of the electrons becomes very important. In 3D, the electrons form a body-centered cubic (bcc) structure. In 2D, they form a triangular lattice (Fig. 5) and in 1D, the electrons become evenly spaced.

The first experimental observation of the Wigner crystallization of electrons was reported by Grimes and Adams (27) in 1979. They found that, under certain circumstances, electrons deposited on a 2D substrate of liquid helium would arrange themselves in a triangular lattice, just like predicted by Wigner.

More recently, in 2009, an experimental and numerical study (28) also reported the formation of Wigner crystal structures using trapped electrons on the surface of liquid helium. Even more, by experimentally manipulating electrons one by one, the authors were able to calculate the energy spectrum to add (or to extract) one electron from the trap with occupation number N. Depending on N, the system of electrons would arrange itself into ring structures. Previously, in 1994, Bedanov and Peeters (26) showed a theoretical prediction of the formation of these ring structures (Fig. 6) by means of numerical and analytical calculations.

Nowadays, Wigner crystals are also referred to as crystal phases found in non-electronic systems (*e.g.*, soft condensed matter systems) at low density regimes. For instance, these phases have been observed experimentally in dusty plasmas (31). In this experiment, dust particles dispersed in a weakly ionized argon plasma acquire a negative charge (due to the ions present in the plasma) on their surfaces (Fig. 7) and become strongly repulsive. Similar to the colloidal

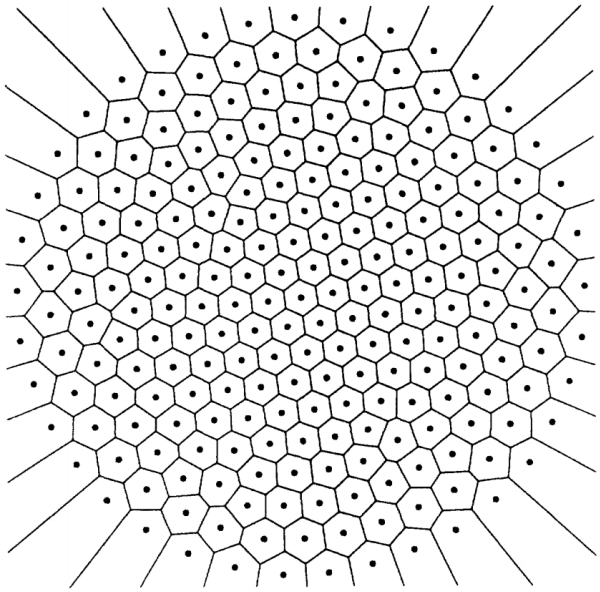

Figure 5 – A 2D system of $N = 230$ electrons confined by a parabolic trap and interacting through a repulsive potential tend to form a Wigner crystal in the center. However, some defects can appear due to the competition between the confinement potential (trap) and the repulsion between the particles. Also, particles in the borders tend to be accommodated in a distorted triangular lattice. Taken from Ref. (26).

particles in water (Sec. 1.3.2), the interaction between dust particles is also screened by a double electric layer. Since the inter-particle interaction potential between these particles is similar to the one presented in Eq. (1.4), there has been a large number of theoretical and experimental investigations about the Wigner crystallization phenomenon using soft condensed matter as model systems.

1.5 Diffusion and Brownian motion

1.5.1 Diffusion equation

Diffusive processes occur frequently in nature and they are directly related to the transport of any given physical quantity in space and time. For instance, the transport of molecules in a fluid (molecular diffusion), the heat conduction in a metal bar (heat diffusion) and the movement of a suspended particle in a viscous fluid (Brownian motion) are a few examples of known diffusive processes.

One of the first mathematical description of a diffusion phenomenon was due to the French mathematician Joseph Fourier, in his *Théorie analytique de la chaleur* (The Analytic Theory of Heat) published in 1822. He studied the heat conduction through a metal bar and showed (32) that the temperature profile $u(x,t)$ of a 1D homogeneous metal bar obeys a heat

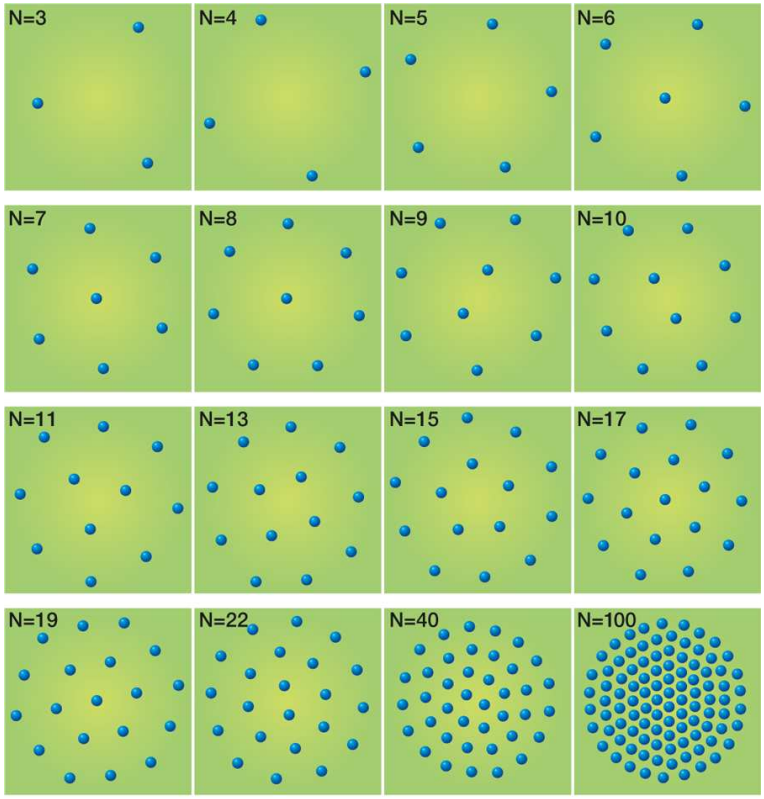

Figure 6 – A series of Wigner crystal structures showing the arrangement of electrons in a circular island from an occupation number of $N = 3$ to $N = 100$. The electrons form ring structures as more electrons are added. For large N, a triangular Wigner lattice forms in the center, while the outer electrons remain in rings. Taken from Ref. (29), illustration by Alan Stonebraker.

equation of the form

$$\frac{\partial}{\partial t}u(x,t) = D_T \frac{\partial^2}{\partial x^2}u(x,t), \tag{1.5}$$

where D_T is known is as the thermal diffusion coefficient and it is a material-specific quantity.

In 1855, German physician Adolf Fick published his work on particle diffusion and established what is known today as the Fick's laws of diffusion. The first Fick's law states that the flux of molecules always goes from regions in space of high concentration of particles to regions of lower concentration, across a gradient of concentration. In mathematical terms, this law is written as

$$\boldsymbol{j} = -D(c)\boldsymbol{\nabla} c(\boldsymbol{r},t), \tag{1.6}$$

where $\boldsymbol{j}$ is flux (amount of matter per unit area per unit time), $D(c)$ is the diffusion coefficient which may depend on the concentration profile $c(\boldsymbol{r},t)$. Note that the negative sign in Eq. (1.6) comes from the postulate that the flux of molecules goes from the regions of higher to lower concentrations, as stated above. Considering the simplest situation where the continuity equation

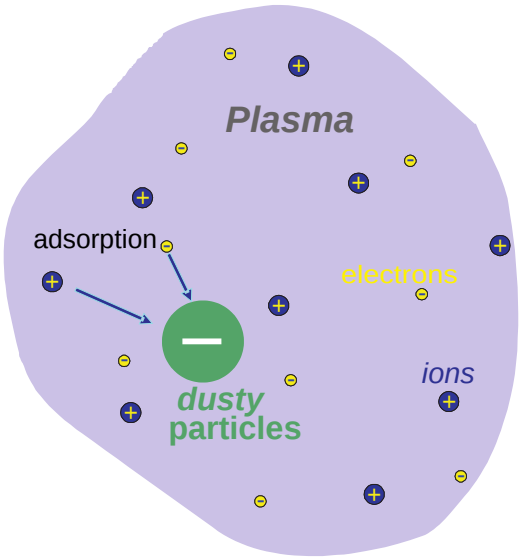

Figure 7 – Representation of a dusty plasma. The free positive ions in the plasma adhere to the surface of the dust particles creating a strong electrostatic repulsive interaction between these particles. Taken and adapted from Ref. (30).

$$\frac{\partial}{\partial t}c(\boldsymbol{r},t)+\nabla\cdot\boldsymbol{j}=0, \tag{1.7}$$

is valid (there are no sinks or sources, *i.e.*, there is no effective creation or destruction of matter), the combination of Eqs. (1.6) and (1.7) leads to a similar diffusion equation as obtained by Fourier

$$\frac{\partial}{\partial t}c(\boldsymbol{r},t)=\nabla\cdot(D(c)\nabla c(\boldsymbol{r},t)). \tag{1.8}$$

Note that if the diffusion constant is independent of the concentration profile $c(\boldsymbol{r},t)$, Eq. (1.8) reduces to

$$\frac{\partial}{\partial t}c(\boldsymbol{r},t)=D\nabla^2 c(\boldsymbol{r},t), \tag{1.9}$$

which is similar to the heat diffusion equation and also usually called the second Fick's law. A solution to Eq. (1.9), considering an initial condition $c(\boldsymbol{r},0)=\delta(\boldsymbol{r}-\boldsymbol{r}_0)$ (where $\boldsymbol{r}_0$ is the initial position of the concentration of particles) and assuming isotropy of space, is given by a Gaussian propagator (33)

$$c(\boldsymbol{r},t)=\frac{1}{h(t)}\exp\left(-\frac{|\boldsymbol{r}-\boldsymbol{r}_0|^2}{m(t)}\right), \tag{1.10}$$

where[3] $h(t)\propto\sqrt{t}$ and $m(t)\propto t$.

From the distribution $c(\boldsymbol{r},t)$ it is possible to calculate its moments. The first two moments are the commonly studied ones, i.e., the average displacement

$$\langle r\rangle=\int_{-\infty}^{\infty} r\,c(\boldsymbol{r},t)dV, \tag{1.11}$$

[3] For instance, in the 1D case, $h(t)=\sqrt{4\pi Dt}$ and $m(t)=4Dt$.

and the mean square displacement (MSD)

$$\langle r^2 \rangle = \int_{-\infty}^{\infty} r^2 \, c(\boldsymbol{r},t) dV. \tag{1.12}$$

These quantities are important because they can be obtained through experiments. Furthermore, they are directly related to macroscopic quantities, such as temperature and viscosity, as we will show in the following.

1.5.2 Brownian motion

The random movement of suspended particles on a fluid was first observed by Scottish botanist Robert Brown in his work *A Brief Account of Microscopical Observations* (34) published in 1828, where he reported the irregular motion of pollen grains in water. Brown was intrigued by the phenomenon but could not explain it in terms of any previously known theory at the time.

Much longer after Brown's reports, in 1888, the French physicist Louis-Georges Gouy made some important remarks about these random movements. Among these remarks, we cite a few: (i) The motion is extremely irregular (Fig. 8), the trajectory seems to be not differentiable, and the motion never ceases; (ii) the motion is most active[4] in less viscous liquids; (iii) the motion is most active at higher temperatures.

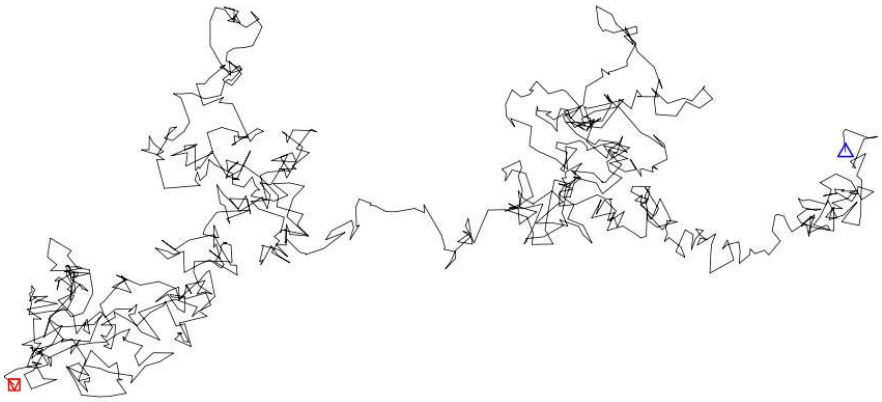

Figure 8 – Trajectory of a particle executing a Brownian movement. Note that the movement is very irregular and experiments by Robert Brown showed that the movement is most active in less viscous liquids and less active for lower temperatures.

These observations were important for the later development of a Brownian motion theory by Albert Einstein (35) published in 1905 and subsequent independent works by Paul Langevin (36) in 1908, Marian Smoluchowski (37) in 1915, and others.

[4] In this context, "active" means that the particle experiences larger displacements from a given origin in the same time interval.

The Einstein theory of Brownian motion is based on the arguments presented now. Consider a set of N independent (non-interacting) particles performing successive random displacements. In the time interval τ, the coordinates of each particle are changed by $\Delta x = \varepsilon$. The fraction of particles which changes their positions between x and $x+\varepsilon$ in the time interval τ can be expressed by

$$\frac{dN}{N} = p(\varepsilon)d\varepsilon, \tag{1.13}$$

where $p(\varepsilon)$ is a distribution of displacements. It is evident that this distribution must obey the normalization condition

$$\int_{-\infty}^{\infty} p(\varepsilon)d\varepsilon = 1. \tag{1.14}$$

The concentration of particles (number of particles per unit length) is $c(x,t)$. Let us now calculate the distribution of particles at a time $t+\tau$ from their previous distribution at instant t. By the definition of $p(\varepsilon)$, the number of particles in the interval x and $x+\varepsilon$ at the instant $t+\tau$ is

$$c(x,t+\tau)dx = dx\int_{-\infty}^{\infty} c(x+\varepsilon,t)p(\varepsilon)d\varepsilon. \tag{1.15}$$

If we consider that the time interval τ is sufficiently small and that the displacement ε is also small, we can expand $c(x,t)$ in powers of τ and ε up to second order. By doing so and replacing the results into Eq. (1.15), we get

$$\begin{aligned} c(x,t)+\frac{\partial c(x,t)}{\partial t}\tau+\frac{\partial^2 c(x,t)}{\partial t^2}\frac{\tau^2}{2} = c(x,t)\int_{-\infty}^{\infty} p(\varepsilon)d\varepsilon+ \\ +\frac{\partial c(x,t)}{\partial x}\int_{-\infty}^{\infty}\varepsilon p(\varepsilon)d\varepsilon+\frac{\partial^2 c(x,t)}{\partial x^2}\int_{-\infty}^{\infty}\frac{\varepsilon^2}{2}p(\varepsilon)d\varepsilon. \end{aligned} \tag{1.16}$$

From the normalization condition [Eq. (1.14)] and from the fact that the second term on the r.h.s. of Eq. (1.16) vanishes[5], we obtain the following differential equation for the concentration $c(x,t)$

$$\frac{\tau}{2}\frac{\partial^2 c(x,t)}{\partial t^2}+\frac{\partial c(x,t)}{\partial t} = D\frac{\partial^2 c(x,t)}{\partial x^2}, \tag{1.17}$$

where D is defined by the expression

$$D \equiv \frac{1}{\tau}\int_{-\infty}^{\infty}\frac{\varepsilon^2}{2}p(\varepsilon)d\varepsilon. \tag{1.18}$$

In the limit where the concentration of particles varies very slowly in time ($\frac{\partial}{\partial t}c(x,t) \gg \tau\frac{\partial^2}{\partial t^2}c(x,t)$), we can drop the first term on the l.h.s. of Eq. (1.17) and find

$$\frac{\partial}{\partial t}c(x,t) = D\frac{\partial^2}{\partial x^2}c(x,t), \tag{1.19}$$

[5] From the construction of the function $p(\varepsilon)$, it is clear that it must be an even function (otherwise the normalization condition would not be satisfied), *i.e.*, $p(\varepsilon) = p(-\varepsilon)$. Therefore, since $\varepsilon p(\varepsilon)$ is an odd function, $\int_{-\infty}^{\infty}\varepsilon p(\varepsilon)d\varepsilon = 0$.

which is the same as the second Fick's law [Eq. (1.9)]. Therefore, by this analysis, Einstein showed that the movement of the now called Brownian particles in a viscous fluid is governed by a diffusion equation. The solution of this equation is given by Eq. (1.10) and in a 1D system of non-interacting particles, the propagator $c(x,t)$ has the exact form (33)

$$c(x,t) = \frac{1}{\sqrt{4\pi Dt}} \exp\left(-\frac{|x-x_0|^2}{4Dt}\right), \tag{1.20}$$

which is a Gaussian around x_0 and has a width proportional to the diffusion coefficient D. Plugging Eq. (1.20) into Eq. (1.12) one obtains the well-known result (38)

$$\langle x^2(t)\rangle \equiv W(t) = 2Dt, \tag{1.21}$$

which shows that the mean square displacement of a Brownian particle in a fluid grows linearly in time[6]. This is usually called the normal diffusion regime sometimes also known as Einstein (or Fickian) diffusion.

1.5.3 Single-file diffusion (SFD)

In 1955, physiologists Hodgkin and Keynes (39) were studying the passage (dynamics) of molecules through narrow pores. These channels were so narrow that molecules could only enter one by one, and therefore they would conserve the original sequence of molecules in a file. This 1D process is now referred to as the single-file diffusion (SFD) problem.

As opposed to 2D and 3D diffusion, where normal diffusion (Einstein or Fickian diffusion) is expected, i.e., the mean square displacement of a tagged particle in the long-time limit grows linearly in time ($W(t) \propto t$), the dynamics of a tagged particle in a file of interacting particles exhibits anomalous diffusion, i.e.,

$$W(t) = 2F\sqrt{t}, \tag{1.22}$$

where F is the so-called single file diffusion mobility.

The first mathematical description of the SFD problem was introduced in the seminal paper of Harris (40), in 1965, where he obtained the result of Eq. (1.22). The model of Harris consisted in the following. Consider N point-like particles diffusing in a 1D infinite straight line with the fixed condition $x_1(t) < x_2(t) < \ldots < x_{N-1}(t) < x_N(t)$ for all times $t \geq 0$. This condition implies that the particles are not allowed to pass each other[7]. Harris showed that the probability distribution of a tagged particle is given by a Gaussian propagator, similar to the one described in Eq. (1.20) but where the width of the distribution is proportional to the square root of time,

[6] This result holds at long-times, *i.e.*, $t \to \infty$.

[7] The model of Harris also assumed periodic boundary conditions and that particles interact through a hard-core potential.

i.e.,

$$P_{\mathrm{T}}(x_{\mathrm{T}},t) \sim \frac{1}{\sqrt{2\pi\langle x_{\mathrm{T}}^2(t)\rangle}} \exp\left(-\frac{x_{\mathrm{T}}^2}{2\langle x_{\mathrm{T}}^2(t)\rangle}\right), \tag{1.23}$$

with

$$\langle x_{\mathrm{T}}^2(t)\rangle = (2/\rho)\sqrt{Dt/\pi} \;\text{ as }\; t \to \infty, \tag{1.24}$$

where ρ is the average density of particles (in an uniform system, $1/\rho$ is the average distance between neighboring particles) and D is the diffusion coefficient. Note that comparing Eqs. (1.22) and (1.24), one arrives at

$$F = \frac{1}{\rho}\sqrt{\frac{D}{\pi}}, \tag{1.25}$$

which relates the single-file diffusion mobility with the diffusion coefficient.

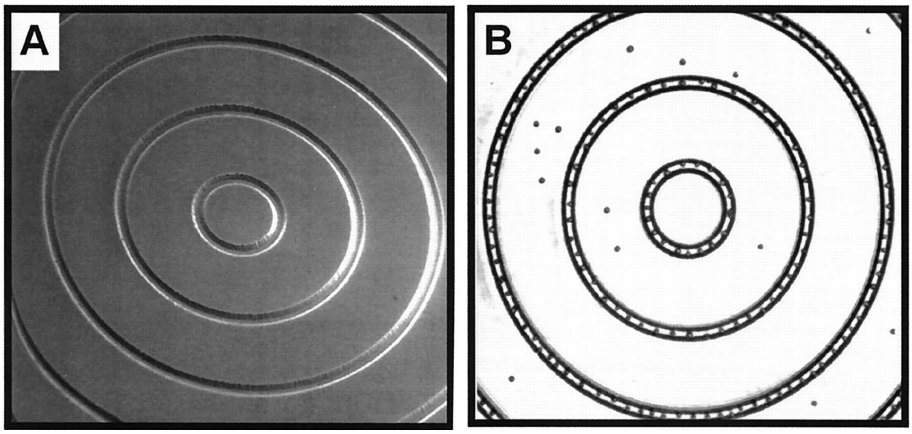

Figure 9 – (a) Circular narrow channels created by photolithography. (b) Image of the channels with the particles (black dots) inside. Taken from Ref. (41).

Eq. (1.24) is the main result of the theory of SFD and it has been obtained analytically (42, 43, 44, 45, 46, 47, 48, 49, 50) by several different approaches. Furthermore, it has also been observed experimentally in different contexts, including in soft matter systems (colloidal dispersions) (41, 51, 52) and in NMR (nuclear magnetic resonance) studies of diffusion in zeolites (53, 54). The heuristic argument to justify the anomalous diffusive behavior reported by Harris is that the dynamics of a tagged particle in a file are correlated with its neighboring particles due to the special geometric constraint (*i.e.*, the single-file condition). This means that for a given particle to diffuse a certain distance its neighbors also needed to have diffused the same amount.

For instance, one of the first experimental evidences of the anomalous diffusion behavior [Eq. (1.22)] was reported by Wei *et al.* (41) in 2000. In this experiment, the authors constructed 1D circular narrow channels by a photolithography process (Fig. 9) where super-paramagnetic colloidal particles where dispersed to diffuse. The 3.6 μm diameter particles were subjected to Brownian motion (thermal bath) and the narrow channel was constructed so that the single-file

condition was fulfilled, i.e., particles could not pass each other. Besides, the interaction between particles was controlled by an external magnetic field, which induced a magnetic moment to each particle. By following the trajectories of the particles over long periods of time with a video microscopy technique, the authors showed that the mean square displacement of a tagged particle followed Eq. (1.22) and its probability distribution was given by Eq. (1.23).

The single-file diffusion mobility factor, F, has also been extensively investigated, both theoretically and experimentally. In the seminal work of Kollmann (46), the author showed analytically that, regardless of the inter-particle interaction potential, the SFD law is always obtained. Kollmann imposed some restrictions in his model: the inter-particle potential has to be of finite range and the system must be homogeneous and in the liquid state. Another result of Kollman's work was relation between F and the structure factor $S(q)$, given by

$$F = \frac{1}{\rho}\sqrt{\frac{DS(q)|_{q\to 0}}{\pi}}, \tag{1.26}$$

where $S(0) = S(q)|_{q\to 0}$ is the structure factor calculated in the limit of long wavelengths ($q \to 0$). The transition from a liquid to a solid-like state in a 1D colloidal system has been recently analyzed by Herrera-Velarde *et al.* (55). For finite-size particles (with diameter σ) interacting through a hard-core potential, Lizana and Ambjörnsson showed (56) that $F = \frac{1-\rho\sigma}{\rho}\sqrt{D/\pi}$, which reduces to the point-like particle ($\sigma = 0$) case [Eq. (1.25)]. Last but not least, Leibovich and Barkai recently showed (57) that F depends on the initial conditions of the system.

Part II

Methods

2 Computer simulation

In this chapter we will discuss briefly some aspects about computer simulation. We will present methods commonly used in simulations, for instance, the Molecular Dynamics (MD) method, as well as variations of this method, specifically Langevin Dynamics (LD) and Brownian Dynamics (BD). Although we try to cover a fair amount of information on the subject, the reader is referred to much more specialized and complete texts, *e.g.*, "Molecular Dynamics Simulations", by J. M. Haile, "The Art of Molecular Simulations" by D. C. Rapaport, and "Computer Simulation of Liquids" by M. P. Allen.

2.1 Introduction

Computer simulation techniques were initially developed during the World War II, mainly through the Manhattan Project[1] in order to model nuclear detonation processes. However, due to the fast development of the electronic industry and the facilitation of access to personal computers (PCs), computer simulations started to be used in several other areas of scientific research, specially in the mathematical modeling of physical, chemical and biological systems, market analysis in economic sciences, social sciences (vote models, disease spreading, etc), and engineering processes of new technologies.

Computational physics, a discipline which uses numerical algorithms to simulate physical systems, is considered an intermediate field between theoretical and experimental physics. Nowadays, the majority areas of Physical Sciences (*e.g.* astrophysics, statistical physics, fluid dynamics, and solid state physics) uses numerical techniques for the solution and analysis of problems which can not be directly solved by analytical methods. The role of computers in scientific research has been very relevant both in the theoretical and in the experimental realms.

From a theoretical point of view, computers allowed a new paradigm for scientists: instead of using some analytical approximations to a specific physical problem, it is now possible to use a computer experiment (computer simulation) to go beyond that approximation and to examine directly the original system. It is clear, however, that computer simulations also use a model system which includes certain approximations. Nevertheless, it is still a very powerful tool to analyze complicated systems, *e.g.*, many-body problems.

[1] The Manhattan Project (MP) was a research project, from 1942 to 1946, led by the United States of America (with the help of Canada and United Kingdom) during the World War II. The main objective was to create the atomic bomb. Among others, the researchers in the MP included American physicists J. R. Oppenheimer (at the time, he was the scientific director of the Los Alamos National Laboratory, where the atomic bombs were designed) and R. P. Feynmann (one of the recipients of the Nobel prize in Physics in 1965).

From an experimental point of view, computers have become a virtual laboratory, where numerical experiments are carried out. The results from a computer simulation can be completely unexpected, *i.e.*, they were not completely evident from the mathematical formulation of the model used to describe the real physical system. A wide variety of computational modeling techniques have been developed over the years.

2.2 Molecular Dynamics (MD)

Molecular Dynamics (MD) simulations refers to a computational set of methods (numerical algorithms) widely used in scientific research, *e.g.*, Physical Sciences, Chemistry, Biophysics, and many others. This method allows one to calculate a set of macroscopic properties of a given physical system (*e.g.*, temperature, pressure, kinetic energy, etc). Furthermore, it allows the calculation of both static and dynamical properties. The starting point of the method is based on a well-defined microscopic description of the physical system under consideration (58). This description can be made through the Hamiltonian or the Lagrangian formalisms, or even directly by using Newton's equations of motion.

In its most simple form, the MD method consists of choosing a set of initial conditions (position and velocity of each particle), an inter-particle interaction potential, an appropriate statistical ensemble, a numerical technique in order to integrate the equations of motion and the implementation of the periodic boundary conditions. The objective of the MD method is then to calculate the trajectories, in phase space, of a collection of particles which individually obey classical coupled equations of motion (58). Therefore, it is necessary to solve numerically (using appropriate algorithms[2]) these coupled equations of motion.

The first MD simulations described in the literature (59, 60, 61) are:

- Simulation of a system of hard spheres, by Alder and Wainwright (1957);
- Simulation of radiation damage events in a model of crystalline cooper, by Vineyard (1960);
- First simulation of a liquid system (liquid Argon), using a Lennard-Jones inter-particle interaction potential, by Rahman (1964).

An important observation should be made: the MD method can be applied, in principle, for both equilibrium systems (where there is conservation of total energy and number of particles, for instance) and for systems out of equilibrium. The reader is refereed to the following literature (62, 63, 64, 65) for a deep reading regarding MD methods for systems out of equilibrium. In this thesis, however, we shall restrict ourselves to equilibrium systems.

[2] As examples, there is the Verlet algorithm, the leapfrog (a variation of the original Verlet algorithm), and the Runge-Kutta-Gill.

2.2.1 Description of the MD method

The starting point of the MD method is to define a set of initial positions and velocities to all the particles in the system. The most common used geometries in 3D are FCC (face-centered cubic) and cubic. In 2D, the preferred initial geometry are square or triangular (hexagonal) lattices. It is also possible to distribute the particles in the simulation box assigning random initial coordinates. However, care should be taken in order to avoid particle overlap[3]. The crystalline arrangements (*e.g.* square or triangular lattices) are most used, in general, due to its simplicity.

In general, the initial velocities for the particles are drawn from either an uniform distribution or a Maxwell–Boltzmann (66) distribution. For instance, if one desires to simulate a system on the micro-canonical ensemble *NVE* (where the total energy E of the system, the total number of particles N, and the volume V of the simulation box are conserved), the distribution of velocities can be drawn following the equipartition theorem[4]:

$$K = \frac{1}{2}\sum_{i=1}^{N} m_i v_i^2 = \frac{3}{2} N k_B T, \tag{2.1}$$

where K is the total kinetic energy, N is the total number of particles in the system, k_B is the Boltzmann constant, T is the absolute temperature of the system, and m_i and v_i are the mass and velocity of the ith particle, respectively. The total linear momentum of the system should be zero, *i.e.*, there should not be external forces acting on the center of mass of the system. Therefore, the initial velocities should be re-scaled in order for the center of mass of the system to remain at rest (67).

Given that all the particles' positions and velocities are known, the following step in the MD method is to obtain the subsequent positions and velocities of all particles. This is done by integrating the coupled equations of motion for each particle, under conditions established by the inter-particle interaction potential defined in the model system.

The choice of the inter-particle interaction potential between particles is a very important step in order to correctly describe the physical system under consideration. In general, an effective pairwise potential[5] is chosen, which considers only interactions between pairs of particles i and j separated by a distance $r_{ij} = |r_i - r_j|$, at each simulation step. Some very known inter-particle interaction potential are, for instance, the hard-sphere potential, the soft Lennard–Jones potential and others much more complex potentials, *e.g.*, the ones used to model interactions between ions and molecules (longitudinal and angular bending, and torsion potentials).

[3] If two particles overlap and the distance between them is very small compared to the length scale of the problem, this could generate an infinite force between a pair of particles, leading to numerical instabilities in the integration algorithm.

[4] See, for instance, F. Bloch, "Fundamentals of Statistical Mechanics" ICP (1989).

[5] The term effective means that this potential incorporates, on average, the interaction of all other particles of the system. Generally speaking, the total potential energy of a set of N particles is of the form $U(r) = \sum_{i<j}^{N} V(\boldsymbol{r}_{ij}) + \sum_{i<j<k}^{N} V(\boldsymbol{r}_{ijk}) + \sum_{i<j<k<l}^{N} V(\boldsymbol{r}_{ijkl}) + \ldots$

The resulting force $\boldsymbol{F}_i$ acting on the ith particle, due to all the other particles in the system, is then obtained by taking the gradient of the inter-particle interaction potential V_{ij}

$$\boldsymbol{F}_i = -\sum_{j \neq i} \boldsymbol{\nabla}_i V_{ij}. \tag{2.2}$$

If we apply Newton's second law for the ith particle, we obtain

$$m_i \frac{d^2 \boldsymbol{r}_i}{dt^2} = \boldsymbol{F}_i + \boldsymbol{F}_i^{\text{ext}}, \tag{2.3}$$

where $\boldsymbol{F}_i^{\text{ext}}$ represents any external forces acting on particle i due to, for instance, a confinement potential, an external electric or magnetic field, etc. Therefore, the main objective of the MD method is to numerically solve the $N-1$ coupled equations of the form (2.3), in order to obtain the new positions $\boldsymbol{r}_i(t)$ of each particle, for any instant t. For this purpose, we can use some computer algorithms for the numerical integration of these equations. We will show a few of these algorithms in the next section.

2.2.2 Numerical integration algorithms

The numerical integration algorithms used to obtain the solutions of the equations of movement are based on the finite-difference method (FDM)[6]. This method consists in expanding the particles' coordinates in a Taylor series around a given point. In these methods, there are two different types of errors introduced by the discretization of the equations of motion: (i) truncation errors and (ii) round-off errors. The first one is related to the precision at which the method of finite differences approaches the real solution for the differential equation to be solved numerically. The round-off errors encompasses all the other errors which comes from the implementation of the method. For instance, the calculation of exponential functions and square roots can introduce this type of error. Another example is the storage of real numbers (*floating point numbers*) in the computer memory.

In the following, we present two integration methods commonly used in MD simulations: the Verlet algorithm and one of its variation, called the *leapfrog* method. We emphasize, however, that there is a plethora of other much more sophisticated integration methods, *e.g.*, the predictor-corrector and the fourth-order Runge-Kutta algorithm[7].

2.2.2.1 The Verlet algorithm

One of the most common numerical integration schemes for solving differential equations (*e.g.*, Newton's equation of motion) was first introduced in computer simulations by the French physi-

[6] One of the most common method is the Euler's method, which is a first-order method where the expansion is such that, given a function $f(x)$, then we should be able to expand it around the point Δx: $f(x+\Delta x) = f(x) + f'(x)\Delta x$, where $f'(x)$ corresponds to the first derivative of the function $f(x)$ in respect to x.

[7] See, for instance, J. M. Haile, "Molecular Dynamics Simulation – Elementary Methods", Wiley-Interscience (1997).

cist Loup Verlet, in 1967 (68). This method consists in expanding the particle coordinate, during a finite time step Δt, in a Taylor series such as

$$\boldsymbol{r}(t+\Delta t) = \boldsymbol{r}(t)+\dot{\boldsymbol{r}}(t)\Delta t+\frac{1}{2}\ddot{\boldsymbol{r}}(t)\Delta t^2+\mathscr{O}(\Delta t^3) \tag{2.4}$$

$$\boldsymbol{r}(t-\Delta t) = \boldsymbol{r}(t)-\dot{\boldsymbol{r}}(t)\Delta t+\frac{1}{2}\ddot{\boldsymbol{r}}(t)\Delta t^2-\mathscr{O}(\Delta t^3). \tag{2.5}$$

By summing Eqs. (2.4) and (2.5), we obtain one estimate for the position of the particle at time $t+\Delta t$

$$\boldsymbol{r}(t+\Delta t) = 2\boldsymbol{r}(t)-\boldsymbol{r}(t-\Delta t)+\ddot{\boldsymbol{r}}(t)\Delta t^2+\mathscr{O}(\Delta t^4). \tag{2.6}$$

The local truncation error in the position is of the order $\mathscr{O}(\Delta t^4)$. Note that the velocity of the particle is not needed in order to obtain the estimate for the position (i.e, to obtain the trajectory of the particle). However, the velocity can be obtained (in order to calculate, for instance, the kinetic energy of the system) by subtracting Eqs. (2.4) and (2.5), which gives

$$\dot{\boldsymbol{r}}(t) \approx \frac{\boldsymbol{r}(t+\Delta t)-\boldsymbol{r}(t-\Delta t)}{2\Delta t}. \tag{2.7}$$

An important consideration is in order. According to Eqs. (2.4) and (2.5), one can see that the Verlet algorithm is appropriately centralized, *i.e.*, $\boldsymbol{r}(t+\Delta t)$ and $\boldsymbol{r}(t-\Delta t)$ are symmetric in time, which makes the algorithm time reversible. Finally, the algorithm is a two-step method, since it estimate the future position $\boldsymbol{r}(t+\Delta t)$ from the actual position $\boldsymbol{r}(t)$ and the previous position $\boldsymbol{r}(t-\Delta t)$. The main characteristics of the method are (i) simplicity of computational implementation and (ii) numerical stability for relatively large time steps. The latter property leads to good conservation of total energy in dynamical systems (67).

2.2.2.2 The *leapfrog* algorithm

The main idea behind the *leapfrog* method is that it is possible to write Eq. (2.4) as

$$\boldsymbol{r}(t+\Delta t) \approx \boldsymbol{r}(t)+\Delta t\left[\dot{\boldsymbol{r}}(t)+\frac{1}{2}\Delta t\ddot{\boldsymbol{r}}(t)\right]. \tag{2.8}$$

Further inspection of Eq. (2.8) leads to the following formula $\dot{\boldsymbol{r}}(t+\frac{1}{2}\Delta t) \approx \dot{\boldsymbol{r}}(t)+\frac{1}{2}\Delta t\ddot{\boldsymbol{r}}(t)$. Similarly, we can also write $\dot{\boldsymbol{r}}(t-\frac{1}{2}\Delta t) \approx \dot{\boldsymbol{r}}(t)-\frac{1}{2}\Delta t\ddot{\boldsymbol{r}}(t)$. By replacing the first formula into Eq. (2.4) and by subtracting both these previous expressions, we obtain the formulas to update the position and the velocity, respectively

$$\boldsymbol{r}(t+\Delta t) \approx \boldsymbol{r}(t)+\dot{\boldsymbol{r}}\left(t+\frac{1}{2}\Delta t\right)\Delta t \tag{2.9}$$

$$\dot{\boldsymbol{r}}\left(t+\frac{1}{2}\Delta t\right) \approx \dot{\boldsymbol{r}}\left(t-\frac{1}{2}\Delta t\right)+\ddot{\boldsymbol{r}}(t)\Delta t, \tag{2.10}$$

which form the *leapfrog* algorithm.

2.2.3 Periodic boundary conditions (PBC)

Usually the MD method is applied to physical systems where the size of the computational unit cell is of the order of hundreds up to thousands particles. Although recently there has been a huge increase in computational power, specially with the use of GPU (Graphical processing units) (69), the MD simulations of many-body systems (*e.g.*, liquids, atomic systems, proteins, etc) are still quite computationally expensive. Systems where the number N of particles ranges from $N = 10^1$ to $N = 10^5$ are dominated by the so-called surface effects (or border effects) (66). In MD simulations where there is no interest in these kind of effects, they can be minimized by using periodic boundary conditions (PBC) (70). The use of PBC is then equivalent to considering a infinite set of identical copies of the main computational unit cell. Fig. 10 shows clearly the concept of PBC. For instance, if a particle in the computational unit cell leaves this region, it re-appears on the opposite side of the simulation box, with the same velocity.

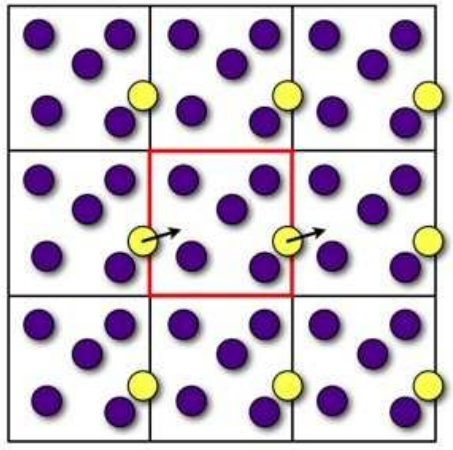

Figure 10 – Pictorial representation of periodic boundary conditions (PBC) for a 2D system. In the center, there is the main computational unit cell, and the identical copies around it. From Ref. (71)

Consider a computational unit cell (simulation box) of size L, where the center of the coordinate axis is situated in the center of the box, and identical copies (images) distributed periodically around the simulation region. Given that $\boldsymbol{r}_i$ is the position of the ith particle, there will be a set of image particles, whose positions are given by $\boldsymbol{r}_i + n\boldsymbol{L}$, where $n = ..., -3, -2, -1, 0, 1, 2, 3, ...$ and $n\boldsymbol{L}$ is a vector which connects the ith particle with its nth image particle. The potential energy of the system (taking into account all the image particles) is given by

$$U(\boldsymbol{r}_i, ..., \boldsymbol{r}_N) = \sum_{i<j} V(\boldsymbol{r}_{ij}) + \sum_{n} \sum_{i<j} V(|\boldsymbol{r}_i - \boldsymbol{r}_j + n\boldsymbol{L}|). \tag{2.11}$$

In order to avoid the numerical calculation of the infinite summation in Eq. (2.11), one should use the concept of the minimal image convention, which states that a particle is not allowed to interact simultaneously with another particle and its image particle. By using this convention,

a particle is able to interact only with particles which are separated by a distance smaller than or equal to $L/2$. However, the use of the minimal image convention is only valid if the inter-particle interaction potential is short-ranged[8]. Therefore, the value of L should be chosen in such a way that the interaction forces between particles are negligible at distances larger than $L/2$. This eliminates finite size effects (67). In the case where the inter-particle interaction potential is long-ranged, there will be a considerable increase in the total potential energy of the system, due to the interaction between particles in the computational unit cell and their image particles. In order to deal with these undesired non-physical effects, there is a common method known as the Ewald summation technique (72). In this thesis, however, we only deal with short-range potentials.

2.2.4 Calculation of physical properties

A typical MD simulation run consists of the following basic steps:

- Initialization of the system, *i.e.*, assign initial coordinates and initial velocities for all the particles in the system);
- Calculation of the interaction force between pairs of particles. This is the most time-consuming part of any MD simulation, since the computational cost to calculate the distances $r_{ij} = |\boldsymbol{r}_i - \boldsymbol{r}_j|$ is of order $\mathcal{O}(N^2)$;
- Use the numerical integration scheme chosen previously, for instance, either the Verlet or the *leapfrog* algorithm;
- Apply the periodic boundary conditions, if necessary.

These are all done in one single time-step. If m is the total number of time-steps in the simulation, then $T_{\text{tot}} = m\Delta t$ is the total time of the simulation run, and Δt is the discrete time interval between time-steps. After a given number of simulation steps, the system should, in principle, attain an equilibrium state. In order to check that the system has indeed reached an equilibrium situation, one could, for instance, calculate the total energy of the system (total potential energy per particle plus the total kinetic energy per particle) over time and check if it has reached a stationary value, *i.e.*, constant over time. The number of time-steps in order for the system to reach this equilibrium situation depends on each problem specifically, therefore a careful analysis should be done for each particular case. The time interval between the beginning of the simulation and the equilibrium state is usually called the thermalization procedure. Only after

[8] An inter-particle interaction potential is considered short-ranged if the interaction between particles decays faster than r^{-d}, where r is the center-to-center distance between a pair of particles and d is the dimension of the system (66).

the thermalization procedure one should calculate physical properties of interest, either structural properties (*e.g.*, radial distribution function (RDF)) or dynamical properties (*e.g.*, mean square displacement (MSD) and velocity autocorrelation function (VACF)).

2.2.4.1 Radial distribution function (RDF)

The radial distribution function $g(r)$ (RDF), sometimes also referred as the pair distribution function, is a measure of how the particles organizes themselves around other particles (73). Specifically, the function $g(r)$ is proportional to the ratio of the probability of finding two particles separated by a distance $r \pm \Delta r$ and the probability for a completely random distribution of particles at the same density (66). From the point of view of statistical mechanics, where usually the number of degrees of freedom is large, the function represents an important physical measure to characterize structural properties of molecular systems, *e.g.*, liquids, glasses and super-cooled liquids, etc. The MD method, as seen previously, calculates individual particles' positions. This allows the function $g(r)$ to be calculated as[9]

$$\rho g(r) = \frac{1}{N} \left\langle \sum_{i}^{N} \sum_{j \neq i}^{N} \delta(r - r_{ij}) \right\rangle, \tag{2.12}$$

where N is the total number of particles, $\rho = N/V$ is the density of particles, r_{ij} is the distance between a pair of particles i and j, and $\langle ... \rangle$ represents an average over several realizations. It is important to note that the distance r_{ij} is invariant under a change of index, *i.e.*, $r_{ij} = r_{ji}$. This property reduces the number of terms in the previous equation to $\frac{1}{2}N(N-1)$ and we can write Eq. (2.12) as

$$\rho g(r) = \frac{2}{N} \left\langle \sum_{i}^{N} \sum_{j < i}^{N} \delta(r - r_{ij}) \right\rangle. \tag{2.13}$$

By integrating both members of Eq. (2.13) over all the possible range of separation between particles and considering that the density ρ is constant, we get

$$\rho \int g(r) d\boldsymbol{r} = \frac{2}{N} \left\langle \sum_{i}^{N} \sum_{j < i}^{N} \int \delta(r - r_{ij}) d\boldsymbol{r} \right\rangle, \tag{2.14}$$

and by the fundamental property of the delta function, $\int \delta(r - r_{ij}) d\boldsymbol{r} = 1$,

$$\rho \int g(r) d\boldsymbol{r} = N - 1. \tag{2.15}$$

This was an expected result and can interpreted as follows. Suppose that we choose a given particle of the system as the origin and by counting the number of remaining particles, the result is $N - 1$ particles.

[9] For uniform systems, the arrangement of particles depends only on the distance r between particles' centers, *i.e.*, it is independent of the orientation of the vector $\boldsymbol{r}$.

Computationally, one can calculate $g(r)$ from Eq. (2.13) by making a histogram to count the number of particles, in a given shell of radius Δr, which are at a distance r from the origin (reference) particle. For a 3D system, consider h_n the number of pairs of atoms (i, j) with the condition $(n-1)\Delta r \leq r_{ij} < n\Delta r$. By counting the pair of atoms in the shell Δr, one would get (67)

$$g(r_n) = \frac{h_n}{2\pi N \rho r_n^2 \Delta r}, \tag{2.16}$$

where $r_n = \left(n - \frac{1}{2}\right)\Delta r$ and n is the index of the each bin of the histogram. If the total extent of the calculation for $g(r)$ is $r_{\max}$, then the total number of bins should be chosen as $N_b = r_{\max}/\Delta r$.

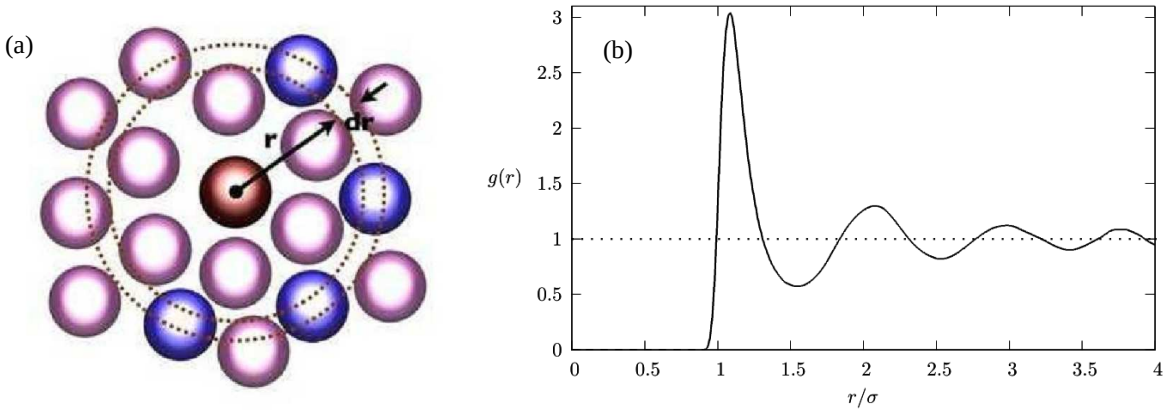

Figure 11 – (a) In the center there is the reference particle (dark circle). The circles around it represents other particles in the system. A centered ring is drawn as reference and it has radius r and width dr. (b) As an example, we show the typical radial distribution function for a Lennard–Jones system in the liquid phase. Taken from Ref. (74).

Furthermore, Eq. (2.12) is useful in the probabilistic interpretation of the radial distribution function. The probability $P(r, dr)$ that a particle is in the region of a spherical shell of radius r and width dr while the spherical shell is centered in the reference particle (cf. Fig. 11) is given by

$$P(r, dr) \equiv \left(\frac{\rho}{N-1}\right) g(r) dr. \tag{2.17}$$

As a final and brief comment, the function $g(r)$ is also commonly used as an auxiliary function to calculate thermodynamic macroscopic properties. For instance, pressure (p), energy (E) and isothermal compressibility ($\kappa_T = (\partial\rho/\partial p)_T$) are related to $g(r)$ by (73)

$$p = \rho k_B T - \frac{2\pi}{3}\rho^2 \int_V r^3 u'(r) g(r, \rho, T) d^3 r, \tag{2.18}$$

$$E = \frac{3}{2} N k_B T + \frac{\rho N}{2} \int_V (4\pi r^2) u(r) g(r, \rho, T) d^3 r, \tag{2.19}$$

$$k_B T \left(\frac{\partial \rho}{\partial p}\right)_T = 1 + \rho \int_V [g(r) - 1] d^3 r, \tag{2.20}$$

where $u(r)$ is the inter-particle interaction potential, k_B is the Boltzmann constant and T is the absolute temperature.

2.2.5 Relation between MD and statistical mechanics

One of the reasons why the method of MD is justified is due to the ergodic principle of statistical mechanics (75), which states that an ensemble average of a given physical quantity is equivalent to a temporal average of the same quantity on the long-time limit (*i.e.*, the limit where $t \to \infty$). In statistical mechanics, one is mainly interested in systems where the number of degrees of freedom is large. For instance, in the canonical ensemble (NVT), where there is conservation of the number of particles, volume and temperature, the ensemble average (in equilibrium) of a physical quantity A can be expressed in terms of phase space integrals taking into account the total potential energy of the system, $U = U(\boldsymbol{r}^N)$, as

$$\langle A \rangle = \frac{\int A(\boldsymbol{r}^N) e^{-\beta U(\boldsymbol{r}^N)} d\boldsymbol{r}^N}{\int e^{-\beta U(\boldsymbol{r}^N)} d\boldsymbol{r}^N}, \tag{2.21}$$

where $\{\boldsymbol{r}^N\}$ is the set of coordinates, $Z = \int e^{-\beta U(\boldsymbol{r}^N)} d\boldsymbol{r}^N$ is the configurational partition function, $\beta = 1/k_B T$ and k_B is the Boltzmann constant. This average corresponds to a series of measurements over an ensemble of independent systems. Therefore, the MD method is based on the assumption that the ergodic principle holds, and then the time that a particle spends in a given region of the phase space is proportional to the volume of this region. In other words, the ergodic principle states that all the accessible microstates are equally likely for the limit $t \to \infty$ (76). Consequently, the temporal average A_m obtained in a MD run should be, in principle, the same as the ensemble average, *i.e.*,

$$A_m = \frac{1}{M} \sum_{i=1}^{M} A_i(\boldsymbol{r}^N) = \langle A \rangle, \tag{2.22}$$

where M is the total number of measurements (independent runs). The usual statistical ensemble used in MD simulations is the microcanonical (NVE), where the number of particles, volume and total energy are the conserved quantities. The system visits the whole phase space in a trajectory where the total energy is constant (*i.e.* there is no heat exchange between the system and its surroundings). However, it is possible to adapt the MD method for different ensembles. For instance, for MD simulations in the canonical ensemble (NVT), one could use the Nosé-Hoover thermostat (77, 78), the Berendsen thermostat (79) or the Langevin Dynamics (LD) simulations, which will be described in details in the next section.

2.3 Langevin Dynamics (LD)

In the previous section we briefly described the MD method, which consists in finding the trajectory of individual particles of a system of N particles by numerical integration of Newton's

equations of motion [cf. Eq. (2.3)]. The usual choice for the MD method is the microcanonical ensemble, where the system is not allowed to exchange heat with its surroundings. One way of introducing thermal fluctuations is to use the method called Langevin Dynamics simulations. In this case, Eq. (2.3) is replaced by the Langevin equation (Sec. 1.5.2), given by

$$m\frac{d\boldsymbol{v}_i}{dt} = -m\eta\boldsymbol{v}_i + \boldsymbol{F}_i + \boldsymbol{F}_i^{\text{ext}} + \boldsymbol{F}_i^T(t), \tag{2.23}$$

where $\boldsymbol{v}_i$ is the velocity of the ith particle, η is the damping constant (related to the dissipation of energy in the system), $\boldsymbol{F}_i$ is the interaction force between particles [cf. Eq. (2.2)], $\boldsymbol{F}_i^{\text{ext}}$ is any external forces acting on the system (*e.g.* confinement forces, electric and/or magnetic fields, etc) and $\boldsymbol{F}_i^T(t)$ is a stochastic force which depends on the absolute temperature T and represents the coupling of the system with a heat bath.

The Langevin equation is a stochastic differential equation where the term proportional to the velocity ($-m\eta\boldsymbol{v}_i$) removes energy from the system while the stochastic force ($\boldsymbol{F}_i^T(t)$) introduces energy into the system in the form of thermal fluctuations. Since the whole system (*i.e.* system of particles + heat bath) should also conserve the total energy, there must be a relation between the dissipation (η) and the coupling with the heat bath (T). This relation is known as the Fluctuation–Dissipation theorem (FDT). The stochastic term $\boldsymbol{F}_i^T(t)$ is called a Wiener process if it obeys the following conditions

$$\langle F_i^T(t)\rangle = 0, \tag{2.24}$$

$$\langle F_{ia}^T(t)F_{jb}^T(t')\rangle = 2m\eta k_B T\delta_{ij}\delta_{ab}\delta(t-t'), \tag{2.25}$$

where (a,b) represents spatial coordinates (*e.g.* x,y,z), δ is the Kronecker delta and $\delta(t-t')$ is the Dirac delta function. Note that such a choice for the stochastic term is basically due to its simplicity. Also, in many real systems (*i.e.* experiments with colloidal particles and soft matter systems in general) it is reasonable to assume a Wiener process (also known as "white noise") to describe the dynamics of the particles embedded in a heat bath. The delta function $\delta(t-t')$ characterizes what is called a process without memory (Markovian process). Therefore, the thermal fluctuations introduced by the stochastic term in the form of Eqs. (2.24)–(2.25) are uncorrelated in time and space.

2.3.1 Brownian Dynamics (BD)

The Brownian Dynamics (BD) method consists in disregarding the inertial term in the equation of motion (2.23), *i.e.*,

$$m\frac{d\boldsymbol{v}_i}{dt} \approx 0. \tag{2.26}$$

This limit is only valid when the particle (usually called the Brownian particle) is suspended in a viscous fluid where the effects of the damping are more relevant than the inertial effects. For instance, if the particle's radius is sufficiently large compared to the size of the molecules of the

fluid (whose effects are implicitly introduced through the stochastic force), then its superficial area will be larger. As a consequence, the damping will have a more relevant effect on the dynamics of the suspended particle. This effect makes the distribution of velocities of the suspended particles reach an equilibrium situation much faster than the change in their positions. Therefore, the velocities of the Brownian particles will have an approximately constant value during this characteristic time interval, which allows one to use the approximation (2.26). This regime is also usually called the over-damped limit.

The BD method is then based on the large difference between the relaxation time scales for the velocities (τ_v) and the relaxation time scales for the positions (τ_s). For instance, for a colloidal particle of diameter 100 nm, one could estimate (80) that $\tau_v \approx 2.2 \times 10^{-9}$ s, while $\tau_s \approx 4.7 \times 10^{-3}$ s. Clearly, $\tau_v \ll \tau_s$, which indicates the large separation between time scales; the velocities of the Brownian particles have relaxed much faster than any significant changes in their positions.

Using the approximation (2.26), Eq. (2.23) can be written as

$$\zeta \frac{d\boldsymbol{r}_i}{dt} = \boldsymbol{F}_i + \boldsymbol{F}_i^{\text{ext}} + \boldsymbol{F}_i^T(t), \tag{2.27}$$

where $\zeta = m\eta$ and $\frac{d\boldsymbol{r}_i}{dt} = \boldsymbol{v}_i$. Note that Eq. (2.27) is valid only for time scales much larger than τ_v. The BD approximation is valid in several real physical systems, specifically in mesoscopic systems where the particles have a diameter of the order of 10 nm up to 10 μm, *i.e.*, the particles are much larger than the particles of the fluid, whose diameters are of the order of a few angstroms. Therefore, the BD method has been widely used for the study of mesoscopic systems, such as suspensions of colloidal particles, proteins in biological systems, and vortex matter in type-II superconductors, just to cite a few examples.

As in the case of the MD method, both the LD and BD methods consists of numerical integration of the equations of motion (2.23) or (2.27). Generally, the algorithms for integration are similar to the ones used in the MD method (*i.e.*, the Verlet or the leapfrog algorithms showed in previous sections) with some modifications in order to take into account the stochastic term. In the following, we will show an Euler-type method based on Refs. (81, 82), and using the Box-Müller (83) technique to generate the stochastic (thermal) forces.

2.3.2 Numerical integration of stochastic differential equations

There are several methods to numerically integrate stochastic differential equations, such as Eqs. (2.23) or (2.27). Here we present one of the simplest algorithm, which is known as the Ermak algorithm (84). It is a first-order method and is similar to the Euler method. We restrict ourselves to the exposure of this method in particular since it is the one we used in the following chapters (Results).

We start by a direct integration of Eq. (2.27) during a finite time interval Δt. This leads to

$$\zeta \int_0^{\Delta t} \frac{d\boldsymbol{r}_i}{dt} dt = \int_0^{\Delta t} \boldsymbol{F}_i dt + \int_0^{\Delta t} \boldsymbol{F}_i^{\text{ext}} dt + \int_0^{\Delta t} \boldsymbol{F}_i^T(t) dt, \tag{2.28}$$

$$\zeta [\boldsymbol{r}_i(\Delta t) - \boldsymbol{r}_i(0)] \approx \Delta t [\boldsymbol{F}_i + \boldsymbol{F}_i^{\text{ext}}] + \int_0^{\Delta t} \boldsymbol{F}_i^T(t) dt, \tag{2.29}$$

$$\boldsymbol{r}_i(\Delta t) \approx \boldsymbol{r}_i(0) + \frac{\Delta t}{\zeta} \left[\boldsymbol{F}_i + \boldsymbol{F}_i^{\text{ext}} \right] + \frac{1}{\zeta} \int_0^{\Delta t} \boldsymbol{F}_i^T(t) dt. \tag{2.30}$$

Note that we assume that the forces $\boldsymbol{F}_i$ and $\boldsymbol{F}_i^{\text{ext}}$ are constant over the time interval Δt. This is a reasonable consideration given that the time interval Δt is sufficiently small. Furthermore, assuming that the stochastic force $\boldsymbol{F}_i^T(t)$ follows properties (2.24)–(2.25), the integral in the r.h.s. of Eq. (2.30) can be replaced by the term $\sqrt{2\zeta k_B T \Delta t}\boldsymbol{R}$ [for details, see Refs. (81, 82)], where $\boldsymbol{R}$ is a dimensionless stationary Gaussian process with zero mean and unit variance (80). Therefore, Eq. (2.30) can be written as

$$\boldsymbol{r}_i(\Delta t) \approx \boldsymbol{r}_i(0) + \frac{\Delta t}{\zeta} \left[\boldsymbol{F}_i + \boldsymbol{F}_i^{\text{ext}} \right] + \sqrt{\frac{2k_B T \Delta t}{\zeta}} \boldsymbol{R}, \tag{2.31}$$

which is known as the Ermak formula to update the position of the particles.

For the Langevin equation (2.23), we may proceed in a similar fashion and obtain the formula to update the position of the particles. The difference now is that the equation of motion has to be integrated for the velocity and then the position of the particles are updated.

We integrate Eq. (2.23) directly during a finite time interval Δt, which gives

$$\boldsymbol{v}_i(\Delta t) = \boldsymbol{v}_i(0) - \eta \int_0^{\Delta t} \boldsymbol{v}_i(t) dt + \frac{1}{m} \int_0^{\Delta t} (\boldsymbol{F}_i + \boldsymbol{F}_i^{\text{ext}}) dt + \frac{1}{m} \int_0^{\Delta t} \boldsymbol{F}_i^T(t) dt, \tag{2.32}$$

$$\boldsymbol{v}_i(\Delta t) \approx \boldsymbol{v}_i(0) - \eta \boldsymbol{v}_i(0) \Delta t + \frac{\Delta t}{m} \left[\boldsymbol{F}_i + \boldsymbol{F}_i^{\text{ext}} \right] + \sqrt{\frac{2\eta k_B T \Delta t}{m}} \boldsymbol{R}. \tag{2.33}$$

Finally, the position of the particles are updated according to

$$\boldsymbol{r}_i(\Delta t) = \boldsymbol{r}_i(0) + \boldsymbol{v}_i(0) \Delta t. \tag{2.34}$$

Part III

Results

3 Single-file to two-dimensional diffusion

Diffusive properties of a mono-disperse system of interacting particles confined to a *quasi*-one-dimensional (q1D) channel are studied using Molecular Dynamics (MD) simulations. We calculate numerically the mean square displacement (MSD) and investigate the influence of the width of the channel (or the strength of the confinement potential) on diffusion in finite-size channels of different shapes (*i.e.*, straight and circular). The transition from single-file diffusion (SFD) to the two dimensional diffusion regime is investigated. This transition (regarding the calculation of the scaling exponent (α) of the MSD $\langle \Delta x^2(t) \rangle \propto t^{\alpha}$) as a function of the width of the channel, is shown to change depending on the channel's confinement profile. In particular the transition can be either smooth (*i.e.*, for a parabolic confinement potential) or rather sharp/stepwise (*i.e.*, for a hard-wall potential), as distinct from infinite channels where this transition is abrupt. This result can be explained by qualitatively different distributions of the particle density for the different confinement potentials.

3.1 Introduction

There is a considerable theoretical and practical interest in the dynamics of systems of interacting particles in confined geometries (85). Single-file diffusion (SFD) refers to a one-dimensional (1D) process where the motion of particles in a narrow channel (*e.g.*, *quasi*-1D systems) is limited such that particles are not able to cross each other. As a consequence, the system exhibits spatial correlations which results in anomalous diffusion. The mechanism of SFD was first proposed by Hodgkin and Keynes (39) in order to study the passage of molecules through narrow pores. Since the order of the particles is conserved over time, this results in unusual dynamics of the system (86, 87), different from what is predicted from diffusion governed by Fick's law. The main characteristic of the SFD phenomena is that, in the long-time limit ($t \gg t_c$, where t_c is a characteristic relaxation time scale which depends on the specificities of the system), the MSD (mean square displacement, defined as $W_x(t) \equiv \langle \Delta x^2(t) \rangle = \langle \sum_{i=1}^{N} (1/N)[x_i(t) - x_i(0)]^2 \rangle$) scales with time as

$$\lim_{t \gg t_c} W_x(t) \propto t^{0.5}. \tag{3.1}$$

This relation was first obtained analytically in the pioneering work of Harris (40). Recent advances in nanotechnology have stimulated a growing interest in SFD, in particular, in the study of transport in nanopores (88, 89). Ion channels of biological membranes and carbon nanotubes (90) are examples of such nanopores. The macroscopic flux of particles through such nanopores is of great importance for many practical applications, *e.g.*, particle transport

across membranes is a crucial intermediate step in almost all biological and chemical engineering processes. SFD was observed in experiments on diffusion of molecules in zeolite molecular sieves (91). Zeolites with unconnected parallel channels may serve as a good realization of the theoretically investigated one-dimensional systems. SFD is also related to growth phenomena (92).

The theoretical background of SFD was developed in early studies on transport phenomena in 1D channels (42, 43, 44). It is also interesting to learn how the size of the system will influence the diffusive properties of the system. SFD in finite size systems has been the focus of increasing attention since there are few exact theoretical results to date (56, 93, 94), which showed the existence of different regimes of diffusion.

Colloidal systems, complex plasmas and vortex matter in type-II superconductors are examples of systems where SFD may occur. The use of colloidal particles is technically interesting since it allows real time and spatial direct observation of their position, which is a great advantage as compared to atoms or molecules, as shown recently in, *e.g.*, the experimental study of defect induced melting (95). One typically uses micro-meter size colloidal particles in narrow channels, as shown in (41, 96). The paramagnetic colloidal spheres of 3.6 μm were confined in circular trenches fabricated by photolithography and their trajectories were followed over long periods of time. Several other studies have focused on the diffusive properties of complex plasmas. A complex plasma consists of micrometer-sized ("dust") particles immersed in a gaseous plasma background. Dust particles typically acquire a negative charge of several thousand elementary charges, and thus they interact with each other through their strong electrostatic repulsion (97).

Systems of particles moving in space of reduced dimensionality or submitted to an external confinement potential exhibit different behavior from their free-of-border counterparts (98). The combined effect of interaction between the particles and the confinement potential plays a crucial role in their physical and chemical properties (99). In Ref. (100), it was found that SFD depends on the inter-particle interaction and can even be suppressed if the interaction is sufficiently strong, resulting in a slower sub-diffusive behavior, where $\langle \Delta x^2(t) \rangle \propto t^{\alpha}$, with $\alpha < 0.5$.

In this chapter we will investigate the effects of confinement potential on the diffusive properties of a Q1D system of interacting particles. In the limiting case of very narrow (wide) channels, particle diffusion can be referred to SFD (2D regime) characterized by a sub-diffusive (normal diffusive) long-time regime where the mean square displacement (MSD) $\langle \Delta x^2(t) \rangle \propto t^{0.5}$ ($\propto t^{1.0}$). Recall that the MSD of a tagged hard-sphere particle in a one dimensional infinite system is characterized by two limiting diffusion behaviors: for time scales shorter than a certain crossover time $\tau_c = 1/D\rho^2$, where D is the diffusion coefficient and ρ is the particle concentration, $\langle \Delta x^2(t) \rangle \propto t^{1.0}$ which is referred to as the normal diffusion regime (101). For times larger than τ_c, the system exhibits a sub-diffusive behavior, with the MSD $\langle \Delta x^2(t) \rangle \propto t^{0.5}$, which char-

acterizes the single-file diffusion regime. Between these two regimes, there is a transient regime exhibiting a non-trivial functional form.

However, in case of a *finite* system of diffusing particles (*e.g.*, a circular chain or a straight chain in the presence of periodic boundary conditions), the SFD regime (*i.e.*, with $\langle \Delta x^2(t) \rangle \propto t^{0.5}$) does not hold for $t \to \infty$, unlike in an infinite system. Instead, for sufficiently long times, the SFD regime turns to the regime of *collective* diffusion, *i.e.*, when the whole system diffuses as a single "particle" with a renormalized mass. This diffusive behavior has been revealed in experiments (41, 102) and theoretical studies (103, 104, 45, 105). This collective diffusion regime is similar to the initial short-time diffusion regime and it is characterized by either $\langle \Delta x^2(t) \rangle \propto t^{1.0}$, for over-damped particles [see, *e.g.*, (41, 100, 103)] or by $\langle \Delta x^2(t) \rangle \propto t^{2.0}$ (followed by the MSD $\propto t^{1.0}$), for under-damped systems (104, 105). Correspondingly, the time interval where the SFD regime is observed becomes *finite* in finite size systems. It depends on the length of the chain of diffusing particles: the longer the chain the longer the SFD time interval. Therefore, in order to observe a clear power-law behavior (*i.e.*, $\langle \Delta x^2(t) \rangle \propto t^{\alpha}$) one should consider sufficiently large systems.

Here we focus on this intermediate diffusion regime and we show that it can be characterized by $\langle \Delta x^2(t) \rangle \propto t^{\alpha}$, where $0.5 < \alpha < 1.0$, depending on the width (or the strength of the confinement potential) of the channel. We analyze the MSD for two different channel geometries: (i) a linear channel, and (ii) a circular channel. These two systems correspond to different experimental realizations of diffusion of charged particles in narrow channels (41, 106). The latter one (*i.e.*, a circular channel) has obvious advantages: (i) it allows a long-time observation of diffusion using a relatively short circuit, and (ii) it provides constant average particle density and absence of density gradients (which occur in, *e.g.*, a linear channel due to the entry/exit of particles in/from the channel). Thus circular narrow channels were used in diffusion experiments with colloids (41) and metallic charged particles (balls) (102). Furthermore, using different systems allows us to demonstrate that the results obtained in our study are general and do not depend on the specific experimental set-up.

3.2 Model system and numerical approach

Our model system consists of N identical charged particles interacting through a repulsive pair potential $V_{int}(\boldsymbol{r}_{ij})$. In this study, we use a screened Coulomb potential (Yukawa potential), $V_{int} \propto \exp(-r/\lambda_D)/r$. In the transverse direction, the motion of the particles is restricted either by a hard-wall or by a parabolic confinement potential. Thus the total potential energy of the system can be written as

$$H = \sum_{i=1}^{N} V_c(\boldsymbol{r}_i) + \sum_{i>j=1}^{N} V_{int}(\boldsymbol{r}_{ij}). \tag{3.2}$$

The first term in the right-hand side (r.h.s.) of Eq. (3.2) represents the confinement potential, where $V_c(\boldsymbol{r}_i)$ is given by

$$V_c(\boldsymbol{r}_i) = \begin{cases} 0 & \text{for } |y_i| \leq R_w/2 \\ \infty & \text{for } |y_i| > R_w/2, \end{cases} \tag{3.3}$$

for the hard-wall confinement,

$$V_c(\boldsymbol{r}_i) = \frac{1}{2} m\omega_0^2 y_i^2, \tag{3.4}$$

for parabolic one-dimensional potential (in the y-direction), and by

$$V_c(\boldsymbol{r}_i) = \beta (r_0 - r_i)^2, \tag{3.5}$$

for parabolic circular confinement.

Here R_w is the width of the channel (for the hard-wall potential), m is the mass of the particles, ω_0 is the strength of the parabolic 1D confining potential, r_0 is the coordinate of the minimum of the potential energy and r_i is the displacement of the ith particle from r_0 (for the parabolic circular potential). Note that in case of a circular channel, $r_0 = r_{ch}$, where r_{ch} is the radius of the channel.

The second term in the r.h.s. of Eq. (3.2) represents the interaction potential between the particles. For the screened Coulomb potential,

$$V_{int}(\boldsymbol{r}_{ij}) = \frac{q^2}{\varepsilon} \frac{e^{-|\boldsymbol{r}_i - \boldsymbol{r}_j|/\lambda_D}}{|\boldsymbol{r}_i - \boldsymbol{r}_j|}, \tag{3.6}$$

where q is the charge of each particle, ε is the dielectric constant of the medium, $r_{ij} = |\boldsymbol{r}_i - \boldsymbol{r}_j|$ is the distance between ith and jth particles, and λ_D is the Debye screening length. Substituting (3.6) into Eq. (3.2), we obtain the potential energy of the system H_Y

$$H_Y = \sum_{i=1}^{N} V_c(\boldsymbol{r}_i) + \frac{q^2}{\varepsilon} \sum_{i>j=1}^{N} \frac{e^{-|\boldsymbol{r}_i - \boldsymbol{r}_j|/\lambda_D}}{|\boldsymbol{r}_i - \boldsymbol{r}_j|}. \tag{3.7}$$

In order to reveal important parameters which characterize the system, we rewrite the energy H_Y in a dimensionless (H_Y') form by making use of the following variable transformations: $H_Y = (q^2/\varepsilon a_0) H_Y'$, $r = r' a_0$, where a_0 is the mean inter-particle distance. The energy of the system then becomes

$$H_Y' = \sum_{i=1}^{N} V_c'(\boldsymbol{r}_i') + \sum_{i>j=1}^{N} \frac{e^{-\kappa|\boldsymbol{r}_i' - \boldsymbol{r}_j'|}}{|\boldsymbol{r}_i' - \boldsymbol{r}_j'|}, \tag{3.8}$$

where $\kappa = a_0/\lambda_D$ is the screening parameter of the interaction potential. In our simulations in Sec. III, we use a typical value of $\kappa = 1.0$ for colloidal systems and $\lambda_D = 10^{-5}$ m.

The hard-wall confinement potential is written as

$$V_c'(\boldsymbol{r}_i') = \begin{cases} 0 & \text{for } |y_i'| \leq R_w'/2 \\ \infty & \text{for } |y_i'| > R_w'/2, \end{cases} \tag{3.9}$$

where $R_w^{'}$ is scaled by the inter-particle distance a_0. We also introduce a dimensionless parameter

$$\chi = \frac{m(\omega_0 a_0)^2}{2k_B T}, \tag{3.10}$$

which is a measure of the strength of the parabolic 1D confinement potential.

For colloidal particles moving in a nonmagnetic liquid, their motion is over-damped and thus the stochastic Langevin equations of motion can be reduced to those for Brownian particles (84)

$$\frac{d\boldsymbol{r}_i}{dt} = \frac{D_i}{k_B T}\Big[-\sum_{j\neq i}\boldsymbol{\nabla}_i V_{int}(\boldsymbol{r}_{ij}) - \boldsymbol{\nabla}_i V_c(\boldsymbol{r}_i) + \boldsymbol{F}_T^i(t)\Big]. \tag{3.11}$$

Note, however, that in Sec. 3.4 we will deal with massive metallic balls and therefore we will keep the inertial term in the Langevin equations of motion.

In Eq. (3.11), $\boldsymbol{r}_i$, D_i and m_i are the position, the self-diffusion coefficient (measured in m^2/s) and the mass (in kg) of the ith particle, respectively, t is the time (in seconds), k_B is the Boltzmann constant, and T is the absolute temperature of the system. Finally, $\boldsymbol{F}_T^i$ is a randomly fluctuating force, which obeys the following conditions: $\langle \boldsymbol{F}_T \rangle = 0$ and $\langle F_T^i(t) F_T^{i'}(t')\rangle = 2\zeta k_B T \delta_{ii'}\delta(t-t')$, where ζ is the viscosity of the medium. Eq. (3.11) can be written in dimensionless form as follows

$$\frac{d\boldsymbol{r}_i'}{dt'} = D_i'\Gamma\Big[-\sum_{j\neq i}\boldsymbol{\nabla}_i' V_{int}'(\boldsymbol{r}_{ij}') - \boldsymbol{\nabla}_i' V_{conf}'(\boldsymbol{r}_i') + \boldsymbol{F}_T'^i(t')\Big], \tag{3.12}$$

where we use the following transformation $V_{int} = (q^2/\varepsilon a_0)V_{int}^{'}$, $D_i' = D_i/a_0^2$, and introduced a coupling parameter Γ, which is the ratio of the average potential energy to the average kinetic energy, $\Gamma = \langle V\rangle/\langle K\rangle$, such that $\Gamma = q^2/k_B T\varepsilon a_0$. The time t' is expressed in seconds and distances are expressed in units of the inter-particle distance a_0.

In what follows, we will abandon the prime ($'$) notation. We have used a first order finite difference method (Euler method) to integrate Eq. (3.12) numerically. In the case of a straight channel, periodic boundary conditions (PBC) were applied in the x-direction while in the y-direction the system is confined either by a hard-wall or by a parabolic potential. Also, we use a timestep $\Delta t = 0.0001$ and the coupling parameter is set to $\Gamma = 10$. For a circular channel, we use polar coordinates (r,ϕ) and model a 2D narrow channel of radius r_{ch} with parabolic potential-energy profile across the channel, *i.e.*, in the r-direction.

3.3 1D versus 2D diffusion in a straight channel

3.3.1 Mean-square displacement (MSD) calculations

In order to characterize the diffusion of the system, we calculate the MSD as follows

$$\langle \Delta x^2(t) \rangle = \left\langle \frac{1}{N} \sum_{i=1}^{N} [x_i(t+\Delta t) - x_i(t)]^2 \right\rangle_{\Delta t}, \tag{3.13}$$

where N is the total number of particles and $\langle ... \rangle_{\Delta t}$ represents a time average over the time interval Δt. Note that in the general case (*e.g.*, for small circular channels with the number of particles $N = 20$ – see Sec. 3.4) the calculated MSD was averaged over time and over the number of ensembles (107, 108, 109, 110). However, we found that for large N (*i.e.*, several hundred) the calculated MSD for various ensemble realizations coincide (with a maximum deviation within the thickness of the line representing the MSD).

To keep the inter-particle distance approximately equal to unity, we defined the total number of particles N for a 1D and Q1D system as

$$N = \frac{L}{\sqrt{1 - R_w^2}} \; ; \; R_w < 1, \tag{3.14}$$

where L is the size of the simulation box (in dimensionless units) in the x-direction. In our simulations for a straight channel geometry, we typically used $N = 400 - 900$ particles. We study the system for two different types of confinement potential: (i) a parabolic 1D potential in the y-direction, which can be tuned by the confinement strength χ and (ii) a hard-wall potential, where particles are confined by two parallel walls separated by a distance R_w.

The results of calculations of the MSD as a function of time for different values of the confinement strength χ [Eq. (3.10)] and the width of the channel R_w are presented in Fig.12(a)-(c) and Fig.13(a)-(c), respectively.

Initially, in both cases (*i.e.*, a parabolic and a hard-wall confinement potential), the system exhibits a short-time normal diffusion behavior, where $\langle \Delta x^2(t) \rangle \propto t^{1.0}$. This is the typical initial "free-particle" diffusion regime. After this initial regime, there is an intermediate sub-diffusive regime (ITR). As discussed in Ref. (111), the ITR shows an apparent power-law behavior (112), where $0.5 < \alpha < 1.0$, and it was also found previously in different diffusion models (113, 114). In the ITR, we found a SFD regime for either a channel with strong parabolic confinement [$\chi = 3.5$ (Fig. 12(a))] or a narrow hard-wall channel [$R_w = 0.20$ (Fig. 13(a))]. This is due to the fact that for large (small) values of χ (R_w), the confinement prevents particles from passing each other. The results for α in the ITR are shown as a function of χ and R_w in Fig. 12(d) and Fig. 13(d), respectively. As can be seen in Fig. 12(d) [Fig. 13(d)], α increases with decreasing χ [with increasing R_w] and thus the SFD condition does not hold any longer. The values of α presented in these figures correspond to the minimum of the effective time dependent exponent $\alpha(t)$. Following Ref. (115), $\alpha(t)$ is calculated using the "double logarithmic

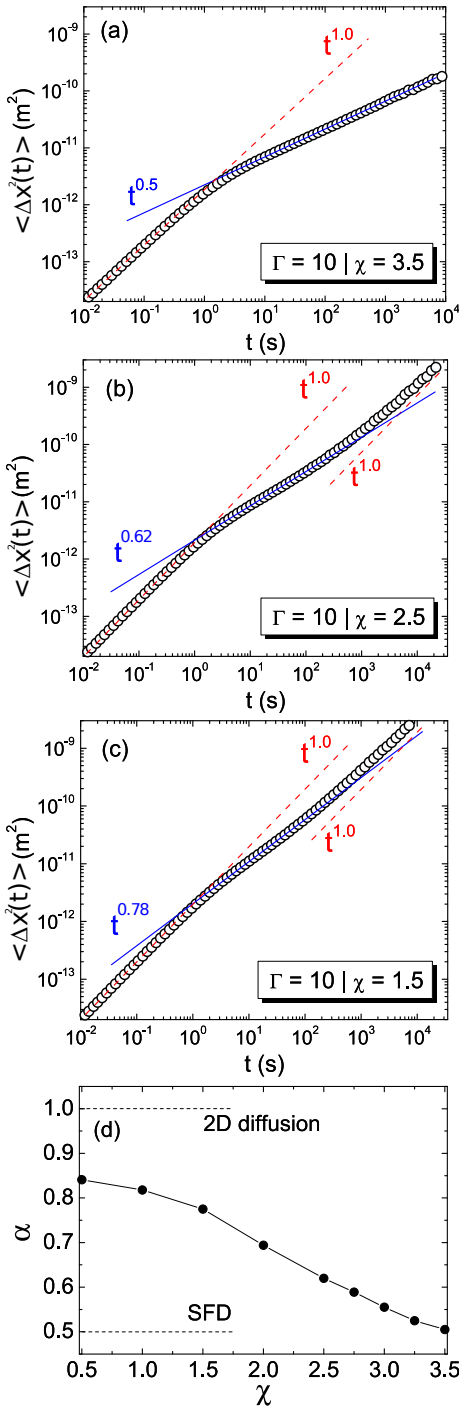

Figure 12 – (a)-(c) Log-log plot of the mean square displacement (MSD) $\langle \Delta x^2(t) \rangle$ as a function of time for different values of χ. Different diffusion regimes can be distinguished: normal diffusion regime ($\alpha = 1.0$) and intermediate sub-diffusive regime (ITR, $\alpha < 1.0$). Note that for the case of χ = 1.5, there is a normal diffusion regime (*i.e.* $\alpha = 1.0$) after the ITR. The dashed and solid lines in (a)-(c) are a guide to the eye. Panel (d) shows the dependence of the slope (α) of the MSD curves (in the ITR, characterized by an apparent power-law; $\langle \Delta x^2(t) \rangle \propto t^{\alpha}$) on the confinement strength χ.

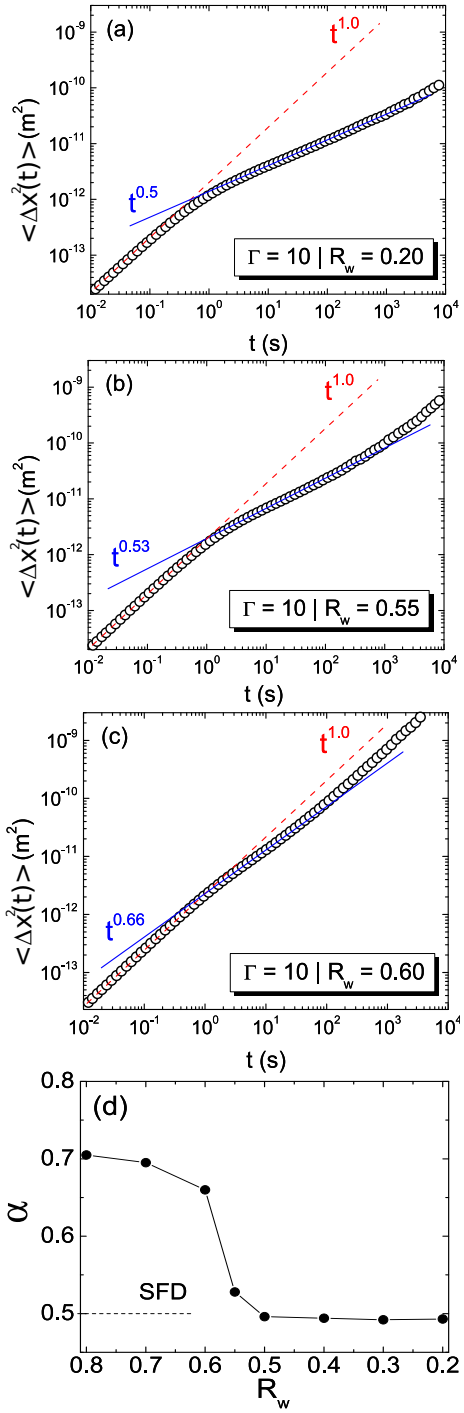

Figure 13 – (a)-(c) Log-log plot of the mean square displacement (MSD) $\langle \Delta x^2(t) \rangle$ as a function of time for different values of R_w. Different diffusion regimes can be distinguished: normal diffusion regime ($\alpha = 1.0$) and intermediate sub-diffusive regime (ITR, $\alpha < 1.0$). Note that for the case of R_w = 0.60, there is a normal diffusion regime (*i.e.* $\alpha = 1.0$) after the ITR. The dashed and solid lines in (a)-(c) are a guide to the eye. Panel (d) shows the dependence of the slope (α) of the MSD curves (in the ITR, characterized by an apparent power-law; $\langle \Delta x^2(t) \rangle \propto t^{\alpha}$) on the confinement parameter R_w.

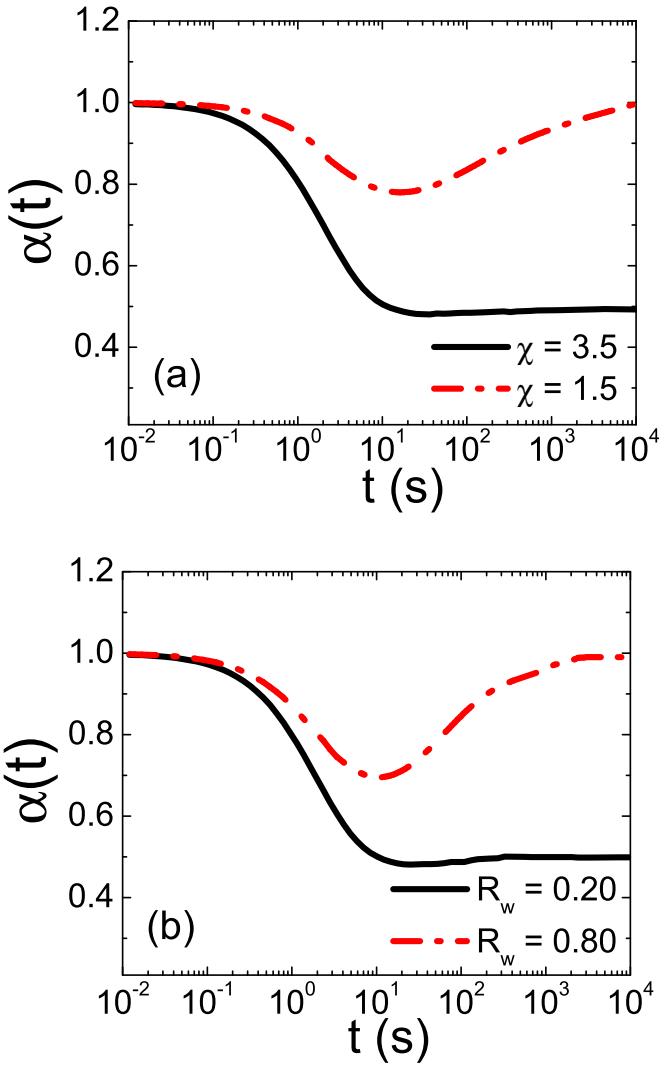

Figure 14 – (a)-(b) Exponent α as a function of time, calculated from Eq. (3.15) for different values of the confinement parameters χ and R_w, respectively.

time derivative"

$$\alpha(t) = \frac{d \log \langle \Delta x^2(t) \rangle}{d \log t}, \tag{3.15}$$

and the results are shown in Fig. 14.

The different diffusive regimes, *i.e.*, normal diffusion regime ($\alpha = 1.0$) and SFD ($\alpha = 0.5$), were also found recently in finite-size systems (104, 45) although the transition from SFD to normal diffusion was not analyzed. The α-dependence on both the confinement parameters (*i.e.*, $\alpha(\chi)$ and $\alpha(R_w)$) presents a different qualitative behavior, namely, the SFD regime is reached after a smoother crossover in the parabolic confinement case as compared to the hard-wall case. A similar smoother crossover is also found in the case of a circular channel with parabolic confinement in the radial direction. A more detailed discussion on these two different types of the behavior of α will be provided in Sec. 3.4.

3.3.2 "Long-time" behavior of the MSD curves and crossing events $C(t)$

For small values of the parabolic confinement (*e.g.*, $\chi = 1.5$), the MSD curves present three different diffusive regimes: (i) a short-time normal diffusion regime, where MSD $\langle \Delta x^2(t) \rangle \propto t^{1.0}$; (ii) a sub-diffusive regime with $\langle \Delta x^2(t) \rangle \propto t^{\alpha}$, where $0.5 < \alpha < 1.0$ and (iii) a "long-time" diffusion regime, which is characterized by $\langle \Delta x^2(t) \rangle \propto t^{1.0}$. Note that the "long-time" term used here is not to be confused with the long-time used for *infinite* systems, as discussed in Sec. 3.1. However, for large values of the parabolic confinement (*e.g.*, $\chi = 3.5$), we observe only two distinct diffusive regimes, namely: (i) a short-time normal diffusion regime ($\langle \Delta x^2(t) \rangle \propto t^{1.0}$) and (ii) a SFD regime (*i.e.*, $\langle \Delta x^2(t) \rangle \propto t^{0.5}$).

One question that arises naturally is whether this normal diffusion regime (*i.e.*, $\langle \Delta x^2(t) \rangle \propto t^{1.0}$ for "long-times") is an effect of the *colletive* motion of the system (center-of-mass motion) or an effect of the single-particle jumping process, since the confinement potential $\chi = 1.5$ allows particles bypass. In order to answer this question, we calculate the number of crossing events $C(t)$ as a function of time and results are shown in Fig. 15(a). We found that for small values of the confinement potential (*e.g.*, $\chi = 1.5$) the number of crossing events grows linearly in time, *i.e.*, $C(t) \propto \omega_c t$, where ω_c is the rate of crossing events. On the other hand, a strong confinement potential (*e.g.*, $\chi = 3.5$) prevents particles from bypassing, and thus $C(t) = 0$ during the whole simulation time.

Therefore, the "long-time" normal diffusive behavior (*i.e.*, $\langle \Delta x^2(t) \rangle \propto t^{1.0}$ for "long-times") found in our simulations for the case where the SF (single-file) condition is broken (*e.g.*, $\chi = 1.5$) is not due to a collective (center-of-mass) diffusion. Instead, this normal diffusive behaviour is due to a single-particle jumping process, which happens with a constant rate $\omega_c > 0$ for the case of small values of the confinement ($\chi = 1.5$) and $\omega_c = 0$ (for $\chi = 3.5$). The same analysis was done for the case of the hard-wall confinement potential, and the results are found to be the same as for the parabolic confinement.

Nevertheless, we point out that the collective diffusion does indeed exist, but our results from simulations do not allow us to observe this collective (center-of-mass) diffusion regime because of the large size of our chain of particles ($N = 400 - 900$). Simulations with $N = 80 - 100$, and excluding the possibility of mutual bypass (strong confinement potential), allowed us to observe that the $\langle \Delta x^2(t) \rangle \propto t^{1.0}$ regime is recovered in the "long-time" limit. In Sec. 3.5, we will further discuss the long-time limit using a model of discrete sites.

As we demonstrated above, the transition from pure 1D diffusion (SFD) characterized by $\alpha = 0.5$ to a *quasi*-1D behavior (with $\alpha > 0.5$) could be either more "smooth" (as in Fig. 12(d), for a parabolic confinement) or more "abrupt" (as in Fig. 13(d), for a hard-wall confinement). One can intuitively expect that this difference in behavior can manifest itself also in the crossing events rate ω_c, *i.e.*, that ω_c as a function of χ (or R_w) should display a clear signature of either "smooth" or "abrupt" behavior.

However, the link between the two quantities, *i.e.*, the exponent, $\alpha(\chi/R_w)$, and the crossing events rate, $\omega_c(\chi/R_w)$ is not that straightforward. To understand this, let us refer to the long-time limit (which will be addressed in detail within the discrete-site model in Sec. 3.5). As we show, in the long-time limit the exponent α is defined by one of the two conditions: $\omega_c = 0$ (then $\alpha = 0.5$) or $\omega_c > 0$ (then $\alpha = 1$) and it does not depend on the specific value of ω_c provided it is nonzero. Therefore, in the long-time limit the transition between 1D to 2D behavior is not sensitive to the particular behavior of the function $\omega_c(\chi/R_w)$.

Although for "intermediate" times (considered in this section) the condition $\omega_c = 0$ or $\omega_c > 0$ is not critical, nevertheless, very small change in the crossing events rate $\omega_c(\chi/R_w)$ strongly influences the behavior of the exponent $\alpha(\chi/R_w)$. This is illustrated in Figs. 15(b)-(c). In Fig. 15(b), the function $\omega_c(\chi)$ gradually decreases from 1.45 to 0 for χ varying in a broad interval from 1.5 to 3 (note that the segment of $\omega_c(\chi)$ for $2.5 < \chi < 3$ is nonzero which can be seen in the inset of Fig. 15(b) showing the derivative $d\omega_c(\chi)/d\chi$). Correspondingly, the transition from $\alpha = 0.5$ to $\alpha \approx 0.8$ in that interval of χ is "smooth" (see Fig. 12(d)). On the other hand, the function $\omega_c(R_w)$ shown in Fig. 15(c) mainly changes [note the change of the slope $d\omega_c(R_w)/dR_w$ shown in the inset of Fig. 15(c)] in a narrow interval $0.5 < R_w < 0.6$. Respectively, the transition for the function $\alpha(R_w)$ occurs in the narrow interval $0.5 < R_w < 0.6$ and thus is (more) "abrupt".

3.3.3 Distribution of particles along the *y*-direction

For the ideal 1D case, particles are located on a straight line. Increasing the width R_w of the confining channel will lead to a zig-zag transition (97, 116). This zig-zag configuration can be seen as a distorted triangular configuration in this transition zone. Further increase of R_w brings the system into the 2D regime, where the normal diffusion behavior is recovered (see Fig. 16).

For the parabolic 1D confinement, we can see [Fig. 17(a)] that the distribution of particles $P(y)$ along the channel is symmetric along the axis $y = 0$. Also, for large values of χ (*e.g.*, $\chi = 3.5$) particles are confined in the *y*-direction and thus can move only in the *x*-direction, forming a single-chain structure. As the confinement decreases ($\chi \to 0$), the distribution of particles $P(y)$ broadens resulting in the crossover from the SFD regime ($\chi = 3.5$) to the 2D normal diffusion regime ($\chi = 0.5$). Note that for small values of χ (*e.g.*, $\chi = 0.5$), the system forms a two-chain structure [represented by two small peaks of $P(y)$ in Fig. 17(a)], thus allowing particles to pass each other.

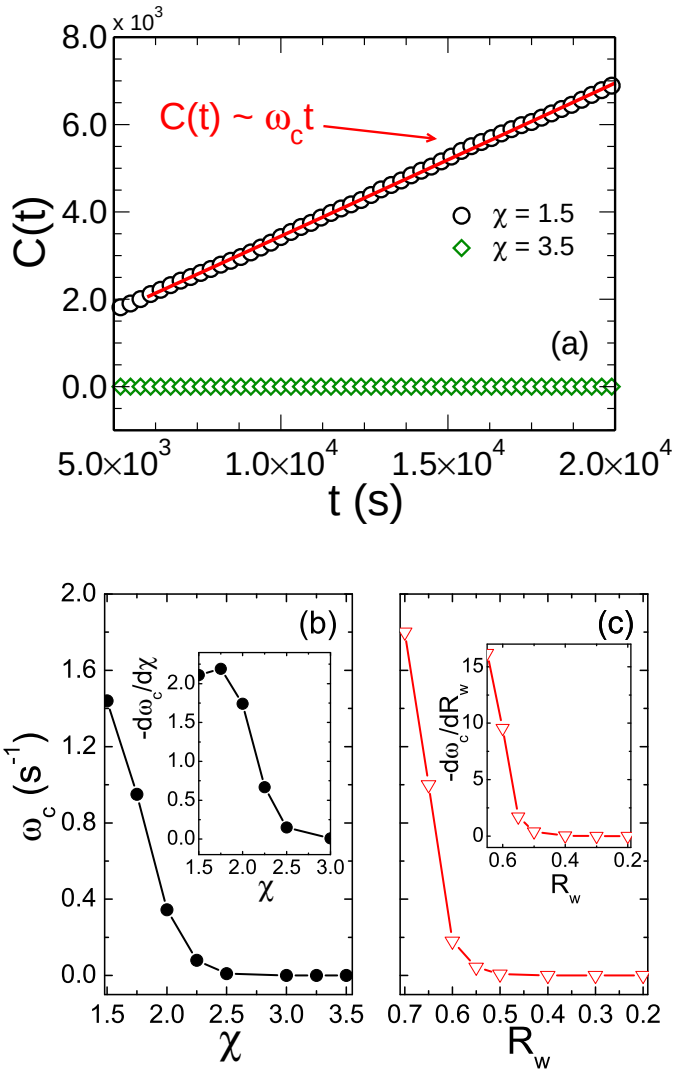

Figure 15 – (a) Number of crossing events $C(t)$ as a function of time for $N = 400$ particles, for $\chi = 1.5$ (black open circles) and $\chi = 3.5$ (green open diamonds). The solid red line is a linear fit to $C(t)$. Panels (b) and (c) show the rate of the crossing events ω_c as a function of the confinement potential parameters (χ and R_w). The insets in the panels (b) and (c) show the derivatives, $d\omega_c(\chi)/d\chi$ and $d\omega_c(R_w)/dR_w$, correspondingly.

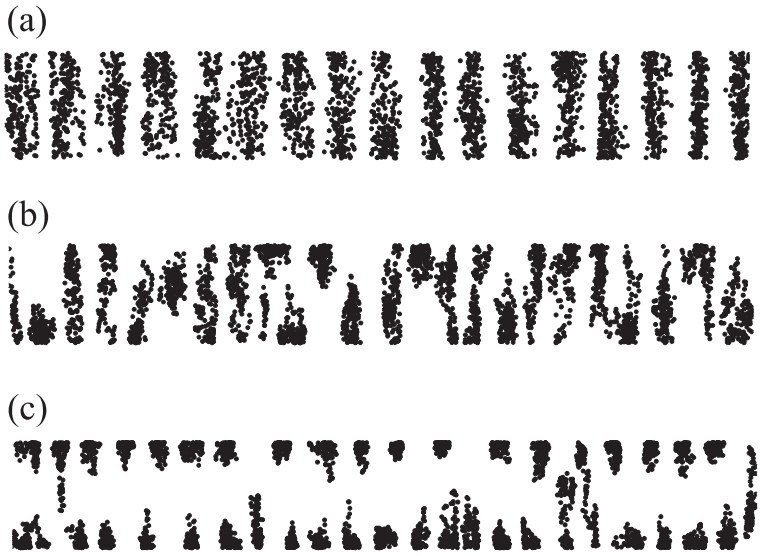

Figure 16 – For the hard-wall confinement case, we show typical trajectories of particles (*i.e.* 10^6 MD simulation steps) confined by the channel of width (a) $R_w = 0.20$, (b) $R_w = 0.60$ and (c) $R_w = 0.80$.

3.4 Diffusion in a circular channel

In the previous section, we analyzed the transition (crossover) from the SFD regime to 2D diffusion in narrow channels of increasing width. The analysis was performed for a straight channel with either hard-wall or parabolic confinement potential. However, in terms of possible experimental verification of the studied effect, one faces an obvious limitation of this model: although easy in simulation, it is hard to experimentally fulfill the periodic boundary conditions at the ends of an open channel. Therefore, in order to avoid this difficulty, in SFD experiments (41, 102) circular channels were used.

In this section, we investigate the transition (crossover) from SFD to 2D-diffusion in a system of interacting particles diffusing in a channel of *circular* shape. In particular, we will study the influence of the strength of the confinement (*i.e.*, the depth of the potential profile across the channel) on the diffusive behavior. Without loss of generality, we will adhere to the specific conditions and parameters of the experimental set-up used in Ref. (102). An additional advantage of this model is that the motion of the system of charged metallic balls is not over-damped, and we will solve the full Langevin equations of motion to study the diffusive behavior of the system.

We consider N particles, interacting through a Yukawa potential [Eq. (3.6)], which are embedded in a ring channel of radius r_{ch}. We define a parabolic confinement potential across

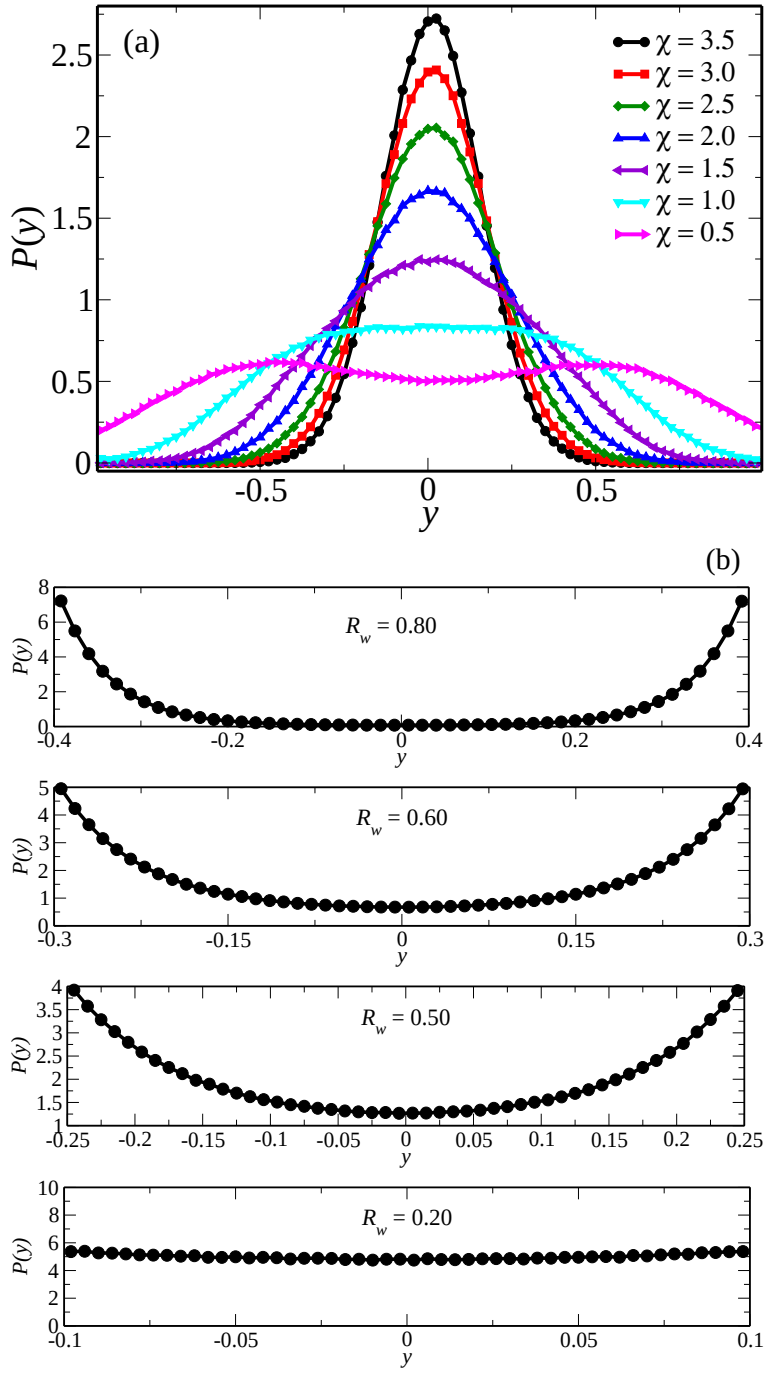

Figure 17 – Probability distribution of the particle density $P(y)$ along the y-direction are shown for (a) different values of χ (parabolic 1D confinement) and (b) four different values of the width R_w of the channel (hard-wall confinement).

the channel in the form of Eq. (3.5) where parameter β is chosen as follows

$$\beta = \frac{V_0}{\gamma r_0^2}, \quad V_0 = \frac{q^2}{\varepsilon} \sum_{i \neq j} \frac{\exp\left[-2\kappa r_{ch} \sin\left(\frac{\phi_i - \phi_j}{2}\right)\right]}{2 r_{ch} \sin\left(\frac{\phi_i - \phi_j}{2}\right)}, \tag{3.16}$$

when all the particles are equidistantly distributed along the bottom of the circular channel. It should be noted that in this case, V_0 is approximately equal to V_{gs} due to the weak Yukawa interaction, which slightly shifts the particles away from the bottom of the channel. Such a choice of V_0 is related to the fact that we study the influence of the confinement on the diffusion and, therefore, the potential energy of the particles must be of the order of the inter-particle interaction energy. Parameter r_0 characterizes the distance where the external potential reaches the value V_0/γ, and V_{gs} is the energy of the ground state of the system of N particles as defined by Eq. (3.7).

Parameter γ plays the role of a control parameter. By changing γ we can manipulate the strength of the confinement and, therefore, control the fulfillment of the single-file condition. Increase in γ corresponds to a decrease in the depth of the confinement [Eq. (3.5)] which leads to the expansion of the area of radial localization of particles. Therefore, an increase of γ results in a similar effect (*i.e.*, spatial delocalization of particles) as an increase of temperature, *i.e.*, parameter γ can be considered as an "effective temperature". Note that such a choice of the parameter that controls the confinement strength is rather realistic. In the experiment of Ref. (102) with metallic balls, the parabolic confinement was created by an external electric field, and the depth of the potential was controlled by tuning the strength of the field.

To study diffusion of charged metallic balls, we solve the Langevin equation of motion in the general form (*i.e.*, with the inertial term $\propto m$),

$$m\frac{d^2\boldsymbol{r}_i}{dt^2} = -m\eta\frac{d\boldsymbol{r}_i}{dt} - \sum_{j,i\neq j} \boldsymbol{\nabla} V_{int}(\boldsymbol{r}_{ij}) - \boldsymbol{\nabla} V_c(\boldsymbol{r}_i) + \boldsymbol{F}_T^i, \tag{3.17}$$

where $m = 2.5 \times 10^{-6}$ kg is the mass of a particle, and η is the damping constant. Here all the parameters of the system were chosen following the experiment (102), and $\lambda_D = 4.8 \times 10^{-4}$ m, $\Gamma = 1$ [which is a typical experimental value, see, *e.g.*, also (41)]. Correspondingly, mass is measured in kg, length in m, and time in seconds.

Also, we took a channel of radius $r_{ch} = 9$ mm (in the experiment, the external radius of the channel was 10 mm, and the channel width 2 mm; note that in our model we do not define the channel width: the motion of a particle in the transverse direction is only restricted by the parabolic confinement potential). We also took experimentally relevant number of diffusing particles, N, varying from $N = 12$ to $N = 40$ (in the experiment, the ring channel contained $N = 12$ or $N = 16$ diffusing balls).

Fig. 18 shows the results of calculations of the trajectories of $N = 20$ particles diffusing in a ring of radius $r_{ch} = 9$ mm for the first 10^6 MD steps for various values of the parameter

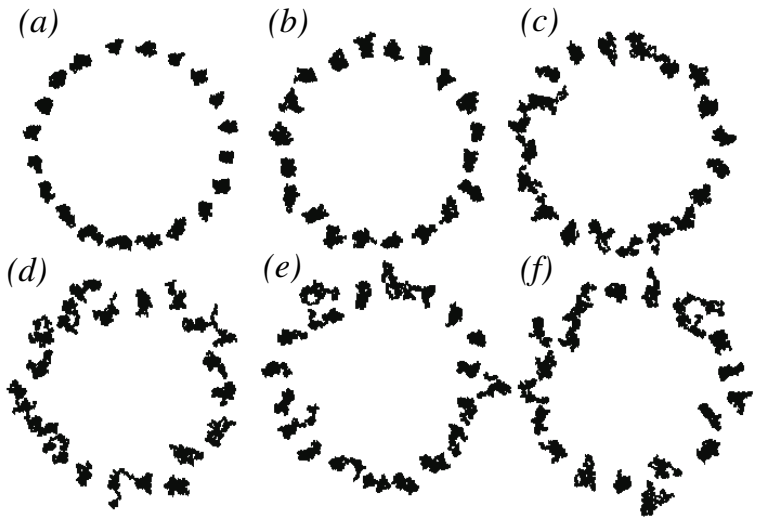

Figure 18 – Trajectories of $N = 20$ particles diffusing in a ring of radius $r_{ch} = 9$ mm for 10^6 consequent time steps for different values of γ. γ=1 (a), 2 (b), 3 (c), 5 (d), 7 (e), 9 (f).

γ. As can be seen from the presented snapshots, the radial localization of particles weakens with increasing γ. At a certain value of γ this leads to the breakdown of the single-file behavior [Figs. 18(c)-(f)].

3.4.1 Breakdown of SFD

It is convenient to introduce the distribution of the probability density of particles in the channel $P_{\rm rad}$ along the radial direction r. In order to calculate the function $P_{\rm rad}(r)$ we divided the circular channel in a number of coaxial thin rings. The ratio of the number of observations of particles in a sector of radius r_i to the total number of observations during the simulation is defined as the probability density $P_{\rm rad}(r_i)$. In Fig. 19, the probability density $P_{\rm rad}(r)$ is presented for different values of γ. With increasing γ, the distribution of the probability density $P_{\rm rad}(r)$ broaden and the maximum of the function $P_{\rm rad}(r)$ shifts away from the center of the channel (see Fig. 19). The latter is explained by the softening of the localization of particles with increasing γ, which tend to occupy an area with a larger radius due to the repulsive inter-particle interaction. Simultaneously, the distribution of the probability density $P_{\rm rad}(r)$ acquires an additional bump indicating the nucleation of a two-channel particle distribution (117). The observed broadening and deformation of the function $P_{\rm rad}(r)$ is indicative of a gradual increase of the probability of mutual bypass of particles [*i.e.*, the violation of the SF (single-file) condition, also called the "overtake probability" (118)] with increasing γ.

Let us now discuss a qualitative criterion for the breakdown of SFD, *i.e.*, when the majority of particles leave the SFD mode. For this purpose, let us consider a particle in the potential created by its close neighbor (which is justified in case of short-range Yukawa inter-

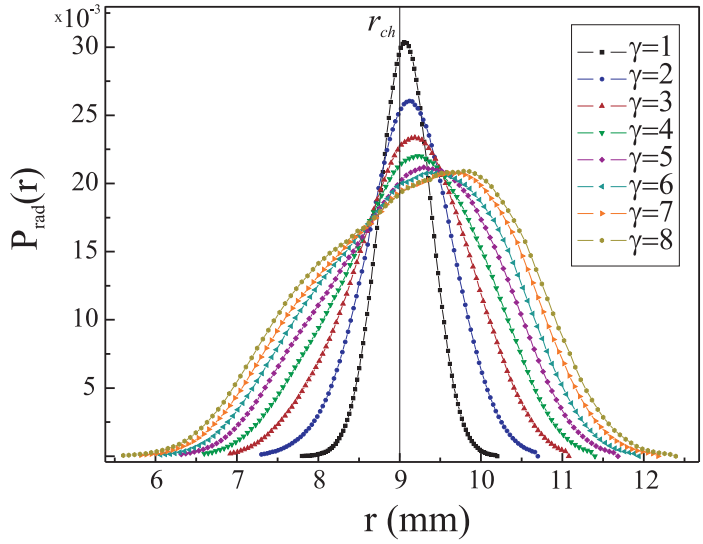

Figure 19 – The distribution of the probability density of particles $P_{\text{rad}}(r)$ in a circular channel of radius $r_{ch} = 9$ mm along the radial direction r. The different curves correspond to various γ. Increasing γ the width of the distribution $P_{\text{rad}}(r)$ increases due to a weakening of the confinement.

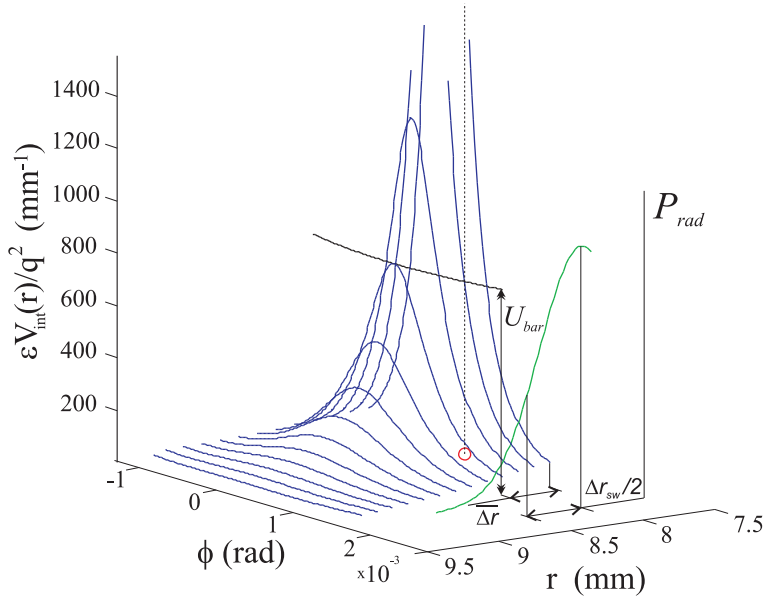

Figure 20 – Spatial distribution of the potential $V_{\text{int}}(r, \phi)$ created by a particle (red (grey) circle) and the qualitative distribution of the probability density of particles in circular channel $P_{\text{rad}}(r)$ (green (light grey) line) along the radial direction r. The function $\overline{\Delta r}$ determines an approximate radial distance between particles when the potential barrier U_{bar} becomes "permeable" for given temperature T. The function Δr_{sw} characterizes a width of the distribution $P_{\text{rad}}(r)$ at this temperature T.

particle interaction and low density of particles in a channel) shown in Fig. 20. Different lines show the inter-particle potential V_{int} as a function of angle ϕ for different radii r.

For small values of γ, the center of the distribution $P_{\text{rad}}(r)$ (see Fig. 19) almost coincides with the center of the channel (*i.e.*, with the minimum of the confinement potential profile) and the distribution $P_{\text{rad}}(r)$ is narrow. Therefore, mutual passage of particles is impossible, *i.e.*, the SF condition is fulfilled. The asymmetric broadening of the function $P_{\text{rad}}(r)$ with increasing γ results in an increasing probability of mutual bypass of particles which have to overcome a barrier U_{bar} (see Fig. 20). This becomes possible when $U_{\text{bar}} \lesssim k_B T$. In other words, the thermal energy $k_B T$ determines some minimal width $\overline{\Delta r}$ between adjacent particles when the breakdown of the SF condition becomes possible.

It is clear that "massive" violation of the SF condition (*i.e.*, when the majority of particles bypass each other) occurs when the halfwidth Δr_{sw} of the distribution of the probability density $P_{\text{rad}}(r)$ obeys the condition

$$\Delta r_{\text{sw}} \gtrsim \overline{\Delta r}. \tag{3.18}$$

The function Δr_{sw} is defined by the ratio of the thermal energy $k_B T$ to the external potential $U_{\text{conf}}(r)$ and is of the same order as $\widetilde{\Delta r}$

$$\frac{V_0}{\gamma r_0^2} \cdot (\widetilde{\Delta r}/2)^2 \approx k_B T. \tag{3.19}$$

Therefore the criterion (3.18) can be presented in the form

$$\Delta r_{\text{sw}} \approx \widetilde{\Delta r} \gtrsim \overline{\Delta r}. \tag{3.20}$$

This qualitative analysis of the breakdown of the SFD regime clarifies the role of the width and the shape of the distribution of the probability density influenced by the asymmetry of the circular channel. Note that the shape of the distribution is a signature of the breakdown of the SF condition. This breakdown is caused by the mechanism of minimization of the repulsive inter-particle interaction energy.

3.4.2 Diffusion regimes

The MSD $\langle \Delta\phi^2(t) \rangle$ is calculated as a function of time t as

$$\left\langle \Delta\phi^2(t) \right\rangle = \left\langle \frac{1}{N_{\text{par}} N_{\text{ens}}} \sum_{i,j} \left[\Delta\phi_{ij}(\tau + t) - \Delta\phi_{ij}(t) \right]^2 \right\rangle_t, \tag{3.21}$$

where N_{par} is the total number of particles of an ensemble and N_{ens} is the total number of ensembles. In our calculations, the number of ensembles was chosen 100 for a system consisting of 20 particles.

The time dependence of the MSD for different values of γ is shown in Fig. 21(a)–(c). Initially the system exhibits normal diffusion, where $\langle \Delta\phi^2 \rangle \propto t^{1.0}$. This regime is followed by an intermediate sub-diffusive regime, where the $\langle \Delta\phi^2 \rangle \propto t^{\alpha}$ ($0.5 < \alpha < 1.0$). For longer times, the system recovers "long-time" normal diffusion (see discussions in Sec. 3.3.2), with $\langle \Delta\phi^2 \rangle \propto t^{1.0}$. As in the case of straight channel geometry, this second crossover (*i.e.*, from intermediate sub-diffusion to "long-time" normal diffusion) can also be due to two other reasons: (i) due to a collective (center-of-mass) diffusion or (ii) due to a single-particle jumping process. However, for the simulations in the case of a circular geometry, the number of particles is relatively small (taking the fact that this is a finite-size system), and therefore, the crossover from sublinear to linear regime is due to a collective (center-of-mass) diffusion. We further address this issue in Sec. 3.5, where we consider a discrete site model and we exclude the center-of-mass motion.

Fig. 21(d) shows α as a function of γ. The function $\alpha(\gamma)$ experiences a monotonic gradual crossover from the $\alpha = 0.5$ to a $\alpha \lesssim 1$ regime. Note that the observed deviation from the normal diffusion behavior for large γ (Fig. 21) is related to the presence of, though weak but nonzero, external confinement in the radial direction. This change of the diffusive behavior is explained by a weakening of the average radial localization of particles with increase of γ (Fig. 19) and, as a consequence, by an increase of the probability of mutual bypass of particles.

The observed crossover between the 1D single-file and 2D diffusive regimes, *i.e.*, $\alpha(\gamma)$-dependence, shows a significant different qualitative behavior as compared to the case of a hard-wall confinement potential considered in Sec. 3.3, where a rather sharp transition between the two regimes was found [Fig. 13(d)]. The different behavior is due to the different confinement profiles and can be understood from the analysis of the distribution of the probability density of particles for these two cases. In the case of a hard-wall channel, the uncompensated (*i.e.*, by the confinement) inter-particle repulsion leads to a higher particle density near the boundaries rather than near the center of the channel [see Fig. 16 and Fig. 17(b)]. As a consequence, the breakdown of the SF condition – with increasing width of the channel – happens simultaneously for many particles in the vicinity of the boundary resulting in a sharp transition (see Fig. 13(d)). On the contrary, in the case of parabolic confinement, the density distribution function has a maximum — sharp or broad, depending on the confinement strength — near the center of the channel [see Figs. 17(a) and 19]. With increasing the "width" of the channel (*i.e.*, weakening its strength), only a small fraction of particles undergoes the breakdown of the SF condition. This fraction gradually increases with decreasing strength of the confinement, therefore resulting in a smooth crossover between the two diffusion regimes.

3.5 Discrete site model: The long-time limit

The calculated MSD for different geometries and confinement potentials allowed us to explain the evolution of the sub-diffusive regime with varying width of the channel (or potential strength

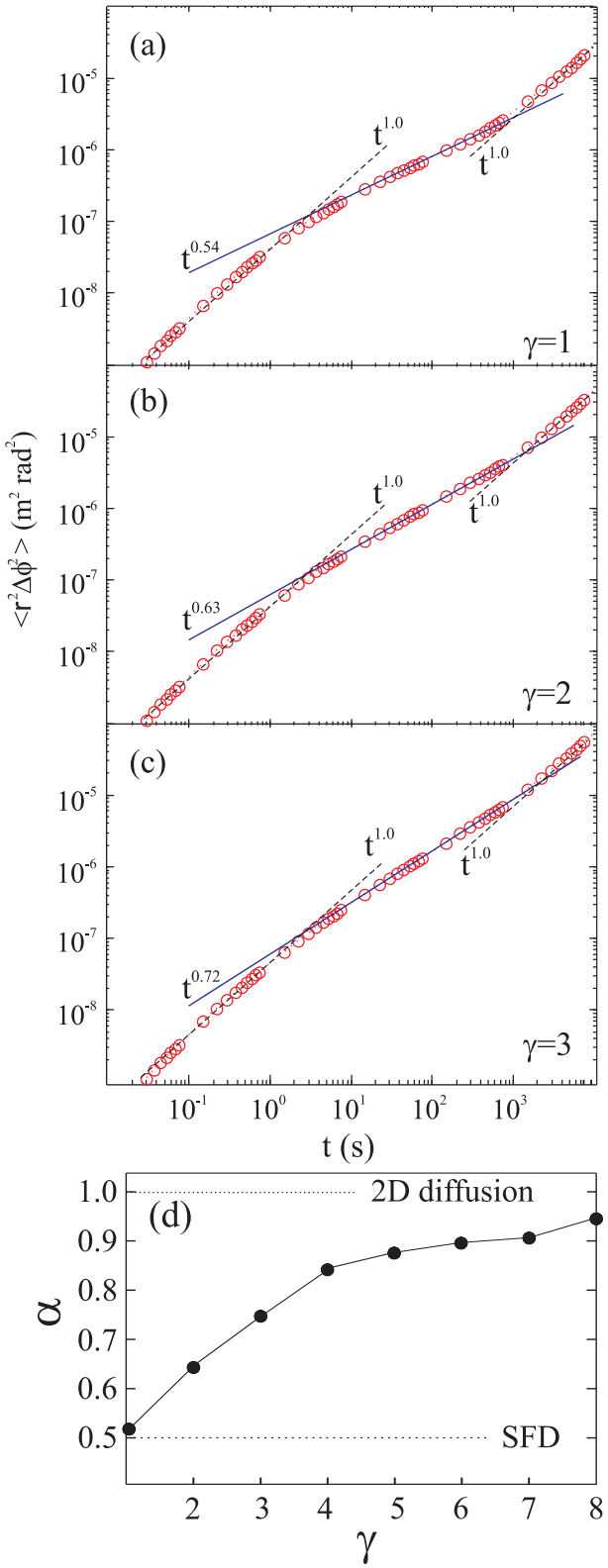

Figure 21 – (a)–(c): Log-log plot of the mean square displacement (MSD) $\langle \Delta\phi^2 \rangle$ as a function of time for different values of the "effective" temperature γ = (a) 1, (b) 2, and (c) 3. Here $(N_{\text{ens}} = 100, N_{\text{par}} = 20)$. (d) The diffusion exponent α as a function of γ. Increase of the "effective" temperature γ leads to the gradual transformation of the single-file regime of diffusion into the diffusion regime of free particles.

in case of a parabolic potential). However, the obtained results are only valid for the intermediate regime and therefore they only describe the "onset" of the long-time behavior. The problem of accessing the long-time behavior in a finite chain is related to the fact that sooner or later (*i.e.*, depending on the chain length) the interacting system will evolve into a collective, or "single-particle", diffusion mode which is characterized by $\alpha = 1.0$. Thus the question is whether the observed behavior holds for the long-time limit, *i.e.*, is the transition from $t^{0.5}$ to $t^{1.0}$ behavior smooth?

To answer this question, we considered a simple model, *i.e.*, a linear discrete chain of fixed sites filled with either particles or "holes" (sites not occupied by particles) [this model was also recently used in Ref. (119)]. The particles can move along the chain only due to the exchange with adjacent vacancies (with holes). Within this model, the long-time diffusion behavior was described analytically for an infinite linear chain as well as for a finite cyclic chain (113). In particular, this model predicts that: (i) If the chain is infinite then the long-time power law of the diffusion curve α is 0.5 (MSD $\langle \Delta x^2(t) \rangle \propto t^{0.5}$); (ii) If the chain is finite then the sub-diffusive regime with $\alpha = 0.5$ is followed by either $\alpha = 1.0$ regime (if the cyclic boundary condition is realized), or by $\alpha = 0$ regime, *i.e.*, the regime of saturation (if no cyclic boundary condition is imposed (56)). The latter regime is reached for times longer than the "diffusion time" of a "hole" along the whole chain t_{chain}.

Let us now apply this model to a finite-size chain of particles. For this purpose, we assume that adjacent particles are able to exchange their positions with some probability P at every time step. For example, probability $P = 0.1$ means that a couple of any adjacent particles certainly exchange their positions once for every 10 time steps. The results of our calculations of the MSD performed using this model are presented in Fig. 22(a). We used the following parameters: the chain length is $N_s = 150$ sites and $N_h = 1$ hole. Averaging was done over 1000 ensembles. The calculation was performed for the following values of the probability: $P = 0, 10^{-5}, 10^{-4}, 10^{-3}, 0.01, 0.1$, and 1.

We see in Fig. 22(a) clearly the above-mentioned two diffusion regimes, *i.e.*, with the MSD $\langle \Delta x^2(t) \rangle \propto t^{0.5}$ and $\propto t^{1.0}$. The characteristic time t_{chain} shifts towards lower values with increasing P. However this analysis (Fig. 22(a)) does not allow to distinguish the contributions to the long-time behavior ($\propto t^{1.0}$) due to: (i) the breakdown of single-file condition (diffusion due to particle exchanges), and (ii) the "collective" diffusion (chain "rotation"). To overcome this difficulty, we exclude the "collective" diffusion of the system and introduce a modified MSD $\langle \Delta x^2(t) \rangle_{\text{corr}}$ (which is so-called "roughness" of the system of particles, as discussed in Ref. (45)) as follows

$$\langle \Delta x^2 \rangle_{\text{corr}} = \langle (x - \bar{x})^2 \rangle, \tag{3.22}$$

where $\langle \ldots \rangle$ is the average over time; $\bar{x}$ is the average of an ensemble of particles at a given time, or "collective" coordinate. It should be noted that $\langle x \rangle \neq \bar{x}$. If the system does not experience

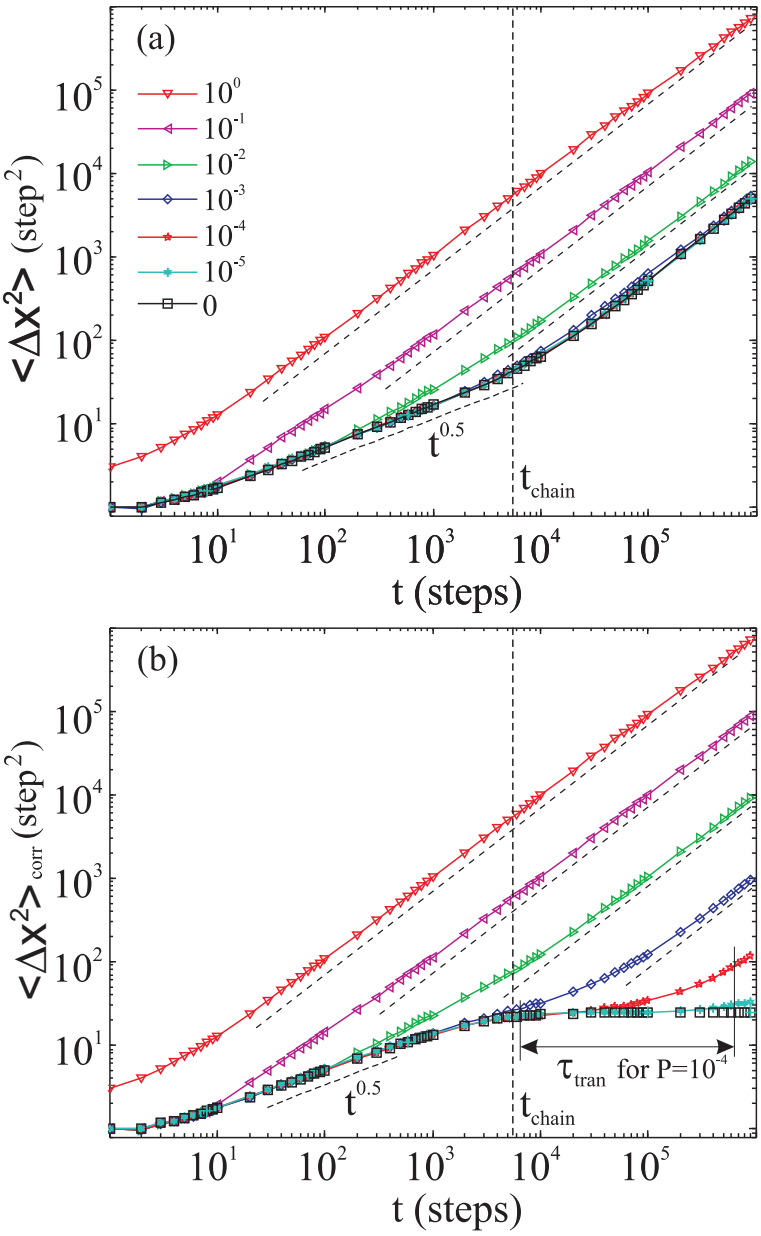

Figure 22 – Log-log plot of the MSD $\langle \Delta x^2(t) \rangle$ (a) and corrected MSD $\langle \Delta x^2(t) \rangle_{\text{corr}}$ (b) as a function of time for different values of the probability P of bypassing. Averaging was done over $N_{\text{sim}} = 1000$ ensembles.

"collective" diffusion then $\bar{x}(t) = 0$ and the modified MSD coincides with the conventional one

$$\langle \Delta x^2 \rangle_{\text{corr}} = \langle x^2 \rangle. \tag{3.23}$$

The diffusion curves calculated by using the modified MSD are presented in Fig. 22(b). For $P = 0$, the diffusion curve (shown by black open squares) after the sub-diffusive regime reaches saturation ($\langle \Delta x^2(t) \rangle_{\text{corr}}$ = const). The observed behavior is similar to that of a finite linear chain with fixed ends (see Ref. (56)). For $P \neq 0$, all the diffusion curves in the long-time limit are characterized by $\alpha = 1.0$, *independent* of the value of the probability P, as seen

in Fig. 22(b). In other words, the long-time diffusion does not depends on the probability of mutual exchanges of particles and has the same long-time behavior for any probability $P \neq 0$. Here we would like to emphasize again that the long-time behavior of the diffusion curves is free from the "collective" diffusion effect and is only determined by particle jump diffusion.

Increasing the number of sites in the model corresponds, in fact, to approaching the model of infinite chain. We have found that the increasing number of sites leads to growth of the $\langle \Delta x^2(t) \rangle_{\text{corr}}$ limit of saturation, on the one hand, and to a shift of t_{chain} to larger t, on the other hand. Hence, extrapolating our results to the case of infinite chain, we can conclude that in this case as well as in the case of finite-size chain, the breakdown of single-file condition leads to an abrupt transition from sub-diffusive to the normal diffusion regime. The difference in the diffusive curves is just the time τ_{tran} from sub-diffusive regime to the normal regime: for low P it (τ_{tran}) is long enough while for high P it (τ_{tran}) is short. It is easy to see that $\tau_{\text{tran}} \sim 1/P(\%)$. Thus, we can conclude that in the long-time limit the transition from $t^{0.5}$ to $t^{1.0}$ behavior is abrupt. Note that our calculations performed using the modified MSD $\langle \Delta x^2(t) \rangle_{\text{corr}}$ reproduce the results of Ref. (56) for a closed "box". This is explained by the fact that in the closed "box" geometry the center of mass (or collective) diffusion is zero, and it is natural that the roughness [see Ref. (45)] and the particles diffusion coincide.

3.6 Concluding remarks

We have studied a monodisperse system of interacting particles subject to three types of confinement potentials: (i) a 1D hardwall potential, (ii) a 1D parabolic confinement potential which both characterize a *quasi*-1D system, and (iii) a circular confining potential, which models a finite size system. In order to study the diffusive properties of the system, we have calculated the mean square displacement (MSD) numerically through molecular dynamics (MD) simulations. For the case where particles diffuse in a straight line in a Q1D channel, different diffusion regimes were found for different values of the parameters of the confining potential (χ or R_w).

We have found that the normal diffusion is suppressed if the channel width R_w is between 0.20 and 0.50 (or by $2.0 < \chi < 3.5$, for the case of parabolic 1D confinement), leading the system to a SFD regime for intermediate time scales. For values of $R_w \geqslant 0.56$, particles will be able to cross each other and the SFD regime will be no longer present. The case of a circular channel corresponds to, *e.g.*, the set-up used in experiments with sub-millimetric metallic massive balls diffusing in a ring with a parabolic potential profile created by an external electric field. The strength of the potential (which determines the effective "width" of the channel) can be tuned by the field strength.

Contrary to the case of hard-wall confinement, where the transition (regarding the calculation of the scaling exponent (α) of the MSD $\langle \Delta x^2(t) \rangle \propto t^{\alpha}$) is sharp, a smooth crossover

between the 1D single-file and the 2D diffusive regimes was observed. This behavior is explained by different profiles for the distribution of the particle density for the hard-wall and parabolic confinement profiles. In the former case, the particle density reaches its maximum near the boundaries of the channel resulting in a massive breakdown of the SF condition and thus in a sharp transition between the different diffusive regimes. In the latter case, on the contrary, the density distribution function has a maximum near the center which broadens with decreasing strength of the confinement. This results in a smooth crossover between the two diffusion regimes, *i.e.*, SFD and 2D regime.

The analysis of the crossing events, *i.e.*, the rate of the crossing events ω_c as a function of the confinement parameter χ or R_w, supports these results: the function $\omega_c(\chi/R_w)$ displays a clear signature of either "smooth" or "abrupt" behavior. We also addressed the case of a finite discrete chain of diffusing particles. It was shown that in this case the breakdown of the single-file condition (when the probability P of particles bypassing each other is non-zero) leads to an abrupt transition from a sub-diffusive regime to the normal diffusion regime.

Related publications

• **D. Lucena**, D. Tkachenko, K. Nelissen, V. R. Misko, W. P. Ferreira, G. A. Farias, and F. M. Peeters, *Transition from single-file to two-dimensional diffusion of interacting particles in a quasi-one-dimensional channel*, Phys. Rev. E **85**, 031147 (2012).

4 Tunable diffusion of magnetic particles

The diffusion of a system of ferromagnetic dipoles confined in a *quasi*-one-dimensional parabolic trap is studied using Brownian dynamics simulations. We show that the dynamics of the system is tunable by an in-plane external homogeneous magnetic field. For a strong applied magnetic field, we find that the mobility of the system, the exponent of diffusion and the crossover time among different diffusion regimes can be tuned by the orientation of the magnetic field. For weak magnetic fields, the exponent of diffusion in the sub-diffusive regime is independent of the orientation of the external field.

4.1 Introduction

The study of magnetic colloids is of great importance both from a theoretical and an experimental point of view. Recently there has been an increased interest in the study of the structural and the dynamical properties of magnetic confined (in particular on the meso- and nano-scale) systems due to the possibility of biomedical (120, 121, 122) and engineering applications (123). Examples of these magnetic systems are ferrofluid nanofilms (124, 125, 126) and magnetorheological (MR) fluids (127, 128). For instance, the translational dynamics of a mesoscopic 3D system of permanent magnetic dipoles was studied in Ref. (129), and it was found that the system displays signatures of sub-diffusive motion due to the strong suppression of orientational fluctuations of the magnetic dipoles by the presence of an homogenous external magnetic field. The formation of chains of magnetic dipoles [coagulation effect (130, 131, 132)] is also relevant for the dynamical properties of these magnetic systems and may lead to different regimes of diffusion. Magnetic clusters of dipolar particles were recently investigated experimentally (133, 134, 135) and they may serve, *e.g.*, as drug delivery mechanisms in biological applications. The structural properties of magnetic colloids were recently analyzed experimentally (136) and by means of molecular dynamics simulations (137), where novel field-induced structural transitions were observed in confined ferrofluid nanofilms.

In comparison with infinite 3D or 2D systems, confined systems exhibit a particular behavior due to the competition between the confining potential and the inter-particle interaction potential. For instance, for a 2D system of repulsive particles confined in a circular parabolic potential, previous studies clearly identified the effect of the boundaries on the structural and dynamical properties of the system, as well as on the melting (138, 139, 140, 141, 142, 143). Another interesting possibility of confined systems is realised when the 2D system is subjected to an external confining potential (*e.g.* parabolic) in one direction. The system is called *quasi*-one-dimensional (q1D). Such a q1D system of repulsive interacting particles self-organize in a

chain-like structure that was recently studied experimentally (144, 145, 146, 147), and through analytical and numerical calculations (148, 149, 150, 151, 152).

Diffusion is strongly modified in confined systems, and may lead to single-file diffusion (SFD) (153, 154, 155, 156, 157), which is directly related to the geometrical constrains imposed by an external confining potential. Furthermore, q1D systems can be used as models for the study of collective phenomena in low dimensional systems, *e.g.*, vortex matter in type-II superconductors (158), colloidal particles (159) and dusty plasmas. In addition, the mechanisms of ion transport in narrow channels (160) and DNA manipulation using magnetic particles (161, 162) can be studied by modelling q1D systems.

In this chapter we investigate numerically the properties of a system of ferromagnetic dipolar particles confined in a one-dimensional parabolic trap (which models a q1D channel) coupled to a thermal bath. The orientation and strength of an in-plane external magnetic field **B** are now control parameters that are able to influence the dynamics of the particles. For diluted systems, particles are arranged in a single chain structure in the center of the parabolic channel. When **B** is perpendicular to the channel, the magnetic particles interact through a pure repulsive potential. For any other orientation of **B**, an extra attractive term is present in the particle-particle interaction potential. The latter can be dominantly attractive or repulsive, depending on the orientation of the external magnetic field. In our numerical analysis, we perform extensive Brownian dynamics (BD) simulations and calculate the mean square displacement (MSD) $W(t)$ of the particles for different parameters which characterizes the system. For the case of normal diffusion regime (Einstein or Fickian diffusion), one has $W(t) = D_0 t^{\alpha}$, where D_0 is the "free particle" diffusion coefficient, α is the so-called exponent of diffusion (in this case, $\alpha = 1.0$) and t is time. For values of $\alpha \neq 1.0$, diffusion is said to be anomalous. For instance, in the case of SFD, $W(t) = 2Ft^{\alpha}$ (with $\alpha = 0.5$) where F is the single-file diffusion mobility factor. We show that the application of an in-plane homogeneous external magnetic field leads to different regimes of diffusion depending on the orientation and strength of the field.

We emphasize here that our analysis of the exponent of diffusion (α) is restricted to the intermediate regime (ITR), which is found before the onset of the true "long-time" limit (*i.e.* $t \to \infty$) (46). See also discussion in Ref. (157) and references therein. Note that in the limit $t \to \infty$, the MSD $W(t) \propto t^{0.5}$ for any pairwise interaction potential if the system fulfills the SF (single-file) condition, *i.e.*, no particle crossings are allowed. The reason is that the clustering of particles, observed in our work due to the attractive interaction, can be considered as a system of bigger particles with lower effective particle density and smaller diffusion constant. These clusters should have the MSD $W(t) \propto t^{0.5}$ but now at a much larger time scale, which we do not consider in this work.

4.2 Model and Numerical Methods

4.2.1 Model System

Our system consists of N interacting dipolar ferromagnetic particles confined in a *quasi*-one-dimensional (q1D) channel and which is in contact with a thermal bath at absolute temperature T. The pair interaction potential $V_{\rm pair}(r)$ is given by the sum of the dipole-dipole term $V_{\rm dip}(r)$ and the short-range repulsion $V_{\rm ss}(r)$, such as

$$V_{\rm pair}(r_{ij}) = \frac{\boldsymbol{\mu}_i \cdot \boldsymbol{\mu}_j}{|\mathbf{r}_{ij}|^3} - \frac{3(\boldsymbol{\mu}_i \cdot \mathbf{r}_{ij})(\boldsymbol{\mu}_j \cdot \mathbf{r}_{ij})}{|\mathbf{r}_{ij}|^5} + 4\varepsilon \left(\frac{\sigma}{|\mathbf{r}_{ij}|}\right)^{12}, \tag{4.1}$$

where $\mathbf{r}_{ij}$ is the inter-particle separation vector between a pair of particles i and j, $\boldsymbol{\mu}_i$ is the permanent magnetic moment of particle i, σ is the diameter of each particle and ε is an energy parameter which characterizes the short-range repulsion between the particles and prevent them from coalescing in a single point (163). We assume identical particles, *i.e.*, $|\boldsymbol{\mu}_i| = |\boldsymbol{\mu}_j| = \mu$. The q1D channel is modeled by a parabolic confinement potential defined as $V_{\rm conf} = m\omega^2 y_i^2/2$, where m, ω and y_i are the mass of each particle, the confinement strength (frequency) and the y coordinate of the ith particle, respectively. We also apply an in-plane homogenous external magnetic field $\mathbf{B}$, which forms an angle ϕ with respect to the x-axis. The interaction torque $\boldsymbol{\tau}_i$ between particles is given by $\boldsymbol{\tau}_i = \boldsymbol{\mu}_i \times \sum_{j>i} \mathbf{B}_{ij}^{\rm int}$ (cf. A.1). The coupling between the magnetic moment of each particle and the external field is given by $\boldsymbol{\tau}_i^B = \boldsymbol{\mu}_i \times \mathbf{B}$. In Fig. 23, we show a schematic representation of the system under study together with the relevant parameters.

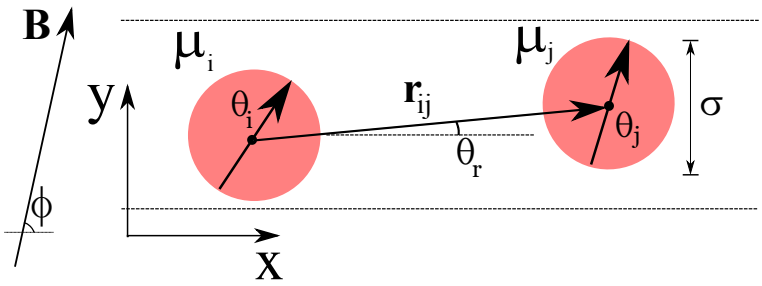

Figure 23 – Schematic representation of the system. The particles have diameter σ and dipole moment $\boldsymbol{\mu}_i$, which forms an angle θ_i with respect to the x-axis. An in-plane external magnetic field $\mathbf{B}$ is applied with magnitude B and ϕ is the angle between $\mathbf{B}$ and the x-axis.

We assume that the motion of the particles is over-damped which is typical for colloids moving in a liquid. The equations of motion for the ith magnetic dipolar particle are

$$\zeta \dot{\mathbf{r}}_i = -\sum_{j>i} [\boldsymbol{\nabla}_i (V_{\rm dip} + V_{\rm ss})] - \boldsymbol{\nabla}_i V_{\rm conf} + \boldsymbol{\xi}_i(t), \tag{4.2}$$

$$\zeta \sigma^2 \dot{\theta}_i \hat{\mathbf{z}} = \boldsymbol{\tau}_i + \boldsymbol{\tau}_i^B + \sigma \xi_i(t) \hat{\mathbf{z}}, \tag{4.3}$$

where $\mathbf{r}_i = x_i\hat{\mathbf{x}} + y_i\hat{\mathbf{y}}$ is the position vector of particle i and θ_i is the angle between the vector $\boldsymbol{\mu}_i$ and the x-axis. Furthermore, ζ is the viscosity of the medium and $\boldsymbol{\xi}_i(t)$ is a stochastic white-noise with the properties: (i) $\langle \boldsymbol{\xi}_i(t) \rangle = 0$ and (ii) $\langle \xi_{im}(t)\xi_{jn}(t') \rangle = 2\zeta k_B T \delta_{ij}\delta_{mn}\delta(t-t')$, where m,n corresponds to the components (x,y,θ), k_B is the Boltzmann constant and T is the absolute temperature of the system.

Note that the first and the second term on the r.h.s. of Eq. (4.3) are related to the potential energy of a dipole due to the magnetic field generated by all the other dipoles

$$U^{\text{int}} = -\boldsymbol{\mu}_i \cdot \sum_{j>i} \mathbf{B}_{ij}^{\text{int}}, \tag{4.4}$$

and the potential energy of a dipole in the presence of the external magnetic field

$$U^{\text{ext}} = -\boldsymbol{\mu}_i \cdot \mathbf{B}, \tag{4.5}$$

respectively. Therefore, for the case of a strong magnetic field (in the following we consider $B = 100$ as an example), the effect of the interaction torque $\boldsymbol{\tau}_i$ can be neglected since the dipoles will tend to align completely to the external field, *i.e.*, $U^{\text{int}} + U^{\text{ext}} \approx U^{\text{ext}}$ (see main panel of Fig. 24). On the other hand, if the external magnetic field is weak (for example, $B = 2.0$), the interaction torque $\boldsymbol{\tau}_i$ can not be neglected since, for this case, we have $U^{\text{int}} \approx U^{\text{ext}}$ (see inset of Fig. 24). Nevertheless, in all our simulations we keep both terms, *i.e.*, $\boldsymbol{\tau}_i$ and $\boldsymbol{\tau}_i^B$.

Finally, our model system does not take into account hydrodynamic interaction (HI) effects (particle-fluid and particle-wall interactions), which usually have only a small effect on the qualitative behavior of the diffusion properties, as recently demonstrated by Euán-Díaz *et al.* (164). A similar approach was adopted for a dilute dipolar colloidal suspension in Refs. (165, 166), where, similar to our work, the interaction potential between particles had both a repulsive and an attractive term. The HI effects can be neglected in our case because we are in the dilute regime, *i.e.*, the low density case. Note that the particles are almost completely uniformly distributed along the x-direction, *i.e.*, the system forms a single-chain configuration. Furthermore, HI effects should play an important role in diffusion (and in general, in dynamical properties) for the case of highly concentrated colloidal suspensions (80), a situation that is not considered in our work.

4.2.2 Numerical Methods

Before we integrate numerically Eqs. (4.2) and (4.3), we introduce the unit of time as $t_0 = \zeta\sigma^2/\varepsilon$, where $\varepsilon = k_B T_0$ is the unit of energy (T_0 is the unit of temperature) and σ is the unit of length. Moreover, $B_0 = \sqrt{\varepsilon/\sigma^3}$ is the unit of magnetic field and $\mu_0 = \sqrt{\varepsilon\sigma^3}$ is the unit of magnetic moment, $\omega_0 = (t_0)^{-1}$ and the dimensionless parameter $\omega^* = m(\omega\sigma)^2/2\varepsilon$ controls the strength of the parabolic confinement potential in the y-direction. These scaling turn all quantities into dimensionless (asterisk) form.

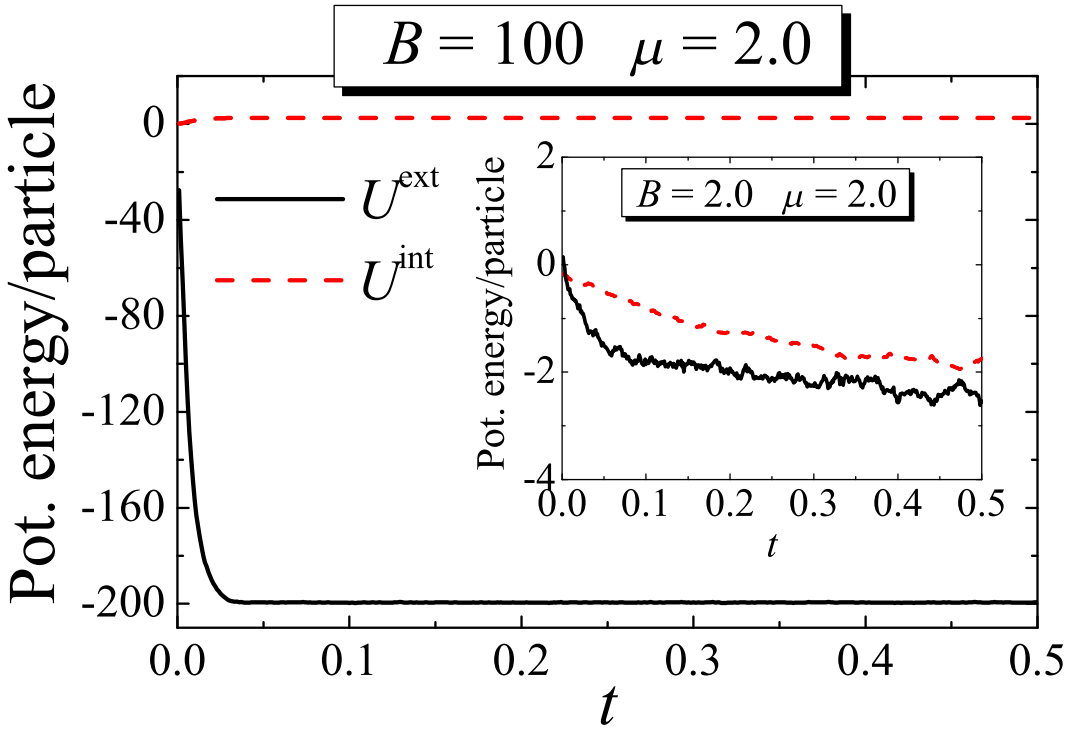

Figure 24 – Potential energy, as defined by Eqs. (4.4)-(4.5), per particle as a function of time t for $B = 100$, $\mu = 2.0$. In the inset we show the same, but for $B = 2$. In both cases, the number of particles in the computational unit cell was $N = 300$ and all the other parameters are given in Sec. 4.2.2.

Integrating the dimensionless over-damped equations of motion, we obtain the following Ermak-type algorithm (84) for updating the position ($\mathbf{r}_i^*$) and angle (θ_i^*) of particle i during the simulation time step Δt^*

$$\begin{aligned} \mathbf{r}_i^*(\Delta t^*) &= \mathbf{r}_i^*(0) + \Delta t^* \mathbf{f}_{ij}^* + \Delta t^* (\omega^*)^2 \mathbf{g}_i^* + \sqrt{2T^* \Delta t^*}\, \boldsymbol{\xi}_i^*, \\ \theta_i^*(\Delta t^*) &= \theta_i^*(0) + \Delta t^* \tau_i^* + \Delta t^* \tau_i^{*B} + \sqrt{2T^* \Delta t^*}\, \xi_i^*, \end{aligned} \tag{4.6}$$

where $\mathbf{f}_{ij}^* = -\sum_j \boldsymbol{\nabla}_i^* [V_{\rm dip}^* + V_{\rm ss}^*]$, $\mathbf{g}_i^* = -\boldsymbol{\nabla}_i^* [(y_i^*)^2]$, $\tau_i^* = |\boldsymbol{\mu}_i^* \times \sum_{j>i} \mathbf{B}_{ij}^{*\rm int}|$ (cf. A.1) and $\tau_i^{*B} = |\boldsymbol{\mu}_i^* \times \mathbf{B}^*|$. Furthermore, $V_{\rm dip}^*$ and $V_{\rm ss}^*$ are given by

$$V_{\rm dip}^* = \frac{\boldsymbol{\mu}_i^* \cdot \boldsymbol{\mu}_j^*}{|\mathbf{r}_{ij}^*|^3} - \frac{3(\boldsymbol{\mu}_i^* \cdot \mathbf{r}_{ij}^*)(\boldsymbol{\mu}_j^* \cdot \mathbf{r}_{ij}^*)}{|\mathbf{r}_{ij}^*|^5}, \tag{4.7}$$

$$V_{\rm ss}^* = 4/|\mathbf{r}_{ij}^*|^{12}. \tag{4.8}$$

From this point onward we will abandon the asterisk notation and all physical quantities are dimensionless, unless stated otherwise. In our simulations, we use the following parameters:

$\Delta t = 1.0 \times 10^{-6}$, $\omega = 10.0$, $\mu = 2.0$ and $T = 1.0$. Note that B and T can be related by the dimensionless parameter $c = |U^{\text{eff}}|/k_B T$, which is defined as the ratio between the coupling energy of a dipole particle with the effective magnetic field ($U^{\text{eff}} = U^{\text{int}} + U^{\text{ext}}$) and the thermal energy ($k_B T$). We also use a simulation box of length (in the x direction) $L_x = 375.0$, and linear density $\rho = N/L_x = 0.8$. We choose this value of L_x in order to cutoff the interaction potential for distances larger than $r = r_c = L_x/2 \approx 187.0$, at which the interaction energy between a pair of particles is approximately $V_{\text{dip}}(r)|_{r_c} \approx 1.0 \times 10^{-6}$. In the x direction, we apply periodic boundary conditions and in the transverse direction, the system is confined by the parabolic trap, which is controlled by the parameter ω. Note that in this work we set a value of ω which is large enough to prevent particles from bypassing each other, as we demonstrated in a previous study (157). This forces the system into a strict 1D chain of particles in the x direction. The initial configuration of the particles is chosen randomly and the system is equilibrated during $(1.0 - 5.0) \times 10^6$ simulation time steps. Other parameters which characterize the system are the magnitude of the external magnetic field (B) and the angle ϕ between $\mathbf{B}$ and the x-axis. Furthermore, the stochastic white noise $\boldsymbol{\xi}_i(t)$ is simulated using the Box-Müller transformation technique (83) and in all the results presented in this work, the error bars in the plots are smaller than the symbol size.

4.3 Interaction potential between two dipoles

Before we study the complete system (the model described in Sec. 4.2), let us first analyze the behavior of the dipole-dipole interaction potential $V_{\text{dip}}(r)$ between two particles as a function of ϕ (cf. Fig. 23), assuming that both dipoles are perfectly oriented in the direction of the external field. In this case, the interaction potential may be written as

$$V_{\text{dip}}(|\mathbf{r}|) = \frac{|\boldsymbol{\mu}|^2}{|\mathbf{r}|^3}\left[1 - 3\cos^2(\phi - \theta_r)\right] + 4|\mathbf{r}|^{-12}, \tag{4.9}$$

where θ_r (cf. Fig. 23) is the angle formed between the vector $\mathbf{r}$ and the x-axis. We assume the simplest case, where $\theta_r = 0^o$, which means that particles are forming a perfect one-dimensional chain along the x direction. The dependence of V_{dip} [Eq. (4.9)] on the distance r between two particles is presented in Fig. 25 for different values of ϕ. We found that for $\phi \gtrapprox 54^o$, the interaction potential is dominantly repulsive. On the other hand, for $\phi \lessapprox 54^o$, the interaction potential has a Lennard-Jones form (*e.g.*, $\phi = 0^o$ in Fig. 25). For small values of r, the repulsive term $4|\mathbf{r}|^{-12}$ is dominant. For intermediate values of r ($1.0 < r < 1.5$), the particle can be trapped in the potential well due to the presence of the attractive part in the interaction potential. For larger distances ($r \to \infty$), the interaction vanishes.

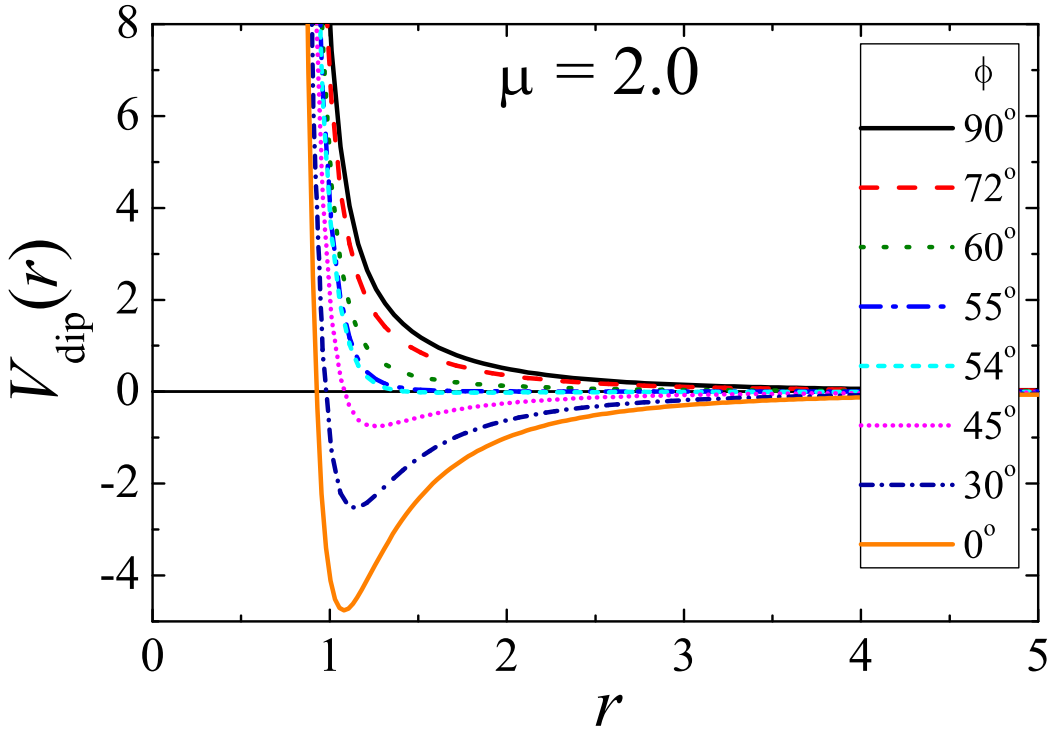

Figure 25 – Dipole-dipole interaction potential $V_{\text{dip}}(r)$ [Eq. (4.9)] as a function of the distance r between two dipoles and for different values of ϕ.

4.4 Influence of a strong external magnetic field on diffusion

The influence of a strong homogeneous external magnetic field on the diffusive properties of the model system described in Sec. 4.2.1 will now be investigated. The external field **B** with magnitude $B = 100$ [which is a typical strong field value used in experiments, see (167)] forms an angle ϕ with respect to the x-axis (cf. Fig. 23). Note that since we set $T = 1.0$, the parameter $c \approx 200 \gg 1$, which means thermal fluctuations are weak. We now investigate how diffusion depends on ϕ.

We will study the diffusive properties of the system through the analysis of the mean square displacement $W(t)$ along the x direction, defined as

$$W(t) = \left\langle \frac{1}{N} \sum_{i=1}^{N} [x_i(\tau + \delta t) - x_i(\tau)]^2 \right\rangle_\tau , \tag{4.10}$$

where N is the number of particles (we use a typical value of N=300–900 particles), τ is an arbitrary time origin (104), δt is the time interval between measurements and $\langle \cdot \rangle_\tau$ is an average over different time origins during the simulation (168).

4.4.1 Region (I): $55^o \lesssim \phi \leq 90^o$

First, we consider the external magnetic field perpendicular to the parabolic confinement channel, *i.e.* $\phi = 90^o$. In this case, the interaction is purely repulsive [$V_{\rm dip}(r) \propto (1/r)^3$] and the mean square displacement $W(t)$ [Fig. 26(a)] of the system exhibits a sub-diffusive regime [single-file diffusion (SFD)], with $W(t) = 2F_a t^{0.5}$ for time scales larger than the short-time normal diffusion regime (STND), which is characterized by $W(t) = D_0 t$ (169). The crossover time t_c between these two distinct regimes of diffusion can be estimated (104) as the time where the curves $D_0 t$ and $2F_a t^{0.5}$ intersect

$$D_0 t_c \approx 2F_a (t_c)^{0.5} \Rightarrow t_c \approx \left(\frac{2F_a}{D_0}\right)^2. \tag{4.11}$$

The mean square displacement for $\phi = 90^o$ and $\phi = 70^o$ are presented in Figs. 26(a)-(b), respectively. We found that for $55^o \lesssim \phi \leq 90^o$, *i.e.*, when the dipole-dipole interaction is purely repulsive (cf. Fig. 25), $W(t)$ has the following behavior

$$W(t) = \begin{cases} D_0 t & \text{for } t < t_c \\ 2F_a t^{0.5} & \text{for } t > t_c, \end{cases} \tag{4.12}$$

where a straightforward calculation using Eq. (4.11) gives $t_c \approx 7.58 \times 10^{-3}$ ($F_a \approx 4.79 \times 10^{-5}$ and $D_0 \approx 0.110 \times 10^{-5}$). In this region (I), the crossover time t_c and the SFD mobility F_a are independent of the value of ϕ.

4.4.2 Region (II): $0^o \leq \phi \lesssim 55^o$

For the case of $0^o \leq \phi \lesssim 55^o$, the attractive term present in the dipole-dipole interaction potential becomes more relevant with decreasing ϕ. As a consequence, we expect that the diffusion of the dipoles to be affected by the orientation of **B**. We found that for this region (II), the system exhibits the STND followed by a sub-diffusive regime, with $W(t) = 2F_b(\phi) t^{0.6}$, where now t_c and F_b depends on the angle ϕ and

$$W(t) = \begin{cases} D_0 t & \text{for } t < t_c(\phi) \\ 2F_b(\phi) t^{0.6} & \text{for } t > t_c(\phi), \end{cases} \tag{4.13}$$

with $t_c(\phi) \approx (2F_b(\phi)/D_0)^{2.5}$. The mean square displacement for $\phi = 50^o$ and $\phi = 0^o$ is presented in Figs. 26(c)-(d), respectively.

In Figs. 27(a)-(b) we show the mobility $F_b(\phi)$ in region (II) and the crossover time t_c as a function of ϕ, respectively. Note that both F_b and t_c decreases with decreasing ϕ in region (II). On the other hand, as stated above, the crossover time t_c is constant in region (I).

The decrease of t_c and F_b, in region (II), with decreasing ϕ can be explained by the decrease of the minimum inter-particle distance between neighbor particles [cf. Fig. 28(a)].

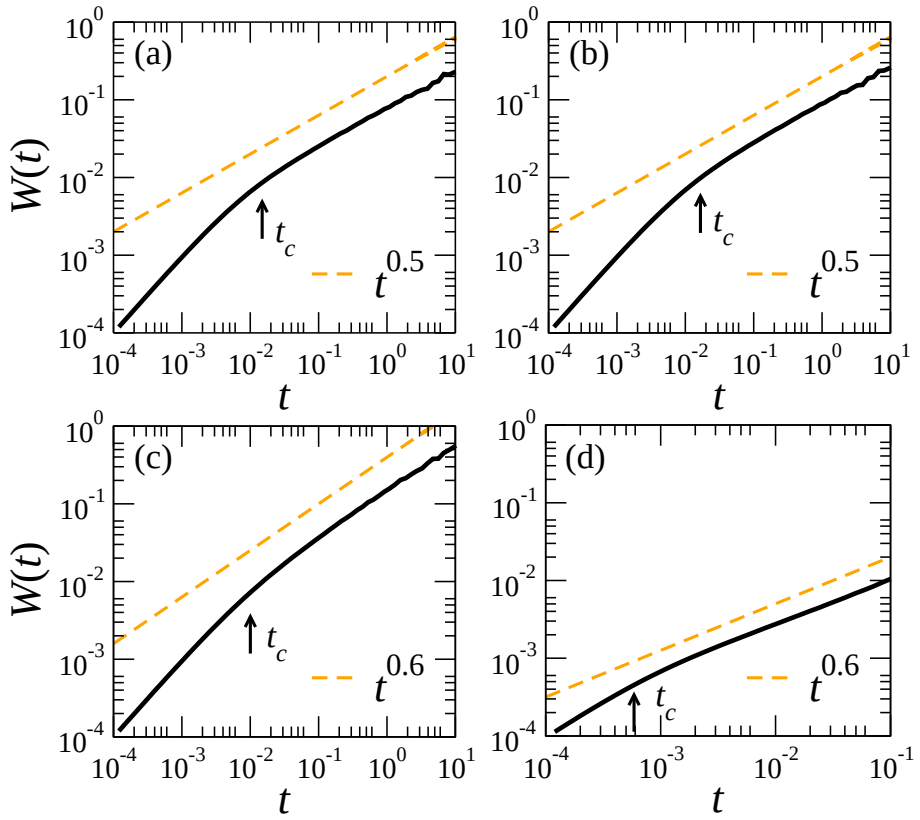

Figure 26 – Log-log plot of the mean square displacement (solid black curves) $W(t)$ as a function of the time t for $B = 100$ and (a) $\phi = 90^o$, (b) $\phi = 70^o$, (c) $\phi = 50^o$ and (d) $\phi = 0^o$. The dashed orange lines are a guide to the eye and the crossover time t_c for each case is indicated by the vertical arrow.

When the interaction potential is dominated by the repulsive part of the potential [region (I)], the particles are distributed homogeneously along the unconfined direction [Fig. 29(a)], *i.e.*, the minimum inter-particle distance between neighbors is approximately constant. In region (II), the attractive term in the interaction potential becomes more relevant, and the system starts to form clusters of chains. Therefore, the particles are no longer homogenously distributed along the channel. The minimum inter-particle distance decreases with decreasing ϕ and the crossover time t_c is smaller than in region (I) because particles "feel" the interaction with neighboring particles much faster. Also, since the particles can be trapped inside the clusters of chains, the mobility (F_b) is reduced with decreasing ϕ.

4.5 Exponent of diffusion (α) in the intermediate (ITR) sub-diffusive regime

In the previous section we showed that the MSD [$W(t)$] exhibits two different regimes of sub-diffusion depending on the region [(I) or (II)]: the exponent of diffusion (α) in the sub-diffusive

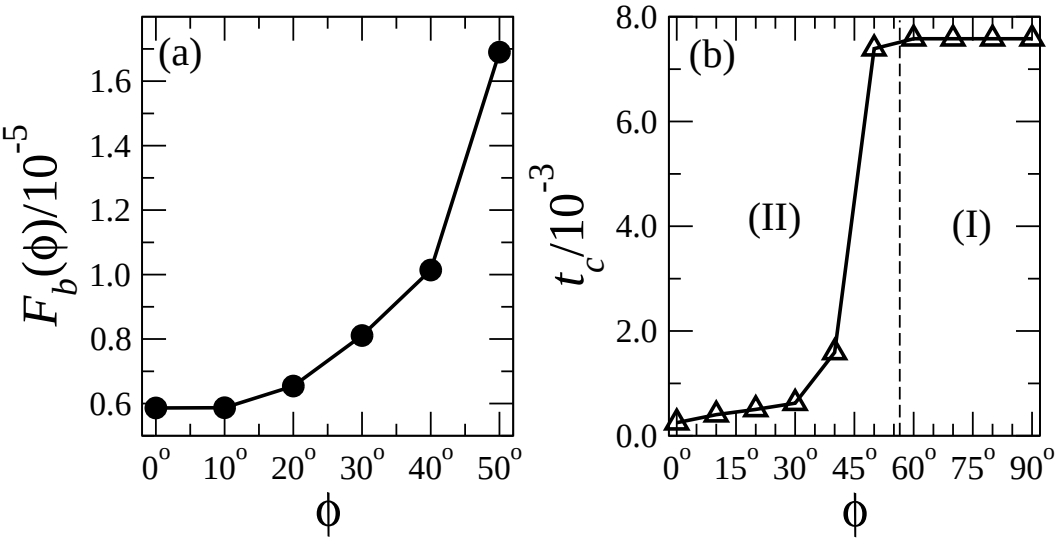

Figure 27 – (a) Mobility F_b in region (II) as a function of ϕ and (b) crossover time t_c between the STND regime and the sub-diffusive regime as a function of ϕ. The solid lines are a guide to the eye. The dashed vertical line in (b) divides regions with (II) and without (I) an attractive part in the inter-particle interaction potential.

regime changes from $\alpha = 0.5$ to $\alpha = 0.6$ as the angle ϕ is decreased from $\phi = 90^o$ to $\phi = 0^o$. The exponent α is calculated by fitting the MSD of our simulation data in the region of interest (for instance, the ITR regime) according to the relation $W(t) \propto t^{\alpha}$. The increase in the diffusion mechanism can be seen in Fig. 28(b), where α is presented as a function of the orientation ϕ. Note that α increases with decreasing ϕ, which can be understood in terms of the dipole-dipole interaction dependence on ϕ. For $\phi \gtrsim 55^o$, the interaction potential is mainly repulsive and therefore it leads the system into a sub-diffusive behavior, where $\alpha = 0.5$. The scaling $W(t) \propto t^{0.5}$ has been observed experimentally in repulsive interacting particles (41), and was also found from simulations (104, 105, 154) and through analytical (56, 45) calculations. In this case, the minimum inter-particle distance is approximately equal to $d \approx (\rho)^{-1} \approx 1.2$. On the other hand, for $\phi \lesssim 55^o$, the interaction potential exhibits a competition between a repulsive and an attractive term (cf. Fig. 25). The attractive part of the potential forces the formation of clusters of chains [Fig. 29(b)], resulting in empty spaces along the unconfined direction. This is illustrated in Fig. 28(a), where the minimum distance between particles d is shown as a function of ϕ. Note that d decreases with decreasing ϕ. Since the system has a fixed density ρ, the empty spaces between the clusters of chains results in an increase of diffusion, which subsequently gives an exponent of diffusion α that is slightly larger than 0.5.

In order to better understand the increase of the exponent of diffusion α, we calculate the mean square displacement of each jth particle $[W_j(t)]$ using an expression similar to Eq. (4.10)

$$W_j(t) = \langle [x_j(\tau + \delta t) - x_j(\tau)]^2 \rangle_\tau, \tag{4.14}$$

where $j = 1, ..., N$ represents each individual particle and $\langle \cdot \rangle_\tau$ is an average over different time

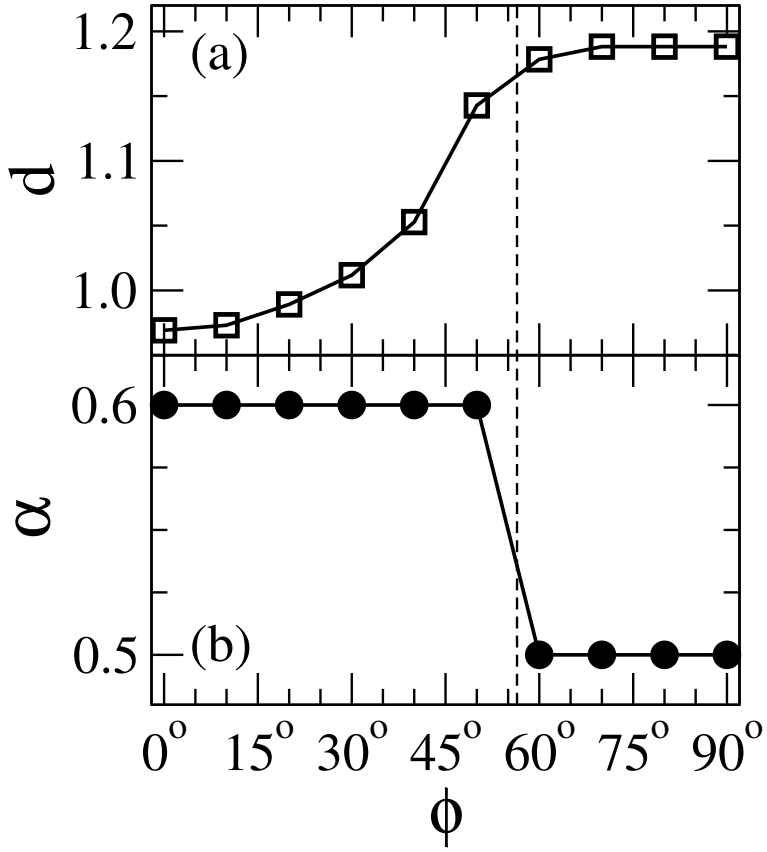

Figure 28 – (a) Minimum inter-particle distance d between neighboring particles for $B = 100$ and $T = 1.0$ as a function of the orientation ϕ of the external field. (b) Exponent of diffusion (α) as a function of the orientation ϕ of the external magnetic field. Note that d decreases with decreasing ϕ in the region $0^o < \phi \lesssim 55^o$, which is the same region where we found the increase of the diffusion mechanism [cf. panel (b)]. The solid lines are a guide to the eye.

origins during the simulation. In Figs. 30(a)-(b) we show $W(t)$ (open black circles) and $W_j(t)$ (gray triangles) for $\phi = 90^o$ and $\phi = 0^o$. Note that for the case $\phi = 90^o$, $W_j(t)$ deviates very little from the mean square displacement of the system $W(t)$. In this case the particles in the system are distributed homogenously along the unconfined direction. Therefore, the diffusion of a tagged particle should be the same as the diffusion of the whole system. On the other hand, for the case of $\phi = 0^o$, $W_j(t)$ deviates [much more] from $W(t)$ [than in the case $\phi = 90^o$]. This is caused by the asymmetry along the unconfined direction. In this case, it is possible that a tagged particle can diffuse differently than the whole system because of the formation of clusters of chains [cf. Fig. 29(b)]. For instance, particles which are located at the borders of the cluster of chains diffuse faster than particles which are inside the cluster. This is the reason for an exponent α that is slightly larger than 0.5 in the case where the interaction potential has both repulsive and attractive terms [Region (II), see Sec. 4.4.2].

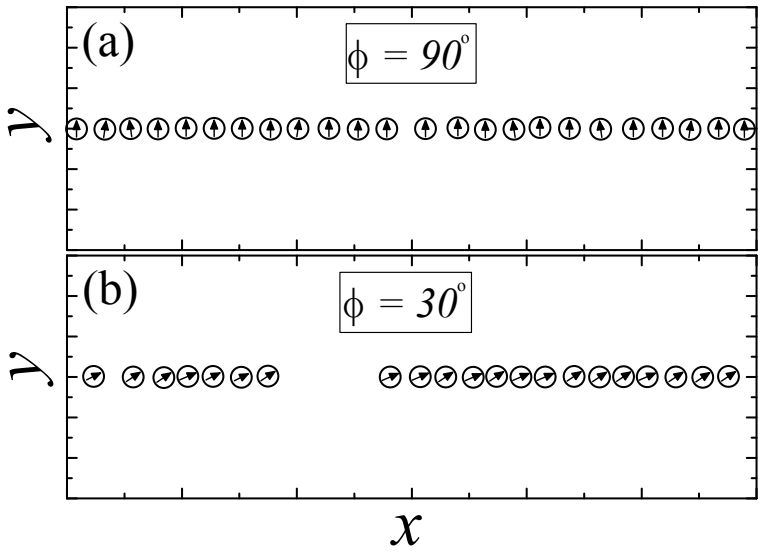

Figure 29 – Typical snapshots of the system after 10^6 simulation time steps for (a) $\phi = 90^o$ and (b) $\phi = 30^o$. Other parameters are $B = 100$ and $T = 1.0$.

4.6 Weak magnetic fields

In the previous section, we showed that the diffusion mechanism of the system is affected by the orientation of the strong external magnetic field. Now, we turn to the question of how the magnitude of **B** influences the diffusive properties of the system. To this end, we perform similar simulations using the same parameters of the previous section, but with a weaker magnetic field $B = 0.1$. Note that since we set $T = 1.0$, the parameter $c \approx 0.2 \ll 1$, which means thermal fluctuations are strong. The mean square displacement (in log-log scale) as a function of the time is presented in Fig. 31 for different values of ϕ.

There are two important observations regarding the results for $B = 0.1$: (i) note that the ITR regime for this case is shifted to larger time intervals as compared to the previous case (see Fig. 26), which is a consequence of the weaker coupling of the dipoles with the external magnetic field, leading the system to larger relaxation (crossover) times. Here, the ITR regime can be identified in the time interval $10^1 \lesssim t < 10^2$; (ii) since the external magnetic field is small (compared to the case of the previous section, $B = 100$), the coupling between the magnetic dipoles and the external field is weaker which results in an approximately ϕ-independent regime of diffusion [cf. Fig. 31]. This means that the exponent of diffusion α in the ITR regime is a constant ($\alpha = 0.35$) which is independent of the orientation of the external magnetic field. We will further discuss this particular value of α in the following section. Note that, as opposed to the case of strong magnetic field, the clustering of particles in a chain-like configuration along the unconfined direction is less pronounced, as illustrated in Fig. 32. Note that the orientation of the dipoles of the ferromagnetic particles is almost random.

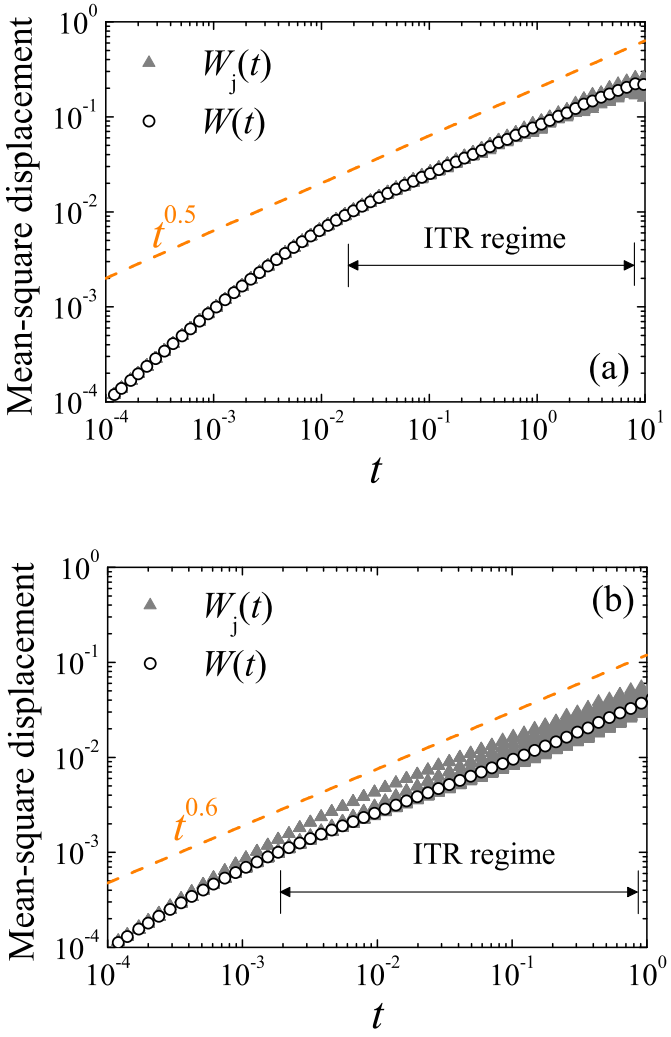

Figure 30 – Mean-square displacement of the system [open black circles, $W(t)$] and mean square displacement of individual particles [gray triangles, $W_j(t)$] as a function of the time t for two different values of $\phi =$ (a) 90^o and (b) 0^o. The dashed orange lines are a guide to the eye. Other parameters are $B = 100$ and $T = 1.0$.

4.7 Influence of the strength of the magnetic field

In this section, we further investigate how the strength B of the external magnetic field influences the diffusion of the system. We analyze the case for $\phi = 90^o$, where the SFD is found in the ITR regime for $B = 100$ [see Fig. 28(b)]. From the calculations of the MSD using Eq. (4.10) for different values of B, we found that for $B \gtrsim 10$, the SFD regime is always present in the ITR regime, *i.e.*, $W(t) \propto t^{0.5}$. Therefore, we only investigate the region $0.1 \leq B \leq 10.0$, and the results are plotted in Figs. 33(a)-(d). For $B = 10$ [Fig. 33(a)], as stated above, the SFD regime is present in the ITR regime, which means $\alpha = 0.5$.

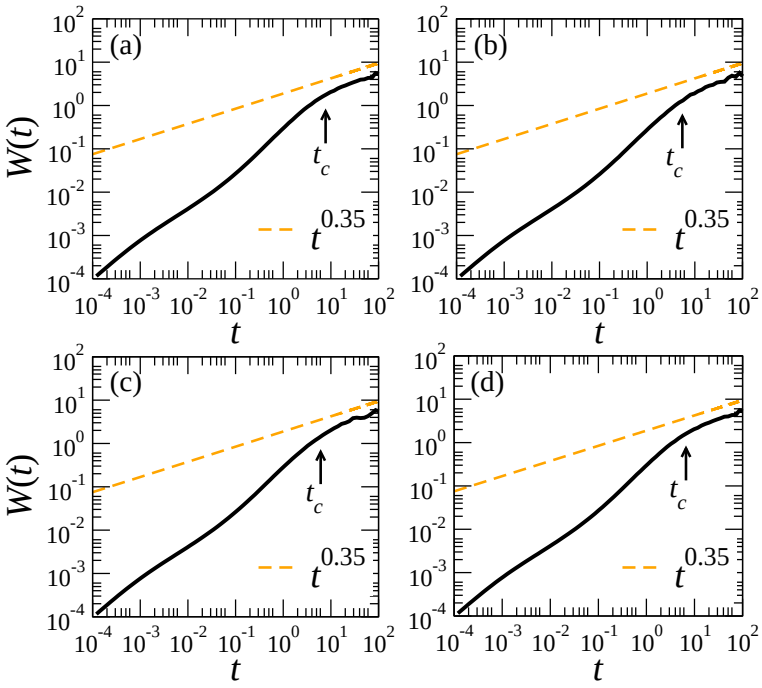

Figure 31 – Log-log plot of the mean square displacement (solid black curves) $W(t)$ as a function of the time t for $B = 0.1$ and (a) $\phi = 90^o$, (b) $\phi = 70^o$, (c) $\phi = 50^o$ and (d) $\phi = 0^o$. The dashed orange lines are a guide to the eye and the crossover time t_c for each case is indicated by the vertical arrow.

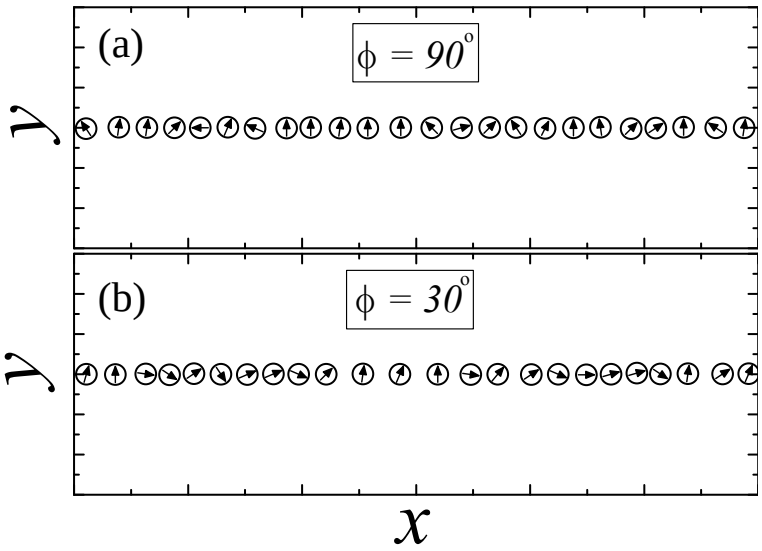

Figure 32 – Typical snapshots of the system after 10^6 simulation time steps for (a) $\phi = 90^o$ and (b) $\phi = 30^o$. Other parameters are $B = 0.1$ and $T = 1.0$.

We found that by decreasing the value of B, the exponent of diffusion (α) decreases from $\alpha = 0.5$ to $\alpha = 0.35$, as shown in Fig. 34. The reason for this behavior is explained by the following: as the magnetic field is decreased, its coupling with the dipoles also decreases, leading to an increase in the rotational movement of the dipoles. Therefore, the energy of a

dipole is more evenly distributed between translational and rotational motion. Recall that for large values of B ($= 100$), the dipoles were almost completely aligned with the field. The increase in the rotation of the dipoles thus leads to a slowing down of the translational diffusion, *i.e.*, α decreases with decreasing B.

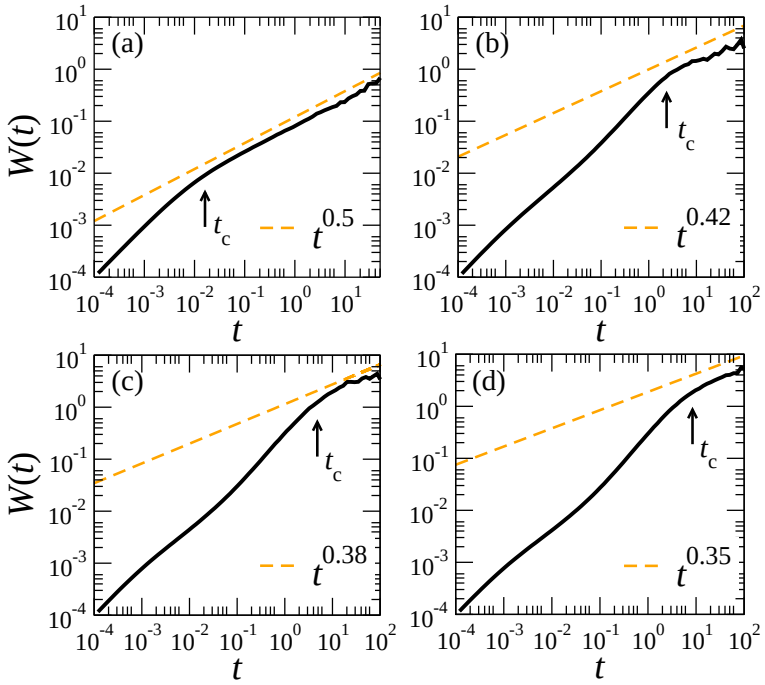

Figure 33 – Log-log plot of the mean square displacement (solid black curves) $W(t)$ as a function of the time t for $\phi = 90^o$ and (a) $B = 10$, (b) $B = 2$, (c) $B = 1$ and (d) $B = 0.1$. The dashed orange lines are a guide to the eye.

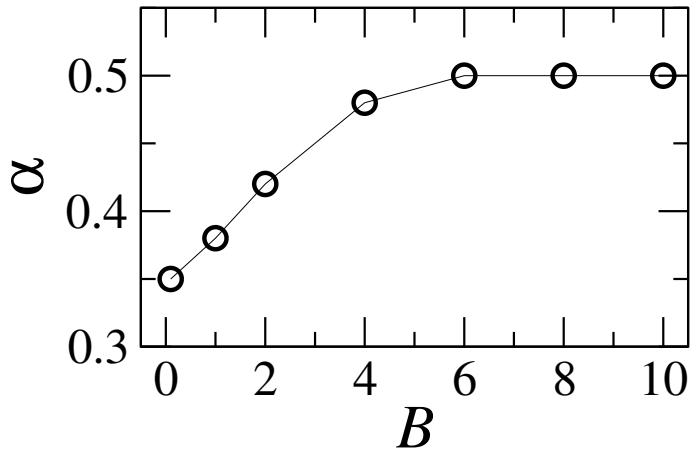

Figure 34 – Exponent of diffusion α (in the ITR regime) as a function of the strength B of the external magnetic field for $\phi = 90^o$. The solid line is a guide to the eye.

In order to strengthen this conclusion, we calculate the mean square angular displace-

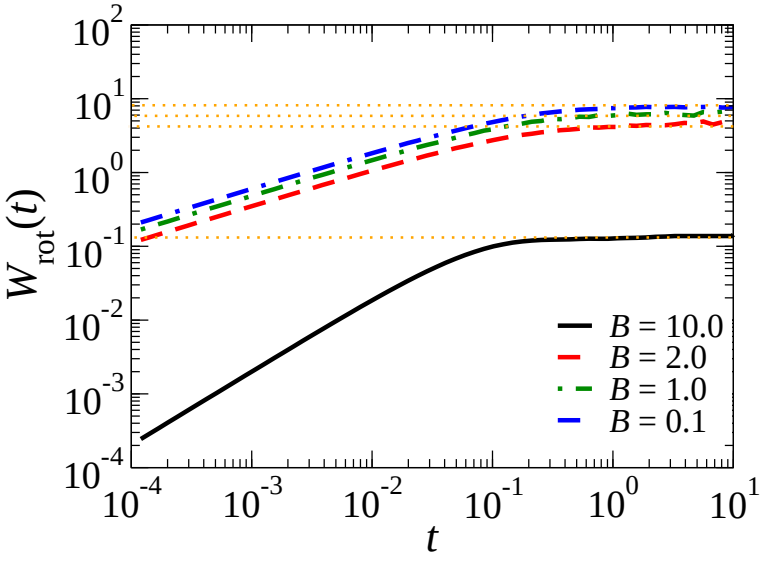

Figure 35 – Log-log plot of the mean square angular displacement $W_{\rm rot}(t)$ as a function of the time t for $\phi = 90^o$ and $B = 10$, $B = 2$, $B = 1$ and $B = 0.1$. The dotted orange horizontal lines correpond to the saturation values of $W_{\rm rot}(t)$.

ment (MSAD) $W_{\rm rot}(t)$, which is defined similary to Eq. (4.10)

$$W_{\rm rot}(t) = \left\langle \frac{1}{N}\sum_{i=1}^{N}[\theta_i(\tau+\delta t) - \theta_i(\tau)]^2 \right\rangle_\tau , \tag{4.15}$$

where θ_i is the angular coordinate of the ith particle (cf. Fig 23). The results of calculations of the MSAD are shown in Fig. 35 for different values of B. Note that for all values of B, $W_{\rm rot}(t)$ saturates after the initial motion. Furthermore, the MSAD curves increases with decreasing B, which indicates that the rotational motion of the dipoles increases with decreasing strength of the external magnetic field.

4.8 Concluding remarks

We studied a system of interacting ferromagnetic dipoles, confined in a q1D channel, that are subjected to a homogeneous external magnetic field. The analysis of the mean square displacement $W(t)$ indicates that the diffusive properties of the system depends on the orientation and on the strength of the external field. For the case of strong magnetic fields (we considered $B = 100$ as an example), we found that the exponent of diffusion α increases with decreasing orientation ϕ [cf. Fig. 28(b)] of the external field, *i.e.*, directing the magnetic field towards the direction parallel to the channel. This increase of diffusion was explained by the dependence of the dipole-dipole interaction potential on ϕ. For $\phi \gtrsim 55^o$, the interaction is dominantly repulsive, leading the system into sub-diffusive motion in the ITR regime. On the other hand, for $\phi \lesssim 55^o$, the interaction potential has a Lennard-Jones form, which creates a competition

between the repulsive and the attractive term of the dipole-dipole potential. The attractive part of the potential leads the system into clusters of chains [Fig. 29(b)]. The empty spaces in the system allow for an increase in diffusion.

For small values of the magnetic field (*e.g.* $B = 0.1$), the coupling between the magnetic dipoles and **B** is weak and the dynamic behavior of the system becomes almost independent of the orientation of **B**. This results in an exponent α, in the sub-diffusive regime, that is a constant ($\alpha = 0.35$) for all values of the orientation of the external magnetic field. The fact that for weak magnetic fields the exponent of diffusion is smaller than 0.5 (the slowing down of translational diffusion) was explained by the weak coupling of the dipoles with the external field, leading to an increase in the rotational motion of the dipoles. Note that the value of $\alpha = 0.35$ only holds for the ITR regime, as discussed in the Introduction. In both cases (strong and weak external magnetic fields), the system is still in the single-file, diluted regime.

Our results show that the diffusion mechanism in this system can be controlled by tuning the orientation and the strength of the external magnetic field. This will allow one to control the dynamics of magnetic particles in narrow channels by simply tuning the parameters which regulate the external magnetic field.

Related publications

• **D. Lucena**, F. F. Munarin, W. P. Ferreira, G. A. Farias, and F. M. Peeters, *Tunable diffusion of magnetic particles in a quasi-one-dimensional channel*, Phys. Rev. E **87**, 012307 (2013).

5 Single-file and normal diffusion of magnetic colloids

Diffusive properties of interacting magnetic dipoles confined in a parabolic narrow channel and in the presence of a periodic modulated (corrugated) potential along the unconfined direction are studied using Brownian dynamics simulations. We compare our simulation results with the analytical result for the effective diffusion coefficient of a single-particle by Festa and d'Agliano (170) and show the importance of inter-particle interaction on the diffusion process. We present results for the diffusion of magnetic dipoles as a function of linear density, strength of the periodic modulation and commensurability factor.

5.1 Introduction

Manipulation and control of magnetic colloidal particles have greatly increased over the last years. Recent advances include fabrication of anisotropic magnetic particles (171) which can have a wide range of applications, from drug deliver mechanisms (121, 172) to fabrication of tunable self-assembly colloidal devices (173, 174). Further examples of applications of anisotropic particles are the so-called colloidal molecules (175, 176), the patchy colloids (177, 178, 179) and the magnetic Janus colloids (180). The use of magnetic dipoles is particularly interesting due to the fact that the inter-particle interaction potential introduces a natural source of anisotropy. This is achieved by the application of a tunable external static homogeneous (131, 181) or oscillating (182, 183) magnetic field ($\boldsymbol{B}$). Diffusion and transport of colloidal particles in periodic modulated (corrugated) channels (184) represent important phenomena which allows the understanding of several mechanisms in soft condensed matter, *e.g.*, molecular and cell crowding in biological systems (185, 186), pinning-depinning transition of vortices in type-II superconductors (187, 188, 189), and elastic strings (190, 191). Theoretical models which describe the trapping dynamics of modulated systems include, for instance, continuous time random walk (CTRW) (192) and random walk with barriers (193). Experimentally, corrugated periodic (12) or random (10) landscapes can be realised, *e.g.*, by light fields allowing the control of the colloidal particles. Furthermore, diffusion in modulated landscapes is often anomalous, *i.e.*, the mean square displacement $W(t)$ (MSD) follows a power-law [$W(t) \propto t^{\alpha}$] with an exponent $0 < \alpha < 1$ (194).

Diffusion in very narrow channels is governed by single-file diffusion (SFD) (195). An interesting quantity in this case is the single-file mobility factor, F. This factor has been previously analysed by Herrera-Velarde and Castañeda-Priego (169) for the case of a system of

repulsive interacting superparamagnetic colloids. In our case, however, the attractive part of the inter-particle interaction potential [Eq. (5.12)] introduces an anisotropy in the system. This means that the external magnetic field, regulated by the magnitude of $\boldsymbol{B}$ and its direction ϕ, now plays an important role in tuning the diffusive properties of the system. The effects of these two parameters in a system without external modulation has been recently investigated by us in Ref. (196). Here we extend these results to the case where the narrow channel is periodically modulated along the unconfined direction. We find that the commensurability between the inter-particle distance and the period of the modulation is an essential factor that strongly influences the diffusion.

5.2 Single-particle in an external periodic potential

First, we consider the simplest case of a single-particle diffusing in one dimension and subjected both to Brownian motion and to an external periodic potential landscape. The equation of motion for the particle is given by the over-damped Langevin equation (197)

$$\zeta \frac{dx}{dt} = -\frac{\partial V(x)}{\partial x} + \xi(t), \tag{5.1}$$

where ζ is the viscosity of the medium, x is the position of the particle, t is time, $V(x)$ is the external one-dimensional periodic potential of the form $V(x) = V_0 \cos(2\pi x/L)$, where V_0 and L are the magnitude and periodicity of the external potential, respectively. Essential here is that $V(x)$ is periodic but it does not necessarily need to be of cosine form. The only condition is that the external potential obeys the periodicity relation, $V(x) = V(x+L)$. Furthermore, $\xi(t)$ is a delta correlated noise which follows the well-known properties (i) $\langle \xi(t) \rangle = 0$ and (ii) $\langle \xi(t)\xi(t') \rangle = 2\zeta k_B T \delta(t-t')$. k_B is the Boltzmann constant and T is the absolute temperature of the heat bath.

In the case where the particle is free, *i.e.*, $V_0 = 0$, it is straightforward to show (197) that the self-diffusion coefficient of the particle is given by the Einstein relation $D_0 = k_B T/\zeta$. In the presence of a periodic potential $V(x)$, previous studies (170, 198, 199) showed that the self-diffusion coefficient of the particle is modified into

$$\frac{D_{\text{eff}}}{D_0} = \frac{L^2}{\int_0^L dx \exp\{V(x)/k_B T\} \int_0^L dz \exp\{-V(z)/k_B T\}}. \tag{5.2}$$

It is easy to see that when $V(x) = 0$, Eq. (5.2) reduces to D_0 as it should be. If we consider the case of $L = 2\pi\sigma$ and $x \to x'\sigma$ [$V(x') = V_0 \cos(x')$], the solutions of the integrals in (5.2) are known (200) and given by

$$\sigma \int_0^{2\pi} dx' \exp\{V(x')/k_B T\} = 2\pi\sigma I_0(V_0/k_B T), \tag{5.3}$$

$$\sigma \int_0^{2\pi} dx' \exp\{-V(x')/k_B T\} = 2\pi\sigma I_0(-V_0/k_B T), \tag{5.4}$$

where $I_0(y)$ are the modified Bessel functions of the first kind and σ is a unit of distance. Therefore, the self-diffusion coefficient $D_{\rm eff}$ depends only on the ratio V_0/k_BT. A series representation of $I_0(y)$ can be written as (201)

$$I_0(y) = 1 + \frac{(y/2)^2}{(1!)^2} + \frac{(y/2)^4}{(2!)^2} + \ldots \tag{5.5}$$

Taking the first order approximation in Eq. (5.5), we have that $D_{\rm eff}/D_0$ is given by

$$\frac{D_{\rm eff}}{D_0} \simeq \frac{1}{[1+(y/2)^2]^2}. \tag{5.6}$$

Note that for $y = V_0/k_BT \ll 1$, $D_{\rm eff}/D_0 \to 1$, as expected. On the other hand, for $y = V_0/k_BT \gg 1$, the modified Bessel function $I_0(y)$ can be written to a first order approximation as (202) $I_0(y) \simeq e^y/\sqrt{2\pi y}$. Therefore, $D_{\rm eff}/D_0$ has the form

$$\frac{D_{\rm eff}}{D_0} \simeq (2\pi y)e^{-2y}. \tag{5.7}$$

For $y = V_0/k_BT \gg 1$, $D_{\rm eff}/D_0 \to 0$. Both limiting cases (5.6) and (5.7) are shown in Fig. 36.

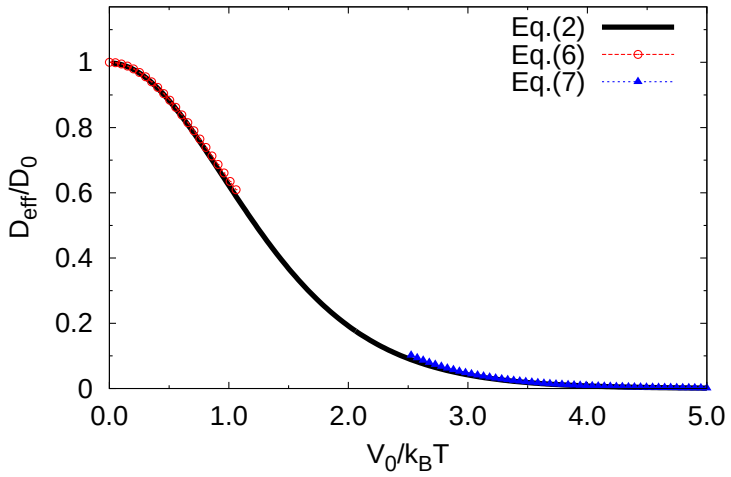

Figure 36 – Effective self-diffusion coefficient $D_{\rm eff}/D_0$ of a single-particle in one dimension in the presence of a thermal bath and a periodic potential $V(x') = V_0\cos(x')$.

5.3 Interacting magnetic dipoles

We now turn to the problem where instead of a single-particle we have N interacting magnetic dipoles of diameter σ and magnetic moment $\boldsymbol{\mu}$ diffusing in the plane (x,y). The geometry of the plane is then modulated by two external potentials, namely (i) a parabolic transversal confinement potential in the y direction and (ii) a periodic potential in the x direction. We also

apply an external homogeneous magnetic field $\boldsymbol{B}$ which can form an angle $0^o \leq \phi \leq 90^o$ with the x axis. In this more complex situation, the equations of motion which describe the dynamics of particle i are given by N over-damped coupled Langevin equations

$$\zeta \dot{\mathbf{r}}_i = -\sum_{j>i} \boldsymbol{\nabla} V_{ij}^{\text{int}} - \boldsymbol{\nabla}[V_{\text{mod}}(x_i) + V_{\text{conf}}(y_i)] + \boldsymbol{\xi}_i(t), \tag{5.8}$$

$$\zeta \sigma^2 \dot{\theta}_i \hat{\mathbf{z}} = \boldsymbol{\tau}_i + \boldsymbol{\tau}_i^{\boldsymbol{B}} + \sigma \xi_i(t) \hat{\mathbf{z}}, \tag{5.9}$$

where $\mathbf{r}_i = x_i\hat{\mathbf{x}} + y_i\hat{\mathbf{y}}$ is the position vector of particle i and θ_i is the angle between the vector $\boldsymbol{\mu}_i$ and the x axis. $\boldsymbol{\tau}_i$ and $\boldsymbol{\tau}_i^{\boldsymbol{B}}$ are the torque due to the magnetic field created on particle i by all other particles and the torque created by the external magnetic field $\boldsymbol{B}$, respectively. A similar set of equations (5.8)-(5.9) was recently used in Ref. (196), and therefore we report only on the results related to the presence of the modulation in the x direction (203, 204)

$$V_{\text{mod}}(x_i) = V_0 \cos\left(\frac{2\pi x_i}{L}\right). \tag{5.10}$$

The parabolic transversal confinement is given by

$$V_{\text{conf}}(y_i) = \frac{1}{2} m\omega^2 y_i^2, \tag{5.11}$$

where ω is the strength of the confinement (frequency) and m is the mass of the identical particles. Furthermore, the pair interaction potential V_{ij}^{int} is given by

$$V_{ij}^{\text{int}} = \frac{\mu_0}{4\pi}\left[\frac{\boldsymbol{\mu}_i \cdot \boldsymbol{\mu}_j}{|\mathbf{r}_{ij}|^3} - \frac{3(\boldsymbol{\mu}_i \cdot \mathbf{r}_{ij})(\boldsymbol{\mu}_j \cdot \mathbf{r}_{ij})}{|\mathbf{r}_{ij}|^5}\right] + 4\varepsilon\left(\frac{\sigma}{|\mathbf{r}_{ij}|}\right)^{12}, \tag{5.12}$$

where μ_0 is the medium permeability, $\mathbf{r}_{ij}$ is the inter-particle separation vector between a pair of particles i and j and ε is an energy parameter in order to prevent particles from coalescing into a single point.

Following previous works (196, 203, 204), we use an Ermak-type algorithm (84) to integrate equations (5.8)-(5.9). The simulations were performed with fixed parameters: $\Delta t = 1.0 \times 10^{-4}(\zeta\sigma^2/k_BT)$, $\mu = 1.0\sqrt{4\pi k_BT\sigma^3/\mu_0}$ and $B = 100\sqrt{k_BT\mu_0/4\pi\sigma^3}$. We choose $\varepsilon = k_BT$ as unit of energy, σ as unit of distance and time is measured in units of $t_B = \zeta\sigma^2/k_BT$. Finally, the stochastic white noise $\boldsymbol{\xi}_i(t)$ is simulated using the Box-Müller transformation technique (83) and in all the results presented in this work, the error bars in the plots are smaller than the symbol size. Similarly to our previous paper (196), hydrodynamic interactions (HI) are not taken into account. Such interactions may have an impact on the diffusion properties [and in general on the dynamical properties, see, *e.g.* Ref. (205)] for the case of highly concentrated colloidal suspensions, which are not considered in the present work.

In order to study diffusion we calculate the mean square displacement (MSD) $W(t)$, defined as (104)

$$W(t) = \left\langle N^{-1}\sum_{i=1}^{N} |\mathbf{r}_i(t) - \mathbf{r}_i(0)|^2 \right\rangle, \tag{5.13}$$

where we use a typical value of $N = 300 - 900$ particles, t is the time and $\langle \ldots \rangle$ is an average over different time origins during the simulation (168). This equation can be split in two terms, namely $W_x(t)$ and $W_y(t)$, where the first refers to the mean square displacement in the x direction and the latter refers to the mean square displacement in the y direction.

The system is tuned by three parameters, namely (i) the linear density, $\rho = N/L_x$ where L_x is the size of the computational unit cell in the x direction and N is the total number of particles, (ii) the angle ϕ of the external magnetic field, and (iii) the strength V_0 of the external modulation in the x direction. Note that since we are using periodic boundary conditions in the x direction, we have to guarantee the continuity of the external modulation at the borders of the computational unit cell. This is achieved by introducing the relation

$$L_x = nL, \tag{5.14}$$

where $n \in Z^+$ and it represents the number of minima (or maxima) of the external modulation within the computational unit cell.

5.4 Normal and single-file diffusion for fixed linear density

5.4.1 Case $\omega = 1.0\sqrt{2k_BT/m\sigma^2}$

In this section, we set the transversal confinement parameter $\omega = 1.0\sqrt{2k_BT/m\sigma^2}$ and $\phi = 90^o$. A snapshot of the configuration of the system together with the contour plot of the periodic modulation and transversal confinement is shown in Fig 37. The mean square displacement in the x direction $W_x(t)$ [Eq. (5.13)] for different values of V_0/k_BT is shown in Fig. 38. Note that for all the values of V_0/k_BT, except for 4.0 and 5.0, $W_x(t)$ exhibits a linear dependence on time t for large time scales

$$\lim_{t \gg t_N} W_x(t) = 2D_s t, \tag{5.15}$$

where D_s is the self-diffusion coefficient and t_N (indicated by gray open diamonds) is the time scale at which this normal diffusion regime is recovered. Note that since the system is coupled to a heat bath (k_BT), the normal diffusion regime should be recovered for any value of the ratio V_0/k_BT, with the condition that $t_N \to \infty$ for $V_0/k_BT \to \infty$. In other words, this means that the intermediate regime (where $W(t)$ exhibits a slower-than-linear dependence on time or $W(t) =$ const) extends over a larger time interval for larger values of V_0/k_BT. This intermediate regime is generally associated with a "cage" effect, which in our case is represented by the localization of particles in the potential minima. A similar effect was found previously in simulations on mono-disperse glassy systems (206) and Lennard-Jones binary mixtures (207). However, in these works, the caging effect was not induced by an external modulation but rather by many-body effects related to the specificities of their system.

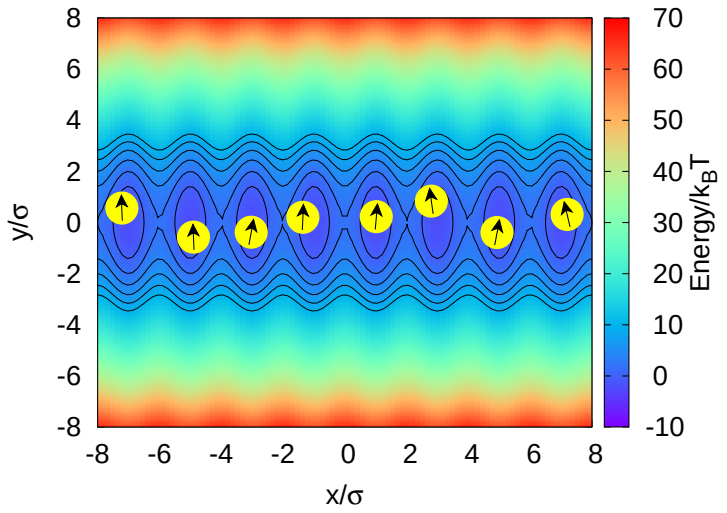

Figure 37 – Snapshot of the configuration of the system for $V_0/k_BT = 2.0$. The particles are represented by yellow circles where the black arrows indicate the direction of the dipoles. The contour plot of the potential $V_{\mathrm{mod}}(x) + V_{\mathrm{conf}}(y)$ is also shown. The linear density is $\rho = 0.5\sigma^{-1}$ and the transversal confinement strength is $\omega = 1.0\sqrt{2k_BT/m\sigma^2}$.

From these results, we also note that, as expected from previous section, the self-diffusion coefficient depends on the ratio V_0/k_BT. This dependence is shown in Fig. 39, where D_s decreases with increasing V_0/k_BT. D_s is obtained by fitting our data with Eq. (5.15). Note that even though the behaviour of D_s as a function of the ratio V_0/k_BT is qualitatively similar to $D_{\mathrm{eff}}(V_0/k_BT)$ for a single-particle, it is clear that $D_s < D_{\mathrm{eff}}$. This difference between D_s and D_{eff} is due to correlations between the particles, which now couples the movement of the dipoles through the interaction potential. We estimate this difference by calculating the ratio $R = D_s/D_{\mathrm{eff}}$ which is shown in the inset of Fig. 39. Note that R drops to zero as V_0/k_BT increases. This means that in both cases, *i.e.*, for single-particle and for interacting particles, the self-diffusion coefficient goes to a value very close to zero [but does not vanish completely, see Sec. IIIB of Ref. (208)] as V_0/k_BT increases. Therefore, there is no diffusion until temperature is sufficiently high to allow the escape of the particles from the potential wells (209). The effect of the linear density ρ on the self-diffusion coefficient, D_s, will be discussed in Sec. 5.5.

5.4.2 Case $\omega = 10.0\sqrt{2k_BT/m\sigma^2}$

In the case where the transversal confinement potential is increased, the fluctuations of the particles in the y direction becomes smaller. This effect of confinement brings the system into the single-file (SF) regime, which means that particles cannot bypass each other (157). This special geometric constraint leads to a phenomenon called single-file diffusion (SFD), in which one of the most striking feature is that the long-time mean square displacement $W_x(t)$ of a

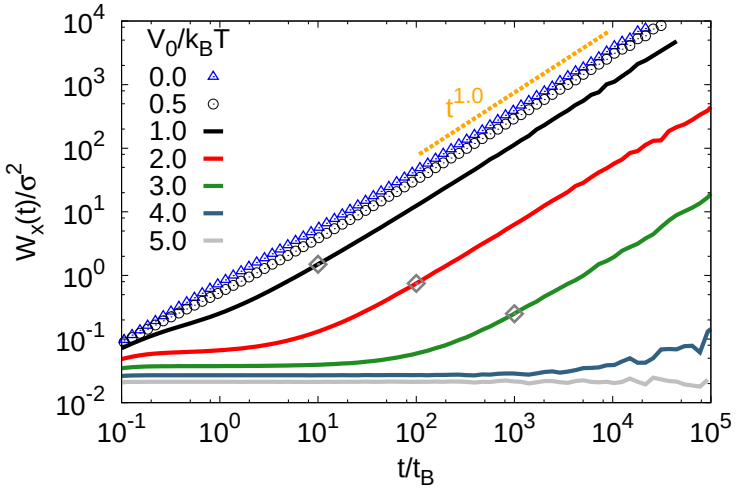

Figure 38 – Log-log plot of the mean square displacement in the x direction $W_x(t)$ as a function of time t for different values of the ratio V_0/k_BT. The yellow dotted line is a guide to the eye. The open diamonds indicate approximately the time scale (t_N) where the normal diffusive regime, *i.e.* $W_x(t) \propto t$, is recovered. The transversal confinement strength is $\omega = 1.0\sqrt{2k_BT/m\sigma^2}$ and the linear density is $\rho = 0.5\sigma^{-1}$.

tagged particle along the unconfined direction (in our case, the x direction) displays typical sub-diffusive motion with

$$\lim_{t \gg t_c} W_x(t) = Ft^{0.5}, \tag{5.16}$$

where F is the so-called single-file diffusion mobility and t_c is a characteristic relaxation time of the system. In particular, F and t_c depend on the specifics of the system (210). Wei *et al.* (41) showed experimentally that for a repulsive inter-particle interaction potential, t_c decreases with increasing strength of the interaction potential. This can be understood from the fact that an increase in the interaction leads to an increase in the collision rate between the particles (113). Nelissen *et al.* (100) recently showed that when the inter-particle interaction is comparable to the viscosity (damping), an intermediate "under" single-file diffusion regime, *i.e.* $W_x(t) \propto t^{\alpha}$ (with $\alpha < 0.5$), is also observed. Such a behaviour was also found in experiments with millimetre metallic balls (102) and in numerical simulations (105) taking into account spatial correlated noises.

In our specific case, the modulation in the x direction adds an additional restriction to the movement of the particles. The effect of V_0/k_BT on the mean square displacement $W_x(t)$ is shown in Fig. 40(a). Two effects are noticed here: First, the relaxation time t_c increases with increasing ratio V_0/k_BT, which means that for higher values of this ratio a longer time is needed for a particle to feel the presence of its neighboring particles. Once this time scale is reached, the sub-diffusive law [Eq. (5.16)] is recovered due to the interaction with its neighbors. Second, the mobility factor F decreases with increasing V_0/k_BT [cf. inset of Fig. 40(a)], which results from the restriction of the motion in the x direction, as stated above. Note that for $V_0/k_BT > 0.0$,

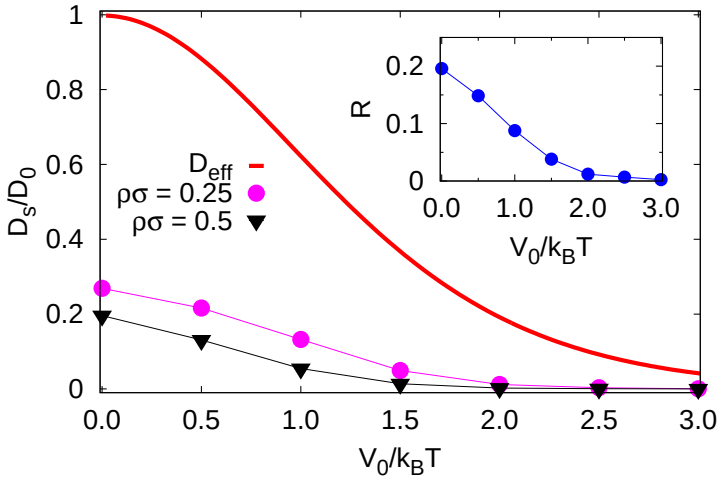

Figure 39 – Long-time self-diffusion coefficient D_s/D_0 as a function of the ratio V_0/k_BT, for different linear densities ρ. The effective self-diffusion coefficient D_{eff}/D_0 [Eq. (5.2)] as a function of V_0/k_BT for a single particle is also shown (solid red curve) for comparison. The inset shows the ratio $R = D_s/D_{\text{eff}}$ as a function of V_0/k_BT for the case $\rho = 0.5\sigma^{-1}$.

the system exhibits an intermediate regime where $W_x(t) \propto t^{\alpha}$, with $\alpha < 0.5$ before it reaches the SFD regime. This intermediate regime extends to larger times scales as the ratio V_0/k_BT increases.

5.5 Effect of linear density on diffusion

In order to investigate the effect of the linear density ρ on the diffusion, we introduce a commensurability factor $p \equiv N/n$, where N is the total number of particles in the computational unit cell and n is the total number of minima (or maxima) of the external periodic modulation along the x direction. Using Eq. (5.14) and the definition for the linear density, we may write the following condition

$$p \equiv \frac{N}{n} = \rho L. \tag{5.17}$$

We start by considering the simplest case ($p = 1$), *i.e.*, where there is one particle per potential well. In this section we analyse the system for three different densities, namely $\rho\sigma = 0.25, 0.50, 0.75$. Also, we fix $\omega = 1.0\sqrt{2k_BT/m\sigma^2}$ and $\phi = 90^o$. In Figs. 41(a)-(b) we show snapshots of the configuration of the system for $\rho = 0.25\sigma^{-1}$ and $\rho = 0.75\sigma^{-1}$, respectively. The mean square displacement $W_x(t)$ for different values of ρ is shown in Figs. 42(a)-(b).

The main effect of different densities on D_s is shown in Fig. 39. The solid curve is the single-particle case discussed in Sec. 5.2, which corresponds to the limiting case of very dilute systems, *i.e.*, very low densities. As the density increases ($\rho = 0.25\sigma^{-1}$ and $\rho = 0.5\sigma^{-1}$),

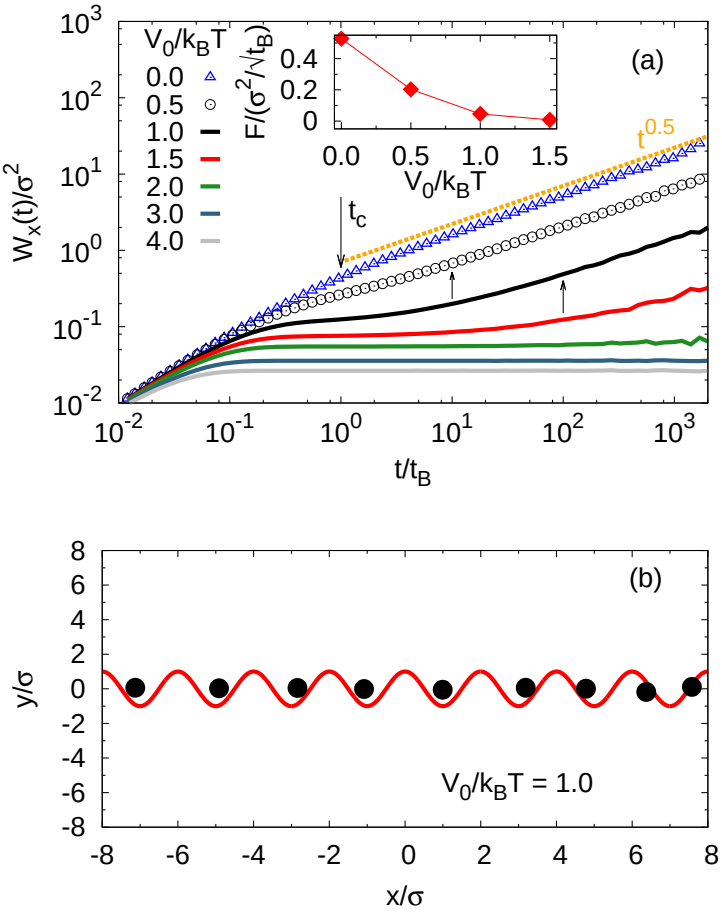

Figure 40 – (a) Log-log plot of the mean square displacement in the x direction, $W_x(t)$, as a function of time t for different values of the ratio V_0/k_BT. The yellow dotted line is a guide to the eye. The transversal confinement strength is $\omega = 10.0\sqrt{2k_BT/m\sigma^2}$ and the linear density is $\rho = 0.5\sigma^{-1}$. Vertical black arrows indicate the relaxation time t_c. Inset: Single-file diffusion mobility F, obtained from the relation (5.16), as a function of V_0/k_BT. (b) Snapshot of the configuration of particles (black dots) for $V_0/k_BT = 1.0$. The modulation $V_{\mathrm{mod}}(x)$ is plotted as the solid red curve.

the self-diffusion coefficient D_s decreases. This effect is related to the coupling between the particles due to the inter-particle interaction potential. For the case of very high densities, the interaction energy is stronger and diffusion should be partially suppressed, *i.e.*, $D_s \approx 0$ for all values of V_0/k_BT. Note that since the system is coupled to a heat bath, the diffusion coefficient is *not exactly* zero but goes to a very small value.

5.6 Effect of commensurability factor

We further investigate the effect of the commensurability factor p on the self-diffusion coefficient. In this section, we fix the linear density to $\rho = 0.5\sigma^{-1}$ and vary p, where we choose two

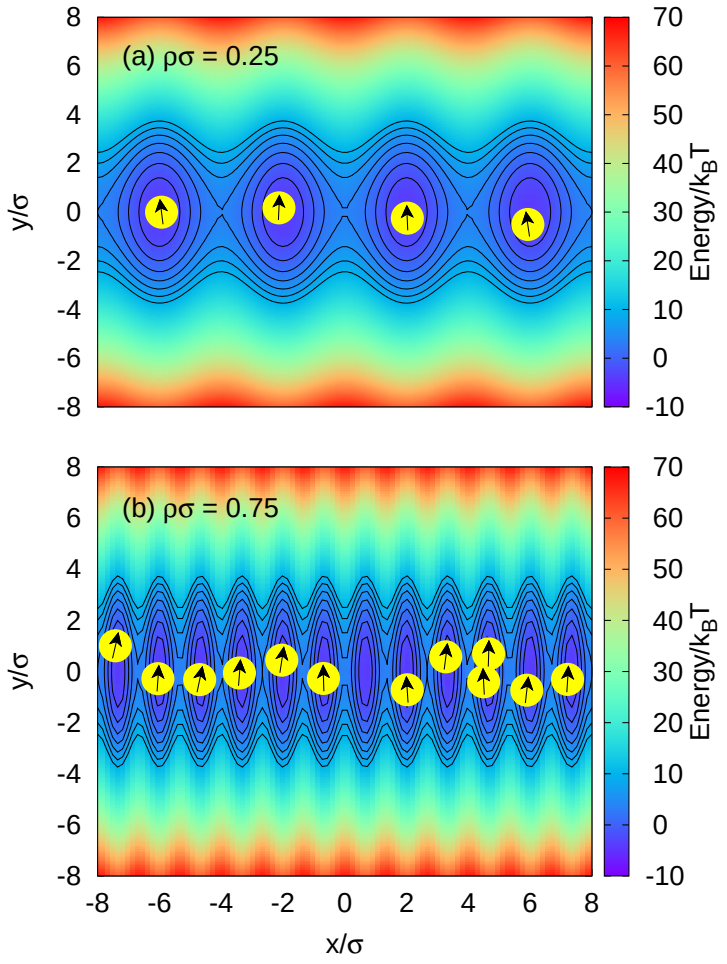

Figure 41 – The same as Fig. 37 but now for $V_0/k_BT = 4.0$. Linear density is (a) $\rho = 0.25\sigma^{-1}$, and (b) $\rho = 0.75\sigma^{-1}$. For both cases, the transversal confinement strength is $\omega = 1.0\sqrt{2k_BT/m\sigma^2}$ and the commensurability factor is $p = 1$.

half-integer values ($p = 1/2$ and $p = 3/2$) and compare these results with the case of previous section ($p = 1$). The effect of p on the mean square displacement $W_x(t)$ is shown in Figs. 43(a)-(c). Note that for all cases, the system exhibits an intermediate regime of diffusion where $W_x(t)$ shows a slower-than-linear dependence on time or $W_x(t) = \text{const}$ before the long-time normal diffusion regime sets in [Eq. (5.15)]. The saturation regime of the MSD in the x direction (*i.e.* $W_x(t) = \text{const}$) is similar to the one discussed previously in Sec. 5.4.1.

An interesting effect of the commensurability factor p on diffusion can be observed in Fig. 43(d). For $V_0/k_BT = 0.0$, the self-diffusion coefficient, D_s, is the same for all the cases ($p = 1/2, 1, 3/2$). This is due to the fact that in the absence of the external modulation, the system is regulated only by the linear density (in this case $\rho = 0.5\sigma^{-1}$). Therefore, the average distance between neighbour particles is the same. On the other hand, for sufficiently large values

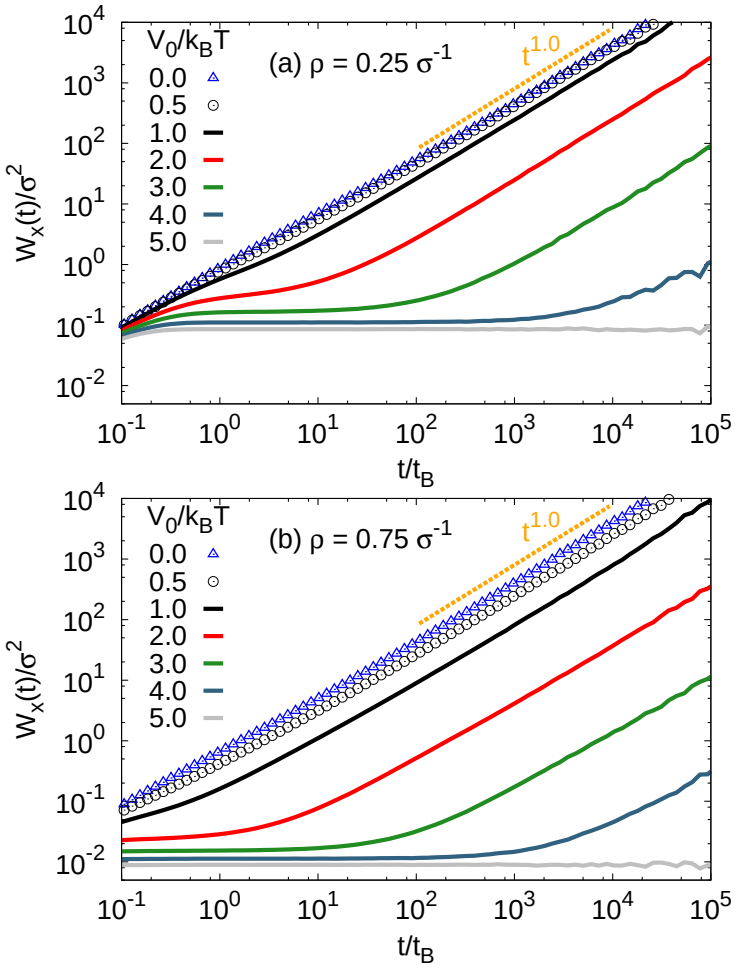

Figure 42 – The same as Fig. 38 but now for density (a) $\rho = 0.25\sigma^{-1}$, and (b) $\rho = 0.75\sigma^{-1}$. The transversal confinement strength is $\omega = 1.0\sqrt{2k_BT/m\sigma^2}$ and the commensurability factor is $p = 1$.

of $V_0/k_BT = 3.0$, the trapping of particles in the wells suppresses the diffusion, and again the self-diffusion coefficient D_s is of the same order (close to zero) for all the cases. However, the effect of p on D_s is more pronounced for intermediate values of $V_0/k_BT = 0.5-2.0$. This effect is explained as follows. First, note that $p = 1/2$ and $p = 1$ have both very similar behaviours, *i.e.*, D_s curve as a function of V_0/k_BT. From the definition of p, we have that for $p = 1/2 \rightarrow L = 1.0\sigma$ and $p = 1 \rightarrow L = 2.0\sigma$. In practice, this means that the neighbour inter-particle *average* distance is the same for both cases, *i.e.*, $d \approx 2.0\sigma$ [cf. Figs. 44(a)-(b)]. For $p = 3/2$ (which means 3 particles per 2 potential wells, on average), the distance between particles in neighbouring wells is larger, $d \approx 3.0\sigma$, which results in a larger self-diffusion coefficient. Interestingly, this case can be thought as a binary system, where one of the wells has one "big" particle formed by two dipoles and the other well has only one particle. Note that for all cases, D_s decreases with increasing V_0/k_BT, although for $p = 3/2$ this decrease is slower compared to the other cases

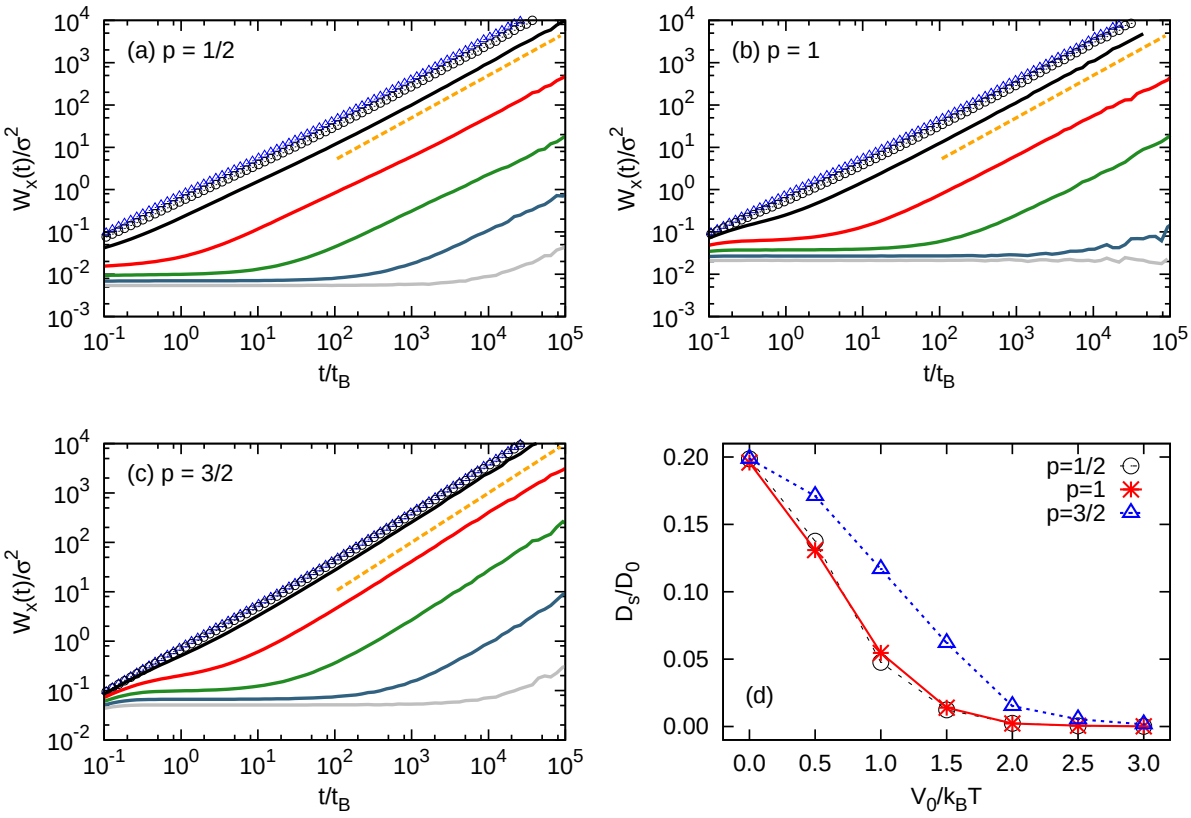

Figure 43 – (a)-(c) Log-log plot of the mean square displacement in the x direction $W_x(t)$, as a function of time t for different values of the ratio V_0/k_BT. The yellow dotted line has a slope of 1 and is a guide to the eye. The transversal confinement strength is $\omega = 1.0\sqrt{2k_BT/m\sigma^2}$ and the linear density is $\rho = 0.5\sigma^{-1}$. Color code is the same as in Fig. 42. (d) Long-time self-diffusion coefficient, D_s, as a function of V_0/k_BT for different values of the commensurability factor p.

($p = 1$ and $p = 1/2$).

5.7 Anisotropic diffusion and transversal sub-diffusion

5.7.1 Two particles per potential well

The competition between the external potentials in the x and y directions (*i.e.* the modulation [Eq. (5.10)] and the parabolic potential [Eq. (5.11)], respectively) leads to an anisotropic diffusion process, *i.e.*, $W_x(t) \neq W_y(t)$[1]. In this section we analyse the effect of the ratio V_0/k_BT on both the parallel (x direction) and transversal (y direction) diffusion independently. For this case, the simulation parameters are $p = 2$, $\rho = 1.0\sigma^{-1}$ and $\omega = 1.0\sqrt{2k_BT/m\sigma^2}$, which al-

[1] Note that the mean square displacement (MSD) in the x and y direction are calculated similarly to Eq. (5.13), where $W_l(t) = \langle N^{-1}\sum_{i=1}^{N}[l_i(t) - l_i(0)]^2\rangle$ and l_i is the x or y coordinate of each ith particle.

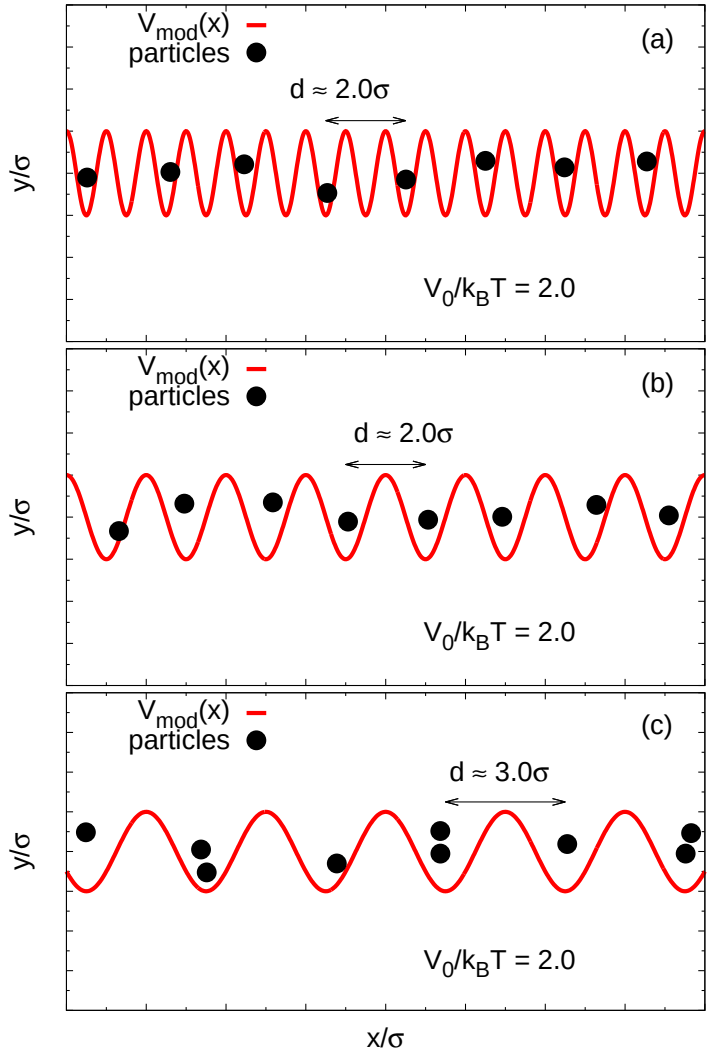

Figure 44 – Snapshot of the configuration of the system for different values of the commensurability factor $p =$ (a) $1/2$, (b) 1 and (c) $3/2$. For all cases, the strenght of the x direction modulation is $V_0/k_BT = 2.0$. Note that L changes according to the value of p.

lows the accommodation of two particles per potential well on *average* [cf. Fig. 45(a)]. As a representative example, we show in Figs. 45(b)-(c) the MSD in the parallel and transversal direction, respectively, for different values of V_0/k_BT. Note that the diffusion in the parallel direction is very different from the transversal direction, which is a direct effect of the anisotropy of space, *i.e.*, the competition between periodic modulation in the x direction and the parabolic confinement in the y direction.

In the x direction (parallel diffusion), the MSD exhibits [cf. Fig. 45(b)] a short-time normal diffusion behaviour for $t < t_B$, which is followed by a saturation regime due to the periodic modulation. Finally, for $t \gg t_B$, the long-time normal diffusion regime is recovered,

with

$$\lim_{t \gg t_B} W_x(t) = D_{||} t, \tag{5.18}$$

where $D_{||}$ is the parallel self-diffusion coefficient. The dependence of $D_{||}$ on V_0/k_BT is shown in Fig. 45(d), and as expected it decreases with increasing V_0/k_BT.

On the other hand, in the y direction (transversal diffusion), the MSD exhibits [cf. Fig. 45(c)] a very different behaviour. The initial short-time normal diffusion is also present. However, for intermediate time scales $t_B < t < t_{\rm sat}$ the system exhibits a sub-diffusive regime with a non-linear time-dependence of the form

$$W_y(t) = K_{\rm trans} t^{\alpha}, \tag{5.19}$$

where $K_{\rm trans}$ is the anomalous transversal diffusion coefficient (211) and $t_{\rm sat}$ is a saturation time scale in which the diffusion is suppressed due to the confinement in the y direction. Note that $\alpha < 0.5$ and thus a smaller power-law behaviour, as compared to the single-file diffusion (SFD) case, is observed. In Fig. 45(c) we show this intermediate regime and find $\alpha \approx 0.35$. Finally, both $K_{\rm trans}$ [cf. Fig. 45(e)] and $t_{\rm sat}$ depends on the periodic modulation strength V_0/k_BT, which is a measure of a type of "effective" confinement in the x direction. This indicates that the periodic modulation in the parallel direction affects directly the diffusion process in the transversal direction. A transversal sub-diffusive behaviour was recently found and analysed by Delfau *et al.* (212) in a *quasi*-one-dimensional system of interacting particles in a thermal bath. Note that our discussion is only valid for an *intermediate regime* (ITR) of sub-diffusion, as discussed previously in Refs. (157, 196) and references therein. The sub-diffusive regime in the transversal direction is a well-defined regime with an exponent of diffusion $\alpha \approx 0.35$, which extends to at least one order of magnitude in time. Note that for $V_0/k_BT > 0.0$, the time scale t_N [cf. Fig. 45(b)] where the system reaches the normal diffusive regime in the x direction, *i.e.* $W_x(t) \propto t$, is approximately the same as the time scale where the system reaches the sub-diffusive regime in the transversal direction [cf. Fig. 45(c)]. For this time scale t_N, a particle crosses the potential barrier imposed by the external modulation and it reaches the neighbor well. Once this time scale is reached, the correlations among particles in different wells give rise to the sub-diffusive regime in the transversal direction, *i.e.*, $W_y(t) \propto t^{0.35}$, before there is a complete saturation regime due to the parabolic confinement potential.

5.7.2 Four particles per potential well

In this section we analyze the transversal diffusion mechanism for $p = 4$, which gives four particles per potential well. As in the previous section, we calculate the transversal MSD $W_y(t)$ as a function of the strength of the external periodic modulation V_0/k_BT, and the results are shown in Fig. 46.

For the case of weak external modulation (*e.g.* $V_0/k_BT = 0.5$), the initial short-time linear MSD [$W_y(t) \propto t$] is followed by a saturation regime due to the finite size of the system in the transversal direction. With the increase of the external modulation, an intermediate sub-diffusive regime takes place before the onset of the saturation regime [cf. Fig. 46, $V_0/k_BT = 4.0$]. This is explained by the formation of a chain of particles along the transversal direction [cf. inset of Fig. 46]. Note that, as opposed to the previous section, where $W_y(t) \propto t^{0.35}$, in this case the MSD presents a clear SFD scaling, *i.e.*, $W_y(t) \propto t^{0.5}$.

These results indicate that even though the chain of particles is relatively small, the correlations between particles is sufficiently strong (212) to induce an intermediate single-file diffusion regime.

5.8 Concluding remarks

We studied the diffusive properties of a system of interacting magnetic dipoles in the presence of a modulated (corrugated) channel along the x direction and confined in the y direction by a parabolic confinement potential. In order to study the diffusion of the system, we used Brownian dynamics simulations. The analysis of the mean square displacement $W(t)$ showed that the system exhibits different regimes of diffusion depending on the external parameters (*i.e.* external modulation, magnetic field) that regulate the particle dynamics. In principle, this system could be realised experimentally using optical tweezer traps and our results could be verified by, *e.g.*, a microscopy imaging technique to track individual particles' trajectories (213).

We characterized the dynamics of the system for several parameters, namely the linear density ρ, the commensurability factor p and the strength of the external periodic modulation V_0/k_BT. Our main results are summarized as follows: (i) the self-diffusion coefficient D_s is modified by the inter-particle interaction potential as compared to the case of a single-particle diffusing in a periodic potential landscape. The difference increases with the linear density of particles; (ii) the effect of the commensurability factor p on the self-diffusion coefficient D_s is pronounced for the case of a semi-integer commensurability factor (as an example we considered $p = 3/2$). The system turns into an effective "artificial" binary system, with the presence of a "big" particle formed by two dipoles in a potential well and a single particle in a neighbour potential well; (iii) the presence of the external modulation affects the diffusion of the magnetic dipoles as compared to the case where there is no modulation [cf. Ref. (196)]; for instance, we found that a transversal sub-diffusive regime, including SFD, can be induced depending on the value of the external modulation V_0/k_BT and on the commensurability factor p.

Related publications

• **D. Lucena**, J. E. Galván-Moya, W. P. Ferreira, and F. M. Peeters, *Single-file and normal diffusion of magnetic dipoles in modulated channels*, Phys. Rev. E **89**, 032306 (2014).

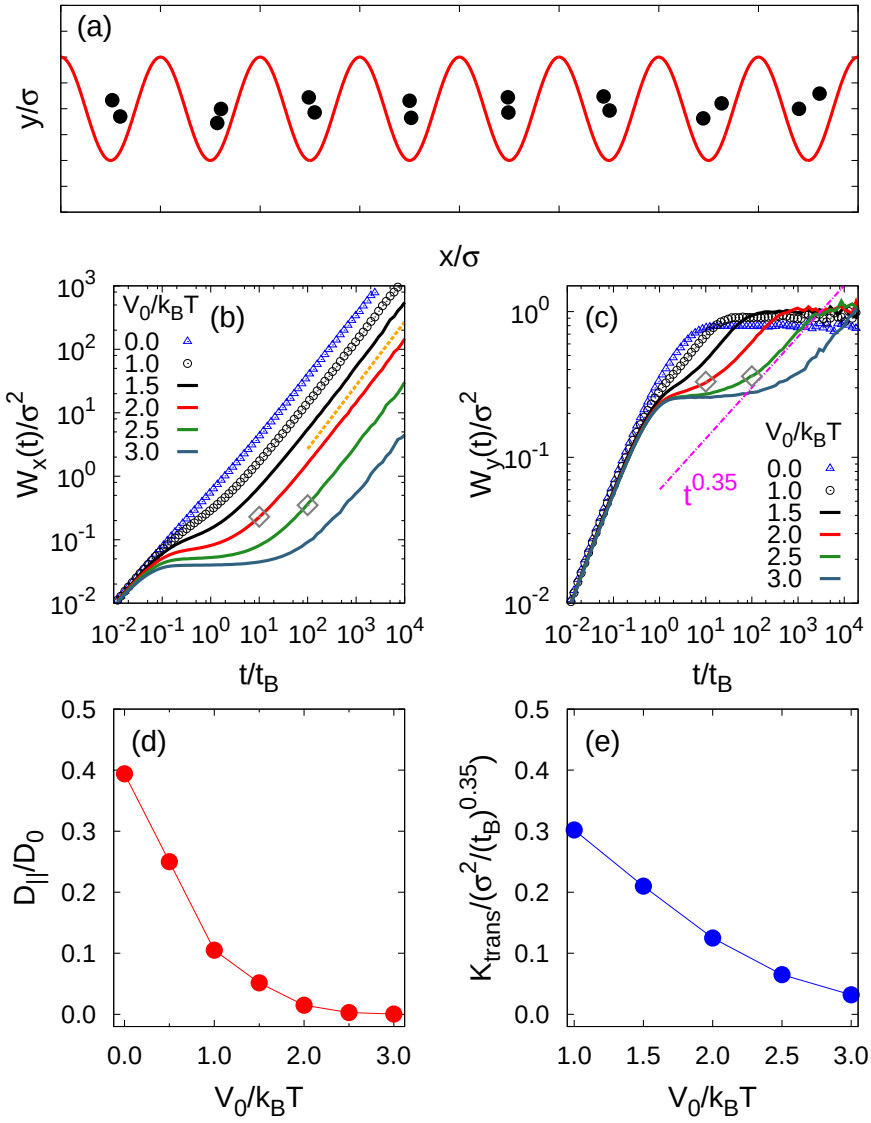

Figure 45 – (a) Snapshot of the configuration of particles (black dots) for $V_0/k_BT = 3.0$. The modulation $V_{\text{mod}}(x)$ is plotted as the solid red curve. (b), (c) Log-log plot of the MSD as a function of time t in the parallel and transversal direction, respectively, for different values of V_0/k_BT. The dotted yellow line has a slope of 1, the magenta dotted-dashed line has a slope of 0.35 and both are guide to the eye. The open diamonds in (b) [(c)] indicate approximately the time scale (t_N) where the normal diffusive regime [sub-diffusive regime] appears. (d) Parallel self-diffusion coefficient $D_{||}$ and (e) anomalous transversal diffusion coefficient K_{trans}, both as a function of V_0/k_BT. Parameters of the simulation are $p = 2$, $\rho = 1.0\sigma^{-1}$ and $\omega = 1.0\sqrt{2k_BT/m\sigma^2}$.

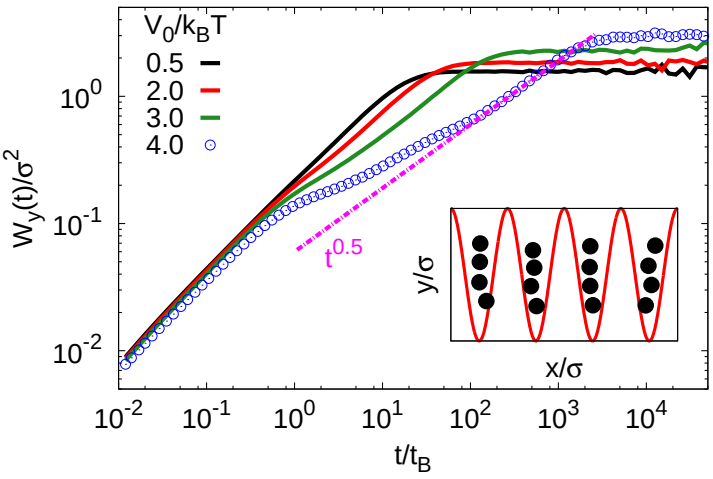

Figure 46 – Log-log plot of the transversal MSD $W_y(t)$ as a function of time t, for different values of V_0/k_BT. The magenta dotted-dashed line has a slope of 0.5 and is a guide to the eye. Inset: snapshot of the configuration of particles (black dots) for $V_0/k_BT = 4.0$. The modulation $V_{\mathrm{mod}}(x)$ is plotted as the solid red curve. Parameters of the simulation are $p = 4$, $\rho = 2.0\sigma^{-1}$ and $\omega = 1.0\sqrt{2k_BT/m\sigma^2}$.

Summary

In this thesis we studied the diffusive properties of soft condensed matter systems under different types of external confinement potentials by using numerical simulation techniques, specifically Langevin and Brownian dynamics simulations. In Chapter 1 we presented an overview of soft condensed matter systems, diffusion (Sec. 1.5) and single-file diffusion (SFD, Sec. 1.5.3), respectively. In Chapter 2 we presented the numerical methods that we used to analyze the systems investigated in the subsequent chapters. The results of our investigations were presented in Chapters 3, 4 and 5, and they can be summarized as follows.

In Chapter 3, the diffusive properties of a mono-disperse system of interacting particles confined to a *quasi*-one-dimensional (q1D) channel were studied using Molecular Dynamics (MD) simulations. We calculated numerically the mean square displacement (MSD) and investigated the influence of the width of the channel (or the strength of the confinement potential) on diffusion in finite-size channels of different shapes (*i.e.*, straight and circular). The transition from single-file diffusion (SFD) to the two dimensional diffusion regime was investigated. This transition (regarding the calculation of the scaling exponent (α) of the MSD $\propto t^{\alpha}$) as a function of the width of the channel, is shown to change depending on the channel's confinement profile. In particular the transition could be either smooth (*i.e.*, for a parabolic confinement potential) or rather sharp/stepwise (*i.e.*, for a hard-wall potential), as distinct from infinite channels where this transition is abrupt. This result could be explained by qualitatively different distributions of the particle density for the different confinement potentials. This transition from SFD to normal diffusion has been recently observed in experiments with super-paramagnetic colloidal particles confined by a hard-wall confinement potential (214). This transition seems to indeed occur in real systems, however one main open question regarding this problem is the following: what is the physical mechanism behind the sub-diffusive regime found in the intermediate regime (ITR)? Also, why is the exponent of diffusion non-universal? These questions are currently under investigation and will be published elsewhere.

In Chapter 4, the diffusion of a system of ferromagnetic dipoles confined in a *quasi*-one-dimensional parabolic trap was studied using Brownian dynamics simulations. We showed that the dynamics of the system is tunable by an in-plane external homogeneous magnetic field. For a strong applied magnetic field, we found that the mobility of the system, the exponent of diffusion and the crossover time among different diffusion regimes could be tuned by the orientation of the magnetic field. For weak magnetic fields, the exponent of diffusion in the sub-diffusive regime was shown to be independent of the orientation of the external field.

In Chapter 5, the diffusive properties of interacting magnetic dipoles confined in a parabolic narrow channel and in the presence of a periodic modulated (corrugated) potential

along the unconfined direction were analyzed using Brownian dynamics simulations. We compared our simulation results with the analytical result for the effective diffusion coefficient of a single-particle by Festa and d'Agliano (170) and we showed the importance of inter-particle interaction on the diffusion process. We presented results for the diffusion of magnetic dipoles as a function of linear density, strength of the periodic modulation and commensurability factor.

Bibliography

1 TAYLOR, P. L. *A Quantum Approach to Condensed Matter Physics*. [S.l.]: Cambridge University Press, 2002. 29 Cited on page 29.

2 PITAEVSKII, L.; STRINGARI, S. *Bose-Einstein Condensation*. [S.l.]: Oxford University Press, 2003. 29 Cited on page 29.

3 TINKHAM, M. *Introduction to Superconductivity*. [S.l.]: Dover Publications, 2004. 29 Cited on page 29.

4 JONES, R. A. L. *Soft Condensed Matter*. [S.l.]: Oxford University Press, 2013. 29 Cited on page 29.

5 PUSEY, P. N.; TOUGH, R. J. A. *Dynamic Light Scattering: Application of Photon Correlation*. [S.l.]: Plenum (New York), 1985. 30 Cited on page 30.

6 BERNE, B. J.; PECORA, R. *Dynamic Light Scattering*. [S.l.]: Wiley (New York), 1976. 30 Cited on page 30.

7 CLARK, G. L. *Nature*, v. 120, p. 119–120, 1927. 31 Cited on page 31.

8 HARLAND, J. L.; VAN MEGEN, W. *Phys. Rev. E*, v. 55, p. 3054, 1997. 31 Cited on page 31.

9 PALBERG, T. *J. Phys.: Condens. Matter*, v. 11, p. R323, 1999. 31 Cited on page 31.

10 HANES, R. D. L.; DALLE-FERRIER, C.; SCHMIEDEBERG, M.; JENKINS, M. C.; EGELHAAF, S. U. *Soft Matter*, v. 8, p. 2714, 2012. 17, 31, 103 Cited 3 times on pages 17, 31, and 103.

11 DEBYE, P. J. W. *The Collected Papers of Peter J. W. Debye*. [S.l.]: Interscience Publishers, 1954. 31, 33 Cited 2 times on pages 31 and 33.

12 DALLE-FERRIER, C.; KRÜGER, M.; HANES, R. D. L.; WALTA, S.; JENKINS, M. C.; EGELHAAF, S. U. *Soft Matter*, v. 7, p. 2064, 2011. 31, 103 Cited 2 times on pages 31 and 103.

13 ASHKIN, A.; DZIEDZIC, J. M.; BJORKHOLM, J. E.; CHU, S. *Opt. Lett.*, v. 11, p. 288, 1986. 31 Cited on page 31.

14 WEI, Q.-H.; BECHINGER, C.; RUDHARDT, D.; LEIDERER, P. *Phys. Rev. Lett.*, v. 81, p. 2606, 1998. 31 Cited on page 31.

15 CHOWDHURY, A.; ACKERSON, B. J.; CLARK, N. A. *Phys. Rev. Lett.*, v. 55, p. 833, 1985. 31 Cited on page 31.

16 DREWSEN, M.; JENSEN, I.; LINDBALLE, J.; NISSEN, N.; MARTINUSSEN, R.; MORTENSEN, A.; STAANUM, P.; VOIGT, D. *International Journal of Mass Spectrometry*, v. 229, p. 83, 2003. 17, 31, 32 Cited 3 times on pages 17, 31, and 32.

17 RUSSEL, S.; SAVILLE, D. A.; SCHOWALTER, W. R. *Colloidal dispersions*. [S.l.]: Cambridge University Press, 1989. 32 Cited on page 32.

18 ISRAELACHVILI, J. N. *Intermolecular and surface forces*. [S.l.]: Academic Press (London), 1992. 32 Cited on page 32.

19 MOTTE, L.; COURTY, A.; NGO, A.-T.; LISIECKI, I.; PILENI, M.-P. Nanocrystals forming mesoscopic structures. In: ____. [S.l.]: Wiley-VCH Verlag, 2005. cap. 1, p. 1. 32 Cited on page 32.

20 BAUMGARTL, J. *Colloids as model systems for condensed matter*. Tese (Doutorado) — Universität Stuttgart, Physikalisches Institut, 2007. 17, 33 Cited 2 times on pages 17 and 33.

21 DUKHIN, S. S.; DERJAGUIN, B. V. *Electrokinetic Phenomena*. [S.l.]: J. Willey and Sons, 1974. 33 Cited on page 33.

22 DEBYE, P.; HÜCKEL, E. The theory of electrolytes. i. lowering of freezing point and related phenomena. *Physikalische Zeitschrift*, v. 24, p. 185, 1923. 33 Cited on page 33.

23 PILENI, M.-P. *J. Chem. Phys. B*, v. 105, p. 3358, 2001. 34 Cited on page 34.

24 PILENI, M.-P. *Adv. Func. Mater.*, v. 11, p. 323, 2001. 34 Cited on page 34.

25 WIGNER, E. *Phys. Rev.*, v. 46, p. 1002, 1934. 34 Cited on page 34.

26 BEDANOV, V. M.; PEETERS, F. M. *Phys. Rev. B*, v. 49, p. 2667, 1994. 17, 34, 35 Cited 3 times on pages 17, 34, and 35.

27 GRIMES, C. C.; ADAMS, G. *Phys. Rev. Lett.*, v. 42, p. 795, 1979. 34 Cited on page 34.

28 ROUSSEAU, E.; PONARIN, D.; HRISTAKOS, L.; AVENEL, O.; VAROQUAUX, E.; MUKHARSKY, Y. *Phys. Rev. B*, v. 79, p. 045406, 2009. 34 Cited on page 34.

29 PEETERS, F. M. *Physics*, v. 2, p. 4, 2009. 17, 36 Cited 2 times on pages 17 and 36.

30 MUNARIN, F. F. *Estudo de sistemas bi-dimensionais de partículas clássicas*. Tese (Doutorado) — Universidade Federal do Ceará, Departamento de Física, 2008. 17, 37 Cited 2 times on pages 17 and 37.

31 THOMAS, H.; MORFILL, G. E.; DEMMEL, V.; GOREE, J.; FEUERBACHER, B.; MÖHLMANN, D. *Phys. Rev. Lett.*, v. 73, p. 652, 1994. 34 Cited on page 34.

32 FIGUEIREDO, D. G. *Análise de Fourier e Equações Diferenciais Parciais*. [S.l.]: Projeto Euclides, 2007. 35 Cited on page 35.

33 DENNERY, P.; KRZYWICKI, A. *Mathematics For Physicists*. [S.l.]: Dover Publications, 1995. 37, 40 Cited 2 times on pages 37 and 40.

34 BROWN, R. *Phil. Mag.*, v. 4, p. 161, 1828. 38 Cited on page 38.

35 EINSTEIN, A. *Annalen der Physik*, v. 17, p. 549, 1905. 38 Cited on page 38.

36 LANGEVIN, P. *C. R. Acad. Sci. (Paris)*, v. 146, p. 530, 1908. 38 Cited on page 38.

37 SMOLUCHOWSKI, M. *Ann. Phys.*, v. 353, p. 1103, 1915. 38 Cited on page 38.

38 LUCENA, D. *Propriedades difusivas de sistemas clássicos confinados*. Dissertação (Mestrado) — Universidade Federal do Ceará, Departamento de Física, 2011. 40 Cited on page 40.

39 HODGKIN, A. L.; KEYNES, R. D. *J. Physiol.*, v. 128, p. 61, 1955. 40, 61 Cited 2 times on pages 40 and 61.

40 HARRIS, T. E. *J. Appl. Probab.*, v. 2, p. 323, 1965. 40, 61 Cited 2 times on pages 40 and 61.

41 WEI, H.-Q.; BECHINGER, C.; LEIDERER, P. *Science*, v. 287, p. 625, 2000. 18, 41, 62, 63, 73, 75, 94, 109 Cited 8 times on pages 18, 41, 62, 63, 73, 75, 94, and 109.

42 LEBOWITZ, J. L.; PERCUS, J. K. *Phys. Rev. E*, v. 155, p. 122, 1967. 41, 62 Cited 2 times on pages 41 and 62.

43 LEVITT, D. G. *Phys. Rev. A*, v. 8, p. 3050, 1973. 41, 62 Cited 2 times on pages 41 and 62.

44 RICHARDS, P. M. *Phys. Rev. B*, v. 16, p. 1393, 1977. 41, 62 Cited 2 times on pages 41 and 62.

45 CENTRES, P. M.; BUSTINGORRY, S. *Phys. Rev. E*, v. 81, p. 061101, 2010. 41, 63, 69, 81, 83, 94 Cited 6 times on pages 41, 63, 69, 81, 83, and 94.

46 KOLLMANN, M. *Phys. Rev. Lett.*, v. 90, p. 180602, 2003. 41, 42, 86 Cited 3 times on pages 41, 42, and 86.

47 RYABOV, A.; CHVOSTA, P. *Phys. Rev. E*, v. 83, p. 020106, 2011. 41 Cited on page 41.

48 RYABOV, A.; CHVOSTA, P. *J. Chem. Phys.*, v. 136, p. 064114, 2012. 41 Cited on page 41.

49 RYABOV, A. *J. Chem. Phys.*, v. 138, p. 154104, 2013. 41 Cited on page 41.

50 RYABOV, A.; CHVOSTA, P. *J. Chem. Phys.*, v. 89, p. 022132, 2014. 41 Cited on page 41.

51 CUI, B.; DIAMANT, H.; LIN, B. *Phys. Rev. Lett.*, v. 89, p. 188302, 2002. 41 Cited on page 41.

52 LIN, B.; MERON, M.; CUI, B.; RICE, S. A.; DIAMANT, H. *Phys. Rev. Lett.*, v. 94, p. 216001, 2005. 41 Cited on page 41.

53 HAHN, K.; KÄRGER, J.; KUKLA, V. *Phys. Rev. Lett.*, v. 76, p. 2762, 1995. 41 Cited on page 41.

54 GUPTA, V.; NIVARTHI, S. S.; MCCORMICK, A. V.; DAVIS, H. T. *Chem. Phys. Lett.*, v. 247, p. 596, 1995. 41 Cited on page 41.

55 HERRERA-VELARDE, S.; ZAMUDIO-OJEDA, A.; CASTANEDA-PRIEGO, R. *J. Chem. Phys.*, v. 133, p. 114902, 2010. 42 Cited on page 42.

56 LIZANA, L.; AMBJÖRNSSON, T. *Phys. Rev. E*, v. 80, p. 051103, 2009. 42, 62, 81, 82, 83, 94 Cited 6 times on pages 42, 62, 81, 82, 83, and 94.

57 LEIBOVICH, N.; BARKAI, E. *Phys. Rev. E*, v. 88, p. 032107, 2013. 42 Cited on page 42.

58 HEERMANN, D. W. *Computer Simulation Methods in Theoretical Physics*. [S.l.]: Springer-Verlag, 1989. 46 Cited on page 46.

59 ALDER, B. J.; WAINWRIGHT, T. E. *J. Chem. Phys.*, v. 27, p. 1208, 1957. 46 Cited on page 46.

60 GIBSON, J. B.; GOLAND, A. N.; MILGRAM, M.; VINEYARD, G. H. *Phys. Rev.*, v. 120, p. 1229, 1960. 46 Cited on page 46.

61 RAHMAN, A. *Phys. Rev. A*, v. 136, p. 405, 1964. 46 Cited on page 46.

62 LEES, A. W.; EDWARDS, S. F. *J. Phys. C*, v. 5, p. 1921, 1972. 46 Cited on page 46.

63 GOSLING, E. M. *Mol. Phys.*, v. 26, p. 1475, 1973. 46 Cited on page 46.

64 ASHURST, W. T.; HOOVER, W. G. *Phys. Rev. Lett.*, v. 31, p. 206, 1973. 46 Cited on page 46.

65 HOOVER, W. G. *Ann. Rev. Phys. Chem.*, v. 34, p. 103, 1983. 46 Cited on page 46.

66 ALLEN, M. P.; TILDESLEY, D. J. *Computer Simulations of Liquids*. [S.l.]: Clarendon Press, 1987. 47, 50, 51, 52 Cited 4 times on pages 47, 50, 51, and 52.

67 RAPAPORT, D. C. *The Art of Molecular Dynamics Simulation*. [S.l.]: Cambridge University Press, 1998. 47, 49, 51, 53 Cited 4 times on pages 47, 49, 51, and 53.

68 VERLET, L. *Phys. Rev.*, v. 159, p. 98, 1967. 49 Cited on page 49.

69 STONE, J. E.; PHILLIPS, J. C.; FREDDOLINO, P. L.; HARDY, D. J.; TRABUCO, L. G.; SCHULTEN, K. *J. Comput. Chem.*, v. 28, p. 2618, 2007. 50 Cited on page 50.

70 BORN, M.; VON KARMAN, T. *Physik Z*, v. 13, p. 297, 1912. 50 Cited on page 50.

71 IACOVELLA, C. R. *Periodic boundary conditions*. [S.l.]: Dept. of Chemical Engineering, Materials Science and Engineering, Macromolecular Science and Physics, University of Michigan, 2006. 18, 50 Cited 2 times on pages 18 and 50.

72 EWALD, P. *Ann. Phys.*, v. 369, p. 253, 1921. 51 Cited on page 51.

73 HAILE, J. M. *Molecular Dynamics Simulation – Elementary Methods*. [S.l.]: Wiley-Interscience, 1997. 52, 53 Cited 2 times on pages 52 and 53.

74 Disponível em: <http://en.wikipedia.org/wiki/Radial_distribution_function>. 18, 53 Cited 2 times on pages 18 and 53.

75 BRIN, M.; GARRETT, S. *Introduction to Dynamical Systems*. [S.l.]: Cambridge University Press, 2002. 54 Cited on page 54.

76 BLOCH, F. *Fundamentals of Statistical Mechanics (Manuscript and Notes of Felix Bloch)*. [S.l.]: Imperial College Press, 2000. 54 Cited on page 54.

77 NOSÉ, S. *J. Chem. Phys.*, v. 81, p. 511, 1984. 54 Cited on page 54.

78 HOOVER, W. G. *Phys. Rev. A*, v. 31, p. 1695, 1985. 54 Cited on page 54.

79 BERENDSEN, H. J.; POSTMA, J. P.; VAN GUNSTEREN, W. F.; DINOLA, A.; HAAK, J. R. *J. Chem. Phys.*, v. 81, p. 3684, 1984. 54 Cited on page 54.

80 NÄGELE, G. Diffusion in condensed matter. In: ____. [S.l.]: Springer-Verlag, Berlin, 2005. 56, 57, 88 Cited 3 times on pages 56, 57, and 88.

81 MANNELLA, R. *Int. J. Mod. Phys. C*, v. 13, p. 1177, 2002. 56, 57 Cited 2 times on pages 56 and 57.

82 MANNELLA, R. *Phys. Rev. E*, v. 69, p. 041107, 2004. 56, 57 Cited 2 times on pages 56 and 57.

83 BOX, G. E. P.; MÜLLER, M. E. *The Annals of Mathematical Statistics*, v. 29, p. 610, 1958. 56, 90, 106 Cited 3 times on pages 56, 90, and 106.

84 ERMAK, D. L.; MCCAMMON, J. A. *J. Chem. Phys.*, v. 69, p. 1352, 1978. 56, 65, 89, 106 Cited 4 times on pages 56, 65, 89, and 106.

85 COTTIN-BIZONNE, C.; BARRAT, J. L.; BOCQUET, L.; CHARLAIX, E. *Nature Mater.*, v. 2, p. 237, 2003. 61 Cited on page 61.

86 KÄRGER, J. *Phys. Rev. A*, v. 45, p. 4173, 1992. 61 Cited on page 61.

87 MARTIN, F.; WALCZAK, R.; BOIARSKI, A.; COHEN, M.; WEST, T.; COSENTINO, C.; SHAPIRO, J.; FERRARI, M. *J. Control. Release*, v. 102, p. 123, 2005. 61 Cited on page 61.

88 BARROZO, P.; MOREIRA, A. A.; AGUIAR, J. A.; ANDRADE JR., J. S. *Phys. Rev. B*, v. 80, p. 104513, 2009. 61 Cited on page 61.

89 ANDRADE JR., J. S.; DA SILVA, G. F. T.; MOREIRA, A. A.; NOBRE, F. D.; CURADO, E. M. F. *Phys. Rev. Lett.*, v. 105, p. 260601, 2010. 61 Cited on page 61.

90 HUMMER, G.; RASAIAH, J. C.; NOWORYTA, J. P. *Nature (London)*, v. 414, p. 188, 2001. 61 Cited on page 61.

91 BAERLOCHER, C.; MCCUSKER, L. B.; OLSON, D. H. *Atlas of Zeolite Structure Types*. [S.l.]: Butterworths-Heinemann, London, 1992. 62 Cited on page 62.

92 HALPIN-HEALY, T.; ZHANG, Y. C. *Phys. Rep.*, v. 254, p. 215, 1995. 62 Cited on page 62.

93 KHARKYANEN, V. N.; YESYLEVSKYY, S. O. *Phys. Rev. E*, v. 80, p. 031118, 2009. 62 Cited on page 62.

94 BARKAI, E.; SILBEY, R. *Phys. Rev. Lett.*, v. 102, p. 050602, 2009. 62 Cited on page 62.

95 ALSAYED, A. M.; ISLAM, M. F.; ZHANG, J.; COLLINGS, P. J.; YODH, A. D. *Science*, v. 309, p. 1207, 2005. 62 Cited on page 62.

96 LUTZ, C.; KOLLMANN, M.; BECHINGER, C. *Phys. Rev. Lett.*, v. 93, p. 026001, 2004. 62 Cited on page 62.

97 PIACENTE, G.; PEETERS, F. M.; BETOURAS, J. J. *Phys. Rev. E*, v. 70, p. 036406, 2004. 62, 71 Cited 2 times on pages 62 and 71.

98 FERREIRA, W. P.; CARVALHO, J. C. N.; OLIVEIRA, P. W. S.; FARIAS, G. A.; PEETERS, F. M. *Phys. Rev. B*, v. 77, p. 014112, 2008. 62 Cited on page 62.

99 YANG, W.; NELISSEN, K.; KONG, M.; ZENG, Z.; PEETERS, F. M. *Phys. Rev. E*, v. 79, p. 041406, 2009. 62 Cited on page 62.

100 NELISSEN, K.; MISKO, V. R.; PEETERS, F. M. *Europhys. Lett.*, v. 80, p. 56004, 2007. 62, 63, 109 Cited 3 times on pages 62, 63, and 109.

101 For underdamped systems, the initial fast growth of the MSD (i.e., ballistic regime) is characterized by $\alpha = 2$. 62 Cited on page 62.

102 COUPIER, G.; SAINT-JEAN, M.; GUTHMANN, C. *Phys. Rev. E*, v. 73, p. 031112, 2006. 63, 73, 75, 109 Cited 4 times on pages 63, 73, 75, and 109.

103 TEPPER, H. L.; HOOGENBOOM, J. P.; VAN DER VEGT, N. F. A.; BRIELS, W. J. *J. Chem. Phys.*, v. 110, p. 11511, 1999. 63 Cited on page 63.

104 DELFAU, J.-B.; COSTE, C.; SAINT-JEAN, M. *Phys. Rev. E*, v. 84, p. 011101, 2011. 63, 69, 91, 92, 94, 106 Cited 6 times on pages 63, 69, 91, 92, 94, and 106.

105 TKACHENKO, D. V.; MISKO, V. R.; PEETERS, F. M. *Phys. Rev. E*, v. 82, p. 051102, 2010. 63, 94, 109 Cited 3 times on pages 63, 94, and 109.

106 LIN, B.; MERON, M.; CUI, B.; RICE, S. A.; DIAMANT, H. *Phys. Rev. Lett.*, v. 94, p. 216001, 2005. 63 Cited on page 63.

107 As recently shown when studying single-trajectory averages (108), time average (TA) may differ from ensemble average (EA) MSD not only for nonergodic processes (for example, for anomalous diffusion described by continuous time random walks (CTRWs) models (109, 110)), but also for some ergodic processes in small complex systems. 66 Cited on page 66.

108 JEON, J.-H.; METZLER, R. *Phys. Rev. E*, v. 85, p. 021147, 2012. 66, 128 Cited 2 times on pages 66 and 128.

109 HE, Y.; BUROV, S.; METZLER, R.; BARKAI, E. *Phys. Rev. Lett.*, v. 101, p. 058101, 2008. 66, 128 Cited 2 times on pages 66 and 128.

110 LUBELSKI, A.; SOKOLOV, I. M.; KLAFTER, J. *Phys. Rev. Lett.*, v. 100, p. 250602, 2008. 66, 128 Cited 2 times on pages 66 and 128.

111 KUTNER, R.; VAN BEIJEREN, H.; KEHR, K. W. *Phys. Rev. B*, v. 30, p. 4382, 1984. 66, 128 Cited 2 times on pages 66 and 128.

112 This apparent power-law behavior is characterized by MSD $\langle \Delta x^2(t) \rangle \propto t^{\alpha}$, and it is an intermediate phenomenon due to the interplay between the crossover from the MSD $\langle \Delta x^2(t) \rangle \propto t^{0.5}$ regime to $\langle \Delta x^2(t) \rangle \propto t^{1.0}$ regime. For details, see Ref. (111). 66 Cited on page 66.

113 VAN BEIJEREN, H.; KEHRA, K. W.; KUTNER, R. *Phys. Rev. B*, v. 28, p. 5711, 1983. 66, 81, 109 Cited 3 times on pages 66, 81, and 109.

114 ALDER, B. J.; ALLEY, W. E. *J. Stat. Phys.*, v. 19, p. 341, 1978. 66 Cited on page 66.

115 CHOU, Y.-L.; PLEIMLING, M.; ZIA, R. K. P. *Phys. Rev. E*, v. 80, p. 061602, 2009. 66 Cited on page 66.

116 PIACENTE, G.; HAI, G. Q.; PEETERS, F. M. *Phys. Rev. B*, v. 81, p. 024108, 2010. 71 Cited on page 71.

117 Note that this is not a zig-zag transition: the function $P_{\mathrm{rad}}(r)$ still has a single maximum which is shifted from the center of the channel. 76 Cited on page 76.

118 AMBJÖRNSSON, T.; SILBEY, R. J. *J. Chem. Phys.*, v. 129, p. 165103, 2008. 76 Cited on page 76.

119 SAVEL'EV, S.; MARCHESONI, F.; TALONI, A.; NORI, F. *Phys. Rev. E*, v. 74, p. 021119, 2006. 81 Cited on page 81.

120 LÜBBE, A. S.; ALEXIOU, C.; BERGEMANN, C. *J. Surg. Res.*, v. 95, p. 200, 2001. 85 Cited on page 85.

121 PANKHURST, Q. A.; CONNOLLY, J.; JONES, S. K.; DOBSON, J. *J. Phys. D: Appl. Phys.*, v. 36, p. R167, 2003. 85, 103 Cited 2 times on pages 85 and 103.

122 BERGEMANN, C.; MÜLLER-SCHULTEB, D.; OSTER, J.; BRASSARD, L.; LÜBBE, A. S. *J. Magn. Magn. Mater.*, v. 194, p. 45, 1999. 85 Cited on page 85.

123 RAJ, K.; MOSKOWITZ, R. *J. Magn. Magn. Mater.*, v. 85, p. 233, 1990. 85 Cited on page 85.

124 ROSENSWEIG, R. E. *Annu. Rev. Fluid Mech.*, v. 19, p. 437, 1987. 85 Cited on page 85.

125 BACRIA, J.-C.; CEBERS, A.; DABADIE, J.-C.; NEVEU, S.; PERZYNSKI, R. *Europhys. Lett.*, v. 27, p. 437, 1994. 85 Cited on page 85.

126 MAHR, T.; REHBERG, I. *Europhys. Lett.*, v. 43, p. 23, 1998. 85 Cited on page 85.

127 TOUSSAINT, R.; HELGESEN, G.; FLEKKOY, E. G. *Phys. Rev. Lett.*, v. 93, p. 108304, 2004. 85 Cited on page 85.

128 FURST, E. M.; GAST, A. P. *Phys. Rev. E*, v. 62, p. 6916, 2000. 85 Cited on page 85.

129 JORDANOVIC, J.; JÄGER, S.; KLAPP, S. H. L. *Phys. Rev. Lett.*, v. 106, p. 038301, 2011. 85 Cited on page 85.

130 MOROZOV, K. I.; SHLIOMIS, M. I. *J. Phys.: Condens. Matter*, v. 16, p. 3807, 2004. 85 Cited on page 85.

131 ANDREU, J. S.; CALERO, C.; CAMACHO, J.; FARAUDO, J. *Phys. Rev. E*, v. 85, p. 036709, 2012. 85, 103 Cited 2 times on pages 85 and 103.

132 MARTIN, J. E.; VENTURINI, E.; ODINEK, J.; ANDERSON, R. A. *Phys. Rev. E*, v. 61, p. 2818, 2000. 85 Cited on page 85.

133 SNEZHKO, I. S. A. A.; KWOK, W.-K. *Phys. Rev. Lett.*, v. 94, p. 108002, 2005. 85 Cited on page 85.

134 BELKIN, M.; SNEZHKO, A.; ARANSON, I. S.; KWOK, W.-K. *Phys. Rev. Lett.*, v. 99, p. 158301, 2007. 85 Cited on page 85.

135 SNEZHKO, A.; BELKIN, M.; ARANSON, I. S.; KWOK, W.-K. *Phys. Rev. Lett.*, v. 102, p. 118103, 2009. 85 Cited on page 85.

136 WAGNER, J.; FISCHER, B.; AUTENRIETH, T.; HEMPELMANN, R. *J. Phys.: Condens. Matter*, v. 18, p. S2697, 2006. 85 Cited on page 85.

137 JORDANOVIC, J.; KLAPP, S. H. L. *Phys. Rev. E*, v. 79, p. 021405, 2009. 85 Cited on page 85.

138 FERREIRA, W. P.; MATULIS, A.; FARIAS, G. A.; PEETERS, F. M. *Phys. Rev. E*, v. 67, p. 046601, 2003. 85 Cited on page 85.

139 FERREIRA, W. P.; PEETERS, F. M.; FARIAS, G. A. *Phys. Rev. E*, v. 68, p. 066405, 2003. 85 Cited on page 85.

140 BEDANOV, V. M.; PEETERS, F. M. *Phys. Rev. B*, v. 49, p. 2667, 1994. 85 Cited on page 85.

141 MELZER, A. *Phys. Rev. E*, v. 67, p. 016411, 2003. 85 Cited on page 85.

142 FERREIRA, W. P.; PARTOENS, B.; PEETERS, F. M.; FARIAS, G. A. *Phys. Rev. E*, v. 71, p. 021501, 2005. 85 Cited on page 85.

143 SCHWEIGERT, V. A.; PEETERS, F. M. *Phys. Rev. B*, v. 51, p. 7700, 1995. 85 Cited on page 85.

144 LIU, B.; AVINASH, K.; GOREE, J. *Phys. Rev. Lett.*, v. 91, p. 255003, 2003. 86 Cited on page 86.

145 LIU, B.; GOREE, J. *Phys. Rev. E*, v. 71, p. 046410, 2005. 86 Cited on page 86.

146 HAGHGOOIE, R.; LI, C.; DOYLE, P. S. *Langmuir*, v. 22, p. 3601, 2006. 86 Cited on page 86.

147 KÖPPL, M.; HENSELER, P.; ERBE, A.; NIELABA, P.; LEIDERER, P. *Phys. Rev. Lett.*, v. 97, p. 208302, 2006. 86 Cited on page 86.

148 HAGHGOOIE, R.; DOYLE, P. S. *Phys. Rev. E*, v. 70, p. 061408, 2004. 86 Cited on page 86.

149 HAGHGOOIE, R.; DOYLE, P. S. *Phys. Rev. E*, v. 72, p. 011405, 2005. 86 Cited on page 86.

150 PIACENTE, G.; SCHWEIGERT, I. V.; BETOURAS, J. J.; PEETERS, F. M. *Phys. Rev. B*, v. 69, p. 045324, 2004. 86 Cited on page 86.

151 PIACENTE, G.; PEETERS, F. M. *Phys. Rev. B*, v. 72, p. 205208, 2005. 86 Cited on page 86.

152 FERREIRA, W. P.; FARIAS, G. A.; PEETERS, F. M. *J. Phys.: Condens. Matter*, v. 22, p. 285103, 2010. 86 Cited on page 86.

153 MACEY, R. I.; OLIVER, R. M. *Biophysical Journal*, v. 7, p. 545, 1967. 86 Cited on page 86.

154 COSTE, C.; DELFAU, J.-B.; EVEN, C.; ; SAINT-JEAN, M. *Phys. Rev. E*, v. 81, p. 051201, 2010. 86, 94 Cited 2 times on pages 86 and 94.

155 TALONI, A.; LOMHOLT, M. A. *Phys. Rev. E*, v. 78, p. 051116, 2008. 86 Cited on page 86.

156 MANZI, S. J.; HERRERA, J. J. T.; ; PEREYRA, V. D. *Phys. Rev. E*, v. 86, p. 021129, 2012. 86 Cited on page 86.

157 LUCENA, D.; TKACHENKO, D. V.; NELISSEN, K.; MISKO, V. R.; FERREIRA, W. P.; FARIAS, G. A.; PEETERS, F. M. *Phys. Rev. E*, v. 85, p. 031147, 2012. 86, 90, 108, 116 Cited 4 times on pages 86, 90, 108, and 116.

158 LIN, N. S.; HEITMANN, T. W.; YU, K.; PLOURDE, B. L. T.; MISKO, V. R. *Phys. Rev. B*, v. 84, p. 144511, 2011. 86 Cited on page 86.

159 TKACHENKO, D. V.; MISKO, V. R.; PEETERS, F. M. *Phys. Rev. E*, v. 80, p. 051401, 2009. 86 Cited on page 86.

160 ALLEN, T. W.; ANDERSEN, O. S.; ROUX, B. *Biophys. Chem.*, v. 124, p. 251, 2006. 86 Cited on page 86.

161 BERENSMEIER, S. *Appl. Microbiol. Biotechnol.*, v. 73, p. 495, 2006. 86 Cited on page 86.

162 WIRTZ, D. *Phys. Rev. Lett.*, v. 75, p. 2436, 1995. 86 Cited on page 86.

163 MUNARIN, F. F.; FERREIRA, W. P.; FARIAS, G. A.; PEETERS, F. M. *Phys. Rev. E*, v. 78, p. 031405, 2008. 87 Cited on page 87.

164 EUÁN-DÍAZ, E. C.; MISKO, V. R.; PEETERS, F. M.; HERRERA-VELARDE, S.; ; CASTANEDA-PRIEGO, R. *Phys. Rev. E*, v. 86, p. 031123, 2012. 88 Cited on page 88.

165 DOMÍNGUEZ-GARCÍA, P.; MELLE, S.; PASTOR, J. M.; RUBIO, M. A. *Phys. Rev. E*, v. 76, p. 051403, 2007. 88 Cited on page 88.

166 MELLE, S.; CALDERÓN, O. G.; RUBIO, M. A.; FULLER, G. G. *J. Non-Newtonian Fluid Mech.*, v. 102, p. 135, 2002. 88 Cited on page 88.

167 KLOKKENBURG, M.; ERNÉ, B. H.; MEELDIJK, J. D.; WIEDENMANN, A.; PETUKHOV, A. V.; DULLENS, R. P. A.; PHILIPSE, A. P. *Phys. Rev. Lett.*, v. 97, p. 185702, 2006. 91 Cited on page 91.

168 FRENKEL, D.; SMIT, B. *Understanding Molecular Simulation*. [S.l.]: Academic Press, 1996. 91, 107 Cited 2 times on pages 91 and 107.

169 HERRERA-VELARDE, S.; CASTANEDA-PRIEGO, R. *Phys. Rev. E*, v. 77, p. 041407, 2008. 92, 103 Cited 2 times on pages 92 and 103.

170 FESTA, R.; D'AGLIANO, E. G. *Physica A*, v. 90, p. 229, 1978. 103, 104, 122 Cited 3 times on pages 103, 104, and 122.

171 SUNG, K. E.; VANAPALLI, S. A.; MUKHIJA, D.; MCKAY, H. A.; MILLUNCHICK, J. M.; BURNS, M. A.; SOLOMON, M. J. *J. Am. Chem. Soc.*, v. 130, p. 1335, 2008. 103 Cited on page 103.

172 CHAMPION, J. A.; MITRAGOTRI, S. *Proc. Natl. Acad. Sci. U.S.A.*, v. 103, p. 4930, 2006. 103 Cited on page 103.

173 SNEZHKO, A.; ARANSON, I. S. *Nat. Mater.*, v. 10, p. 698, 2011. 103 Cited on page 103.

174 LUMAY, G.; OBARA, N.; WEYER, F.; VANDEWALLE, N. *Soft Matter*, v. 9, p. 2420, 2013. 103 Cited on page 103.

175 YIN, Y.; LU, Y.; GATES, B.; XIA, Y. *J. Am. Chem. Soc.*, v. 123, p. 8718, 2001. 103 Cited on page 103.

176 SCIORTINO, F.; ZACCARELLI, E. *Nature (London)*, v. 493, p. 30, 2013. 103 Cited on page 103.

177 JONES, M. R.; MIRKIN, C. A. *Nature (London)*, v. 491, p. 42, 2012. 103 Cited on page 103.

178 MAO, X. *Phys. Rev. E*, v. 87, p. 062319, 2013. 103 Cited on page 103.

179 MAO, X.; CHEN, Q.; GRANICK, S. *Nat. Mater.*, v. 12, p. 217, 2013. 103 Cited on page 103.

180 YAN, J.; BLOOM, M.; BAE, S. C.; LUIJTEN, E.; GRANICK, S. *Nature (London)*, v. 491, p. 578, 2012. 103 Cited on page 103.

181 PYANZINAA, E.; KANTOROVICH, S.; CERDÀ, J. J.; HOLM, C. *J. Magn. Magn. Mater.*, v. 323, p. 1263, 2011. 103 Cited on page 103.

182 JAGER, S.; KLAPP, S. H. L. *Phys. Rev. E*, v. 86, p. 061402, 2012. 103, 137 Cited 2 times on pages 103 and 137.

183 TIERNO, P.; REIMANN, P.; JOHANSEN, T. H.; SAGUÉS, F. *Phys. Rev. Lett.*, v. 105, p. 230602, 2010. 103 Cited on page 103.

184 TIERNO, P. *Phys. Rev. Lett.*, v. 109, p. 198304, 2012. 103 Cited on page 103.

185 GOLDING, I.; COX, E. C. *Phys. Rev. Lett.*, v. 96, p. 098102, 2006. 103 Cited on page 103.

186 SAXTON, M. *Biophys. J.*, v. 92, p. 1178, 2007. 103 Cited on page 103.

187 OLSON, C. J.; REICHHARDT, C.; NORI, F. *Phys. Rev. Lett.*, v. 80, p. 2197, 1998. 103 Cited on page 103.

188 POGOSOV, W. V.; MISKO, V. R.; ZHAO, H. J.; PEETERS, F. M. *Phys. Rev. B*, v. 79, p. 014504, 2009. 103 Cited on page 103.

189 POGOSOV, W. V.; ZHAO, H. J.; MISKO, V. R.; PEETERS, F. M. *Phys. Rev. B*, v. 81, p. 024513, 2010. 103 Cited on page 103.

190 DONG, M.; MARCHETTI, M. C.; MIDDLETON, A. A.; VINOKUR, V. *Phys. Rev. Lett.*, v. 70, p. 662, 1993. 103 Cited on page 103.

191 CHAUVE, P.; DOUSSAL, P. L.; WIESE, K. J. *Phys. Rev. Lett.*, v. 86, p. 1785, 2001. 103 Cited on page 103.

192 KLAFTER, J.; SILBEY, R. *Phys. Rev. Lett.*, v. 44, p. 55, 1980. 103 Cited on page 103.

193 NOVIKOV, D. S.; FIEREMANS, E.; JENSEN, J. H.; HELPERN, J. A. *Nat. Phys.*, v. 7, p. 508, 2011. 103 Cited on page 103.

194 MEROZ, Y.; SOKOLOV, I. M.; KLAFTER, J. *Phys. Rev. Lett.*, v. 110, p. 090601, 2013. 103 Cited on page 103.

195 TALONI, A.; MARCHESONI, F. *Phys. Rev. Lett.*, v. 96, p. 020601, 2006. 103 Cited on page 103.

196 LUCENA, D.; FERREIRA, W. P.; MUNARIN, F. F.; FARIAS, G. A.; PEETERS, F. M. *Phys. Rev. E*, v. 87, p. 012307, 2013. 104, 106, 116, 117 Cited 4 times on pages 104, 106, 116, and 117.

197 RISKEN, H. *The Fokker-Planck Equation: Methods of Solution and Applications*. [S.l.]: Springer Science and Business Media, 1996. 104 Cited on page 104.

198 LIFSON, S.; JACKSON, J. L. *J. Chem. Phys.*, v. 36, p. 2410, 1962. 104 Cited on page 104.

199 REIMANN, P.; VAN DEN BROECK, C.; LINKE, H.; HÄNGGI, P.; RUBI, J. M.; ; PÉREZ-MADRID, A. *Phys. Rev. E*, v. 65, p. 031104, 2002. 104 Cited on page 104.

200 WATSON, G. N. *A Treatise on the Theory of Bessel Functions*. [S.l.]: Cambridge University Press, 1995. 104 Cited on page 104.

201 GRADSHTEYN, I. S.; RYZHIK, I. M. *Table of Integrals, Series, and Products (7th edition)*. [S.l.]: Academic Press, 2007. 105 Cited on page 105.

202 ABRAMOWITZ, M.; STEGUN, I. A. *Handbook of Mathematical Functions with Formulas, Graphs, and Mathematical Tables*. [S.l.]: New York: Dover Publications, 1972. 105 Cited on page 105.

203 HERRERA-VELARDE, S.; CASTANEDA-PRIEGO, R. *J. Phys.: Condens. Matter*, v. 19, p. 226215, 2007. 106 Cited on page 106.

204 CARVALHO, J. C. N.; NELISSEN, K.; FERREIRA, W. P.; FARIAS, G. A.; PEETERS, F. M. *Phys. Rev. E*, v. 85, p. 021136, 2012. 106 Cited on page 106.

205 JÄGER, S.; STARK, H.; KLAPP, S. H. L. *J. Phys.: Condens. Matter*, v. 25, p. 195104, 2013. 106 Cited on page 106.

206 KOB, W.; ANDERSEN, H. C. *Phys. Rev. Lett.*, v. 73, p. 1376, 1994. 107 Cited on page 107.

207 FLENNER, E.; SZAMEL, G. *Phys. Rev. E*, v. 72, p. 011205, 2005. 107 Cited on page 107.

208 HANES, R. D. L.; SCHMIEDEBERG, M.; EGELHAAF, S. U. *Phys. Rev. E*, v. 88, p. 062133, 2013. 108 Cited on page 108.

209 LIU, Y.; AI, B.-Q. *J. Phys.: Condens. Matter*, v. 21, p. 465102, 2009. 108 Cited on page 108.

210 KRAPIVSKY, P. L. *J. Stat. Mech.*, v. 2013, p. P06012, 2013. 109 Cited on page 109.

211 BARKAI, E.; GARINI, Y.; METZLER, R. *Phys. Today*, v. 65, p. 29, 2012. 116 Cited on page 116.

212 DELFAU, J.-B.; COSTE, C.; SAINT-JEAN, M. *Phys. Rev. E*, v. 87, p. 032163, 2013. 116, 117 Cited 2 times on pages 116 and 117.

213 MUKHOPADHYAY, A. K.; GOREE, J. *Phys. Rev. Lett.*, v. 109, p. 165003, 2012. 117 Cited on page 117.

214 SIEMS, U.; KREUTER, C.; ERBE, A.; SCHWIERZ, N.; SENGUPTA, S.; LEIDERER, P.; NIELABA, P. *Scientific Reports*, v. 2, p. 1015, 2012. 121 Cited on page 121.

215 JACKSON, J. D. *Classical Electrodynamics*. [S.l.]: Wiley (New York), 1975. 137 Cited on page 137.

Appendix

APPENDIX A – Appendix

A.1 Interaction torque and external magnetic field torque

In this appendix, we calculate the first ($\boldsymbol{\tau}_i$) and the second term ($\boldsymbol{\tau}_i^B$) present in the r.h.s. of the equation of motion (4.3) in cartesian coordinates. The interaction torque $\boldsymbol{\tau}_i$ is given by the relation

$$\boldsymbol{\tau}_i = \boldsymbol{\mu}_i \times \sum_{j>i} \mathbf{B}_{ij}^{\text{int}}, \tag{A.1}$$

where $\boldsymbol{\mu}_i$ is the magnetic moment of ith particle and $\sum_{j>i}\mathbf{B}_{ij}^{\text{int}}$ is the magnetic field generated by all j particles on the ith particle. Following Refs. (182, 215), we write

$$\mathbf{B}_{ij}^{\text{int}} \simeq \frac{3\hat{\mathbf{n}}(\hat{\mathbf{n}}\cdot\boldsymbol{\mu}_j) - \boldsymbol{\mu}_j}{|\mathbf{r}_{ij}|^3}, \tag{A.2}$$

where $\hat{\mathbf{n}} = \mathbf{r}_{ij}/|\mathbf{r}_{ij}|$. Since the system is (in practice) two-dimensional (2D), we may write

$$\mathbf{B}_{ij}^{\text{int}} = B_{ij}^x\hat{\mathbf{x}} + B_{ij}^y\hat{\mathbf{y}}, \tag{A.3}$$

$$\mathbf{r}_{ij} = \Delta x_{ij}\hat{\mathbf{x}} + \Delta y_{ij}\hat{\mathbf{y}}, \tag{A.4}$$

$$\boldsymbol{\mu}_j = \mu\cos\theta_j\hat{\mathbf{x}} + \mu\sin\theta_j\hat{\mathbf{y}}, \tag{A.5}$$

in cartesian coordinates. Therefore, directly calculation of Eq. (A.1) using Eqs. (A.2)–(A.5) gives

$$\boldsymbol{\tau}_i = \hat{\mathbf{z}}\left[\mu\cos\theta_i\sum_{j>i}B_{ij}^y - \mu\sin\theta_i\sum_{j>i}B_{ij}^x\right], \tag{A.6}$$

where the terms B_{ij}^x and B_{ij}^y are given by

$$B_{ij}^x = \frac{3[\Delta x_{ij}^2\mu\cos\theta_j + \Delta x_{ij}\Delta y_{ij}\mu\sin\theta_j] - \mu\cos\theta_j|\mathbf{r}_{ij}|^2}{|\mathbf{r}_{ij}|^5}, \tag{A.7}$$

$$B_{ij}^y = \frac{3[\Delta x_{ij}\Delta y_{ij}\mu\cos\theta_j + \Delta y_{ij}^2\mu\sin\theta_j] - \mu\sin\theta_j|\mathbf{r}_{ij}|^2}{|\mathbf{r}_{ij}|^5}. \tag{A.8}$$

Similary, we can calculate the torque $\boldsymbol{\tau}_i^B$ due to the external magnetic field $\mathbf{B} = B_x\hat{\mathbf{x}} + B_y\hat{\mathbf{y}}$ on the ith particle as

$$\boldsymbol{\tau}_i^B = \boldsymbol{\mu}_i \times \mathbf{B} = \hat{\mathbf{z}}[\mu\cos\theta_i B_y - \mu\sin\theta_i B_x]. \tag{A.9}$$

Note that since the problem is 2D, the torques $\boldsymbol{\tau}_i$ and $\boldsymbol{\tau}_i^B$ [Eqs. (A.6) and (A.9), respectively] are in the z-direction, *i.e.*, perpendicular to the xy-plane.

Annex

ANNEX A – Annex

A.1 List of publications related with this thesis

1) **D. Lucena**, D. Tkachenko, K. Nelissen, V. R. Misko, W. P. Ferreira, G. A. Farias, and F. M. Peeters, *Transition from single-file to two-dimensional diffusion of interacting particles in a quasi-one-dimensional channel*, Phys. Rev. E **85**, 031147 (2012).

2) **D. Lucena**, F. F. Munarin, W. P. Ferreira, G. A. Farias, and F. M. Peeters, *Tunable diffusion of magnetic particles in a quasi-one-dimensional channel*, Phys. Rev. E **87**, 012307 (2013).

3) **D. Lucena**, J. E. Galván-Moya, W. P. Ferreira, and F. M. Peeters, *Single-file and normal diffusion of magnetic dipoles in modulated channels*, Phys. Rev. E **89**, 032306 (2014).

4) J. E. Galván-Moya, **D. Lucena**, W. P. Ferreira, and F. M. Peeters, *Magnetic particles confined in a modulated channel: Structural transitions tunable by tilting a magnetic field*, Phys. Rev. E **89**, 032309 (2014).

A.2 List of other publications

1) **D. Lucena**, V. R. Misko, W. P. Ferreira, and F. M. Peeters, *Dynamics of vortices in a Corbino disk in the presence of a regular array of pinning sites*, manuscript in preparation.